NASA/TP—2016–219101

Summary Report on Phase I Results From the 3D Printing in Zero-G Technology Demonstration Mission, Volume I

*T.J. Prater, Q.A. Bean, R.D. Beshears, T.D. Rolin, N.J. Werkheiser, E.A. Ordonez,
R.M. Ryan, and F.E. Ledbetter III*
Marshall Space Flight Center, Huntsville, Alabama

July 2016

The NASA STI Program…in Profile

Since its founding, NASA has been dedicated to the advancement of aeronautics and space science. The NASA Scientific and Technical Information (STI) Program Office plays a key part in helping NASA maintain this important role.

The NASA STI Program Office is operated by Langley Research Center, the lead center for NASA's scientific and technical information. The NASA STI Program Office provides access to the NASA STI Database, the largest collection of aeronautical and space science STI in the world. The Program Office is also NASA's institutional mechanism for disseminating the results of its research and development activities. These results are published by NASA in the NASA STI Report Series, which includes the following report types:

- TECHNICAL PUBLICATION. Reports of completed research or a major significant phase of research that present the results of NASA programs and include extensive data or theoretical analysis. Includes compilations of significant scientific and technical data and information deemed to be of continuing reference value. NASA's counterpart of peer-reviewed formal professional papers but has less stringent limitations on manuscript length and extent of graphic presentations.

- TECHNICAL MEMORANDUM. Scientific and technical findings that are preliminary or of specialized interest, e.g., quick release reports, working papers, and bibliographies that contain minimal annotation. Does not contain extensive analysis.

- CONTRACTOR REPORT. Scientific and technical findings by NASA-sponsored contractors and grantees.

- CONFERENCE PUBLICATION. Collected papers from scientific and technical conferences, symposia, seminars, or other meetings sponsored or cosponsored by NASA.

- SPECIAL PUBLICATION. Scientific, technical, or historical information from NASA programs, projects, and mission, often concerned with subjects having substantial public interest.

- TECHNICAL TRANSLATION. English-language translations of foreign scientific and technical material pertinent to NASA's mission.

Specialized services that complement the STI Program Office's diverse offerings include creating custom thesauri, building customized databases, organizing and publishing research results…even providing videos.

For more information about the NASA STI Program Office, see the following:

- Access the NASA STI program home page at <http://www.sti.nasa.gov>

- E-mail your question via the Internet to <help@sti.nasa.gov>

- Phone the NASA STI Help Desk at 757–864–9658

- Write to:
  NASA STI Information Desk
  Mail Stop 148
  NASA Langley Research Center
  Hampton, VA 23681–2199, USA

Summary Report on Phase I Results From the 3D Printing in Zero-G Technology Demonstration Mission, Volume I

T.J. Prater, Q.A. Bean, R.D. Beshears, T.D. Rolin, N.J. Werkheiser, E.A. Ordonez,
R.M. Ryan, and F.E. Ledbetter III
Marshall Space Flight Center, Huntsville, Alabama

TRADEMARKS

EXECUTIVE SUMMARY

Human space exploration to date has been confined to low-Earth orbit and the Moon. The International Space Station (ISS), an orbiting laboratory 200 miles above the Earth, provides a unique opportunity for researchers to prove out the technologies that will enable humans to safely live and work in space for longer periods of time and venture farther into the solar system. The ability to manufacture parts in space, rather than launch them from Earth, represents a fundamental shift in the current risk and logistics paradigm for human spaceflight. In particular, additive manufacturing (or 3D printing) techniques can potentially be deployed in the space environment to enhance crew safety (by providing an on-demand part replacement capability) and decrease launch mass by reducing the number of spare components that must be launched for missions where cargo resupply is not a near-term option to ensure mission success (in the current risk model, sufficient spare parts must be provided for planned maintenance activities and unexpected failures, the likelihood of which increase with the duration of the mission).

In September 2014, NASA launched the 3D Printing in Zero-G (3DP) technology demonstration mission to the ISS to explore the potential of additive manufacturing for in-space applications and demonstrate the capability to manufacture parts and tools on orbit. The printer for this mission was developed by Made In Space, Inc., a small business located in Mountain View, California, under a NASA Small Business Innovative Research phase III contract. The overarching objectives of the 3DP mission were to use ISS as a testbed to further maturation of enhancing technologies needed for long-duration human exploration missions, introduce new materials and methods to fabricate structures in space, enable cost-effective manufacturing for structures and mechanisms made in low-unit production, and enable physical components to be manufactured in space on long-duration missions if necessary. The mission is aligned with NASA technology roadmaps for materials and manufacturing as well as the NASA Human Research Program Decadal Survey, which calls for the "design and develop[ment] of advanced materials that meet new property requirements to enable human exploration at reduced cost using both current and novel materials synthesis and processing techniques." The 3DP unit was integrated into the ISS Microgravity Science Glovebox in November 2014, and phase I printing operations took place from November through December of that year. Phase I flight operations yielded 14 unique parts (21 total specimens) that could be directly compared against ground-based prints of identical geometry manufactured using the printer prior to its launch to ISS. The 3DP unit functioned safely and produced specimens necessary to advance the understanding of the critical design and operational parameters for the fused deposition modeling (FDM) process as affected by the microgravity environment. From the standpoint of operations, 3DP demonstrated the ability to remove parts from the build tray on orbit, teleoperate the printer from the ground, perform critical maintenance functions within defined human factors limits, produce a tool (the ratchet) that could be evaluated for form/fit/function, and uplink a new part file and produce it on the printer. After printing, parts were separated from the build tray, packaged, and stored on station. The flight parts were downmassed from the ISS on the SpaceX Dragon capsule in February 2015 and arrived at NASA Marshall Space Flight Center (MSFC) in Huntsville, Alabama, in April 2015.

Upon arrival at MSFC, the parts were unboxed and underwent testing and evaluation at the Materials and Processes Laboratory from May 2015 through September 2015. During that time, ground and flight prints completed the following phases of testing: photographic/visual inspection, mass and density evaluation, structured light scanning, x-ray and computed tomography, mechanical testing, and optical microscopy. Analysis of test data was performed by Materials and Processes Laboratory personnel from September 2015 to November 2015 and presented to invitees from industry, government, and academia at a technical interchange held at MSFC on December 2 and 3, 2015. Key findings from each phase of testing were presented at this meeting. Broadly stated, the flight specimens (with the exception of the compression specimens) are denser, stronger, and stiffer than the ground prints. Many specimens also exhibit a noticeable variation in density in the through-thickness of the part, with the bottom half of the specimen being denser than the top half. The in-space manufacturing (ISM) team and attendees examined identified influence factors and hypotheses which may explain these observed variations between classes of specimens in the 3DP dataset. Based on the discussions and interactions at this meeting, the ISM team developed a 'go-forward plan' for further evaluation of the ground and flight specimens and ground-based characterization work to answer open questions related to the 3DP dataset.

The primary purpose of the phase I test plan was to verify the process capabilities of FDM in the microgravity environment (i.e., FDM's ability to produce materials with properties that are equivalent/in family with their terrestrially manufactured counterparts). While FDM is not a process that relies on buoyancy driven convection to achieve material consolidation, differences in heat and mass transfer coefficients in microgravity may impact layer adhesion, surface tension, and cooling rate. Even subtle differences in these parameters may result in structurally different materials. Evaluation of the process over a long microgravity time constant in this manner is only possible using the ISS. Data collected from the test plan were intended to quantify any characteristic change in properties, dimensions, etc. that may be a consequence of the operational manufacturing environment and can be used, with the baseline material properties generated through other materials characterization activities, to derive knockdown factors (which allow designers to account for expected variations/degradation in material properties of parts produced using FDM in microgravity).

Phase II printer operations will bring these objectives closer to fulfillment. Phase II prints will allow the ISM team to do the following:

- Gain greater insight into the sources of variability in the 3DP phase I dataset. Phase II prints may lend additional clarity to causes of variability in the phase I data and which concepts/hypotheses are best poised to explain property differences between flight and ground specimens.

- Isolate the effect of microgravity on the FDM process. Several layer quality specimens are part of the phase II print matrix. Evaluation of these specimens using atomic force microscopy or scanning electron microscopy will help to understand any differences in microstructure and/or phase morphology that may be attributable to the operation of the FDM process in microgravity (or point to differences in cooling rate between the ground and flight specimens).

- Collect additional data relevant to the material aging hypothesis. At the time phase II prints occur, the feedstock from canister 11 will be well beyond the 12-month recommended shelf life specified

by the manufacturer. Canister 12 is the same age as canister 11, but has been stored in a sealed container with dessicant since its arrival on ISS (all phase I prints were completed with canister 11). Phase II provides a unique opportunity to evaluate material aging (and the rate of aging for material stored in a controlled environment versus stored in the ISS environment) on orbit and better defines feedstock requirements for future printers.

• Provide greater statistical sampling for mechanical property data. The sample size for mechanical specimens from 3DP phase I is small (a total of eight tensile, six compression, and six flexure, with half of each sample set originating from the flight prints and the other half from the ground). Additional data obtained from mechanical testing of phase II tensile, compression, and flexure specimens will provide insight into whether trends, biases, and characteristic mechanical properties reported based on phase I testing are consistent with further flight operation of the printer.

• Demonstrate critical operational and maintenance requirements for the printer by changing the feedstock and the extruder head. These represent essential operations for closing the 'manufacturing process loop' for 3DP and are also relevant to work on an in-space recycling system for feedstock.

• Demonstrate the ability of 3DP to print functional parts for use on ISS. Two crew tools, the winning entry from the Future Engineers competition, and up to six to be determined/on-demand parts for stakeholders will be printed as part of phase II operations.

The 3DP mission is the first demonstration of manufacturing in space and represents the first step toward a critical paradigm shift from Earth-dependent approaches (increasing space system reliability and/or relying on cargo resupply to fulfill repair and refurbishment needs) to Earth independence (point of use manufacturing for long-duration space missions). Future NASA endeavors will take crew farther than ever before, on missions where cargo resupply is limited and a return home requires months or even years. 3DP is one technique in a portfolio of ISM technologies that can collectively provide on-demand, sustainable operations during NASA exploration missions, both in transit and on the planetary surface (<www.nasa.gov/offices/oct/home/roadmaps/index.html>). 3DP is the initial step on a journey to develop, characterize, and institutionalize the capabilities that stand to fundamentally change the way exploration architectures are designed, and is one very critical piece of the puzzle to settlement of the high frontier.

TABLE OF CONTENTS

LIST OF FIGURES

LIST OF FIGURES (Continued)

LIST OF TABLES

LIST OF TABLES (Continued)

LIST OF ACRONYMS AND DESIGNATORS

3D-CT	3D computed tomography
3DP	3D Printing in Zero-G
ABS	acrylonitrile butadiene styrene
AFM	atomic force microscopy
AMF	Additive Manufacturing Facility
AO	atomic oxygen
ARC	Ames Research Center
ASME	American Society of Mechanical Engineers
ASTM	American Society of Materials Testing
CAD	computer aided design
CT	computed tomography
EDU	energy dispersive x-ray spectroscopy
ETU	engineering test unit
F	flight specimen
FDM	fused deposition modeling
FTIR	Fourier transform infrared spectroscopy
G	ground specimen
GTU	ground test unit
ISM	in-space manufacturing
ISRU	in situ resource utilization

ISS	International Space Station
LDI	low-density indication
LED	light-emitting diode
LEO	low-Earth orbit
MAPTIS	Materials and Processes Technical Information System
MR	moving range
MSFC	Marshall Space Flight Center
MSG	Microgravity Science Glovebox
NDE	nondestructive evaluation
NIST	National Institute of Standards and Technology
RFI	request for information
RT	radiographic testing
SBIR	Small Business Innovative Research
SD	standard deviation
SEM	scanning electron microscopy
STEM	science, technology, engineering, and math
T&E	testing and evaluation
TIM	technical interchange meeting
TP	Technical Publication
TRL	Technology Readiness Level
UV	ultraviolet
V&V	verification and validation

NOMENCLATURE

E	modulus of elasticity
R^2	squared correlation coefficient
α	statistical significance level
Δ	difference
ρ	gravimetric density
σ_{flex}	flexural stress
$\sigma_{max,20\%}$	maximum stress corresponding to 20% strain
σ_{uts}	ultimate tensile strength
σ_{ys}	yield strength

TECHNICAL PUBLICATION

**SUMMARY REPORT ON PHASE I RESULTS FROM THE 3D PRINTING
IN ZERO-G TECHNOLOGY DEMONSTRATION MISSION, VOLUME I**

1. INTRODUCTION

1.1 The 3D Printing in Zero-G Technology Demonstration Mission

NASA Marshall Space Flight Center (MSFC) and the Agency as a whole are currently engaged in a number of in-space manufacturing (ISM) activities that have the potential to reduce launch costs, enhance crew safety, and provide the capabilities needed to undertake long-duration spaceflight. The recent 3D Printing in Zero-G (3DP) experiment conducted on board the International Space Station (ISS) demonstrated that parts of acylonitrile butadiene styrene (ABS) plastic can be manufactured in microgravity using fused deposition modeling (FDM). This project represents the beginning of the development of a capability that is critical to future NASA missions.

The 3DP technology demonstration is the first payload to perform 3D printing (or, synonymously, additive manufacturing) in a microgravity environment over a long time constant. This demonstration represents the first step towards development of an ISM capability which has the potential to enhance crew safety, enable long-duration missions where cargo resupply may not be an option, and disrupt the orbital supply change to reduce reliance on Earth-based platforms.[1] The 3DP payload was developed by the private company Made In Space, Inc., under a NASA Small Business Innovative Research (SBIR) phase III contract. The 3DP technology demonstration was jointly funded by the NASA Human Exploration and Operations Mission Directorate (through the Advanced Exploration Systems and International Space Station programs) and the Space Technology Mission Directorate (Game Changing Development program). The NASA team provided guidance for the payload design, early prototype and flight unit qualification testing, payload integration management, ground operations personnel, the flight to the ISS (SpaceX-4), and crew time for the printer's operation.

The printer was designed to operate within the Microgravity Science Glovebox (MSG), which provided containment, circulation to the outside of the printer and the electronics box, as well as cooling capabilities to prevent the printer from overheating. The 3DP payload used an extrusion-based process, FDM, to create ABS plastic parts. The choice of ABS as feedstock material was driven by its relatively low extrusion temperature, low toxicity, use in other commercial printing units, and strength relative to other feedstocks. 3DP also contains its own environmental control unit, which is designed to regulate cooling and provide filtration of the air within the printer volume. Parts were printed from data files loaded on the device at launch, as well as an additional file uplinked to 3DP on orbit.

3DP was unloaded and remained in stowage until installation in MSG on November 17, 2014. The phase I printing, following the calibration of the device, occurred from November 24, 2014, to December 15, 2014, as crew time allowed. 3DP was removed from the MSG on December 16, 2014, and will remain in stowage until crew time becomes available for phase II prints. The phase I prints were brought to Earth on SpaceX-5 on February 10, 2015, and unboxed at MSFC on April 6, 2015. From April to September 2015, the specimens underwent several phases of testing to characterize differences between analogous flight and ground printed specimens (ground prints were made using the flight printer in the glovebox installation at MSFC prior to the printer's launch to ISS) and assess microgravity effects on the FDM process. The results of each phase of testing (visual inspection, structured light scanning, x-ray and computed tomography (CT), structured light scanning, and optical microscopy) are summarized in this Technical Publication (TP). Results were also outbriefed during a technical interchange meeting (TIM) held on December 2 and 3, 2015, at MSFC. This TP also captures the discussions, input, and recommendations from the broader materials science community regarding analysis and interpretation of the phase I print results. A detailed summary of this meeting and an overview of the results from the 3DP phase I operations that were presented are provided in appendix A.

1.2 An Overview of In-Space Manufacturing

The ISM project is responsible for developing the manufacturing capabilities that will provide on-demand, sustainable operations during future NASA exploration missions. The scope of this work includes testing and advancing the candidate manufacturing technologies for in-space applications, as well as developing the skills and processes (such as defining verification and validation (V&V) activities) that will enable the technologies to become institutionalized. ISM utilizes the ISS as a testbed for technology demonstration missions that will serve as the proving ground to transition these technologies to an orbital platform, enhancing crew safety and reducing reliance on Earth.

While 3D printing (and particularly the 3DP technology demonstration mission) are ISM's highest profile activities, ISM includes work in many development areas that are key to reducing reliance on Earth-based platforms and enabling sustainable, safe exploration. These include:

• Feedstock recycling—The feedstock recycler, which will recycle/reclaim 3D printed parts and/or packing materials into feedstock materials which can then be used to manufacture parts using 3D printing facilities on station.

• Printed electronics—Leverage ground-based developments to enable ISM of functional electronic components, sensors, and circuits.

• Printable satellites—The combination of 3DP coupled with printable electronics enables the on-orbit capability to produce small satellites 'on demand.'

• Multimaterial 3D printing—Additively manufacturing metallic parts in space is a desirable capability for large structures, components with high strength requirements, and repairs. NASA is evaluating various additive manufacturing metal processes for use in the space environment.

- External structures and repairs—Throughout the lifecycle of space structures, astronauts will need to perform repairs on tools, components, and structures in space. A previous project at NASA Johnson Space Center investigated the use of structured light scanning techniques to create a digital model of damage and how additive manufacturing technologies such as 3DP and metallic manufacturing techniques (including electron beam welding) could be used to perform repairs.

- Additive construction—These activities are focused on developing a capability to print structures on planetary bodies or asteroids using available resources.

The ISM program is focused on evolving manufacturing technologies from Earth-reliant to Earth-independent, work that is key to NASA's exploration path. The ISS, currently funded through 2024, will continue to serve as the primary testbed and proving ground for ISM technologies. These include the 3DP technology demonstration that is the focus of this TP, the Additive Manufacturing Facility (AMF) (future hardware that will operate on ISS under the management of the Center for the Advancement of Science in Space), the feedstock recycler, the development of the part utilization catalog, printable electronics, and investigations into additive manufacturing of metallics and external repair.

On Earth, the program includes work on certification and inspection processes, development of a characteristic material properties database for parts manufactured in the space environment using ISM capabilities, design of control systems and supporting software for ISM, and ground-based technology maturation and demonstrations. Many of these activities (such as the Additive Construction for Mobile Emplacement project, which seeks to develop a capability to print custom-designed expeditionary structures from either native concrete or concrete derived from available material on planetary bodies) represent intensive collaborations between the ISM and in situ resource utilization (ISRU) communities.[2]

ISM is also a powerful tool to increase student engagement in science, technology, engineering, and math (STEM) educational activities and develop the next generation of engineers. Recently, NASA and the American Society of Mechanical Engineers (ASME) collaborated on a student competition, called the National Future Engineers STEM program, to design a tool that could be used by an astronaut on ISS.[3] The winning part, a multipurpose maintenance tool, will be printed on ISS as part of phase II operations for the 3D printer currently on station. A similar competition to develop a container for ISS use that can be printed in space is currently underway. More information about these and other NASA/ASME competitions can be found at <www.futureengineers.org>.

In-Space Manufacturing Phased Technology Development Roadmap

Earth-based	Demos: Ground and ISS		Exploration		

3D Print Tech Demo		Plastic Printing Demo / ACME / Recycler SmallSats / Metal Printing / Add Mfctr. Facility / Printable Electronics / Self-repair/Replicate	Asteroids / Lagrange Point	Lunar	Mars
Pre-2012	**2014**	**2015 2016 2017 2018**	**2020–25**	**2025**	**2030–40**
Ground and Parabolic Centric: • Multiple FDM Zero-G Parabolic Flights • Trade/System Studies for Metals • Ground-Based Printable Electronics/Spacecraft • Verification and Certification Processes Under Development • Materials Database • Cubesat Design and Development	• In-space: 3D Print: First Plastic Printer on ISS Tech Demo • NIAC Contour Crafting • NIAC Printable Spacecraft • Small Sat in a Day • AF/NASA Space-based Additive NRC Study • ISRU Phase II SBIRs • Ionic Liquids • Printable Electronics	• *3D Print Demo* • *Future Engineer Challenge* • *Utilization Catalogue* • *ISM Cert Process* • *Add. Mfctr. Facility (AMF)* • *In-Space Recycler SBIR* • *In-space Material Database* • *External In-space 3D Printing* • *Autonomous Processes* • *ACME Simulant Dev and Test for Feedstock; Ground Demo* **ISS:** *Utilization/Facility Focus* • In-space Recycler Demo • Integrated Facility Systems for Stronger Types of Extrusion Materials for Multiple Uses Including Metals and Various Plastics • Printable Electronics Tech Demo • Synthetic Biology Demo • Metal Demo Options • *ACME Ground Demos*	*Lunar, Lagrange FabLabs* • Initial Robotic/Remote Missions • Provision Feedstock • *Evolve to Utilizing In Situ Materials (Natural Resources, Synthetic Biology)* • *Product: Ability to Produce, Repair, and Recycle Parts and Structures on Demand; i.e. "Living Off The Land"* • Autonomous Final Milling to	*Planetary Surfaces Points Fab* • Transport Vehicle and Sites Would Need Fab Capability • *Additive Construction and Repair of Large Structures*	*Mars Multi-Material Fab Lab* • *Provision and Utilize In Situ Resources for Feedstock* • *FabLab: Provides On-Demand Manufacturing of Structures, Electronics, and Parts Utilizing In-Situ and Ex-Situ (Renewable) Resources.* Includes Ability to Inspect, Recycle/Reclaim, and Post-Process as Needed Autonomously to Ultimately Provide Self-Sustainment at Remote Destinations.

ISS Serves as a Key Exploration Test-Bed for the Required Technology Maturation and Demonstrations

Figure 1. ISM phased technology roadmap.

ISM has developed a phased technology roadmap (fig. 1) to capture the chronology of work needed to transition identified manufacturing technologies from Earth-based to exploration-based through the 2030–2040 timeframe. The immediate focus and first step is in-space 3D printing and recycling of plastics, but in future years, the breadth and scope of activities are anticipated to rapidly grow to include printable electronics, ionic liquids (another ISRU collaborative activity), additive manufacturing of metallics, and development and demonstration of external repair capabilities. With the scheduled decommissioning of ISS in 2024, ISM could evolve (based on the technology maturation made possible by ISS technology demonstrations in the preceding years) to include fabrication labs on the Moon, asteroids, in cislunar space, or even the Martian surface. A fabrication lab would provide on-demand manufacturing of structures, electronics, and parts via processes that utilize in situ and ex situ (renewable) resources. The suite of ISM technologies identified in the roadmap will be key enablers for exploration and self-sustainment at any destination.

All of the technology development activities identified in figure 1 will require extensive materials characterization work for materials and parts/systems produced using ISM capabilities. The ISM team at MSFC is working to coordinate an integrated team to define and execute material property development activities to achieve the following objectives:

(1) Identify key material properties needed for design and analysis.

(2) Develop a materials characterization approach to establish baseline material properties for plastic parts manufactured in space using current and future 3DP facilities.

(3) Understand relationships between manufacturing process variables and resulting material properties. This includes characterizing the effects of filament layup/orientation, feedstock types and lots, and operating the FDM process in the microgravity environment. Printer-to-printer (and build-to-build) variability must also be characterized.

(4) Anchor characteristic property data reported in (2) with results from structural tests of printed parts to assess the predictive capability of cataloged property values for design and analysis tasks.

(5) Report characteristic property values for materials and/or material systems in the Materials and Processes Technical Information System (MAPTIS). (A material system may be defined as a particular combination of printer/feedstock/filament layup/operational environment.) Values in the MAPTIS database represent validated properties that can be used for the purposes of design and analysis.

Developing a materials characterization roadmap for ISM that will enable functional use of the 3D printer currently on ISS was the primary focus of the first TIM held in July 2015 (a summary of this meeting can be found in ref. 4). These tasks are foundational for all future ISM activities related to 3D printing of plastics. Materials characterization is also necessary precursor work for V&V activities that will be required for parts to be included in the utilization catalog (a library of approved parts that can be printed on station). Follow-on activities that will also require a materials characterization approach and database capability for materials of interest include the AMF, the in-space recycler ISS technology demonstration, and the launch packaging recycler. The latter two pieces of hardware will recycle 3D printed parts and launch packaging materials into feedstock (which can then be potentially used by 3DP or AMF) to close the logistics loop. Robust materials characterization is essential to ensure that parts produced with ISM capabilities will satisfy NASA's stringent functional requirements for spaceflight hardware, and the integrated team that will be formed through this work represents a vital Agency resource for the future development of evolvable manufacturing systems that promote space sustainability.

2. TEST PLAN FOR PHASE I PRINTS FROM THE 3D PRINTING IN ZERO-G TECHNOLOGY DEMONSTRATION MISSION

This section summarizes the print matrix for phase I and provides details on test procedures and objectives. Ground prints for the 3DP technology demonstration mission took place in June 2015 at MSFC. These prints were made on the flight printer in the ground MSG unit. The printer launched to ISS in September 2014 on Space X-4 and was installed in the MSG on station on November 17, 2014. Phase I flight prints took place between November 24, 2014, and December 15, 2014. 3DP was removed from the glovebox on December 16, 2014. Phase I flight prints returned to Earth on SpaceX-5 on February 10, 2015, and arrived at MSFC on April 6, 2015. From April to September 2015, the parts completed multiple phases of testing, including photographic/visual inspection, x-ray and CT, structured light scanning, mechanical testing, and optical microscopy. The objective of this testing was to compare flight prints against analogous ground prints to evaluate microgravity effects on the FDM process, characterize printer performance, and assess the material quality achievable with the 3DP unit.

2.1 Phase I Print Matrix

Filament of undyed ABS plastic at 1.75 mm diameter was used for the phase I prints. The filament was heated to an extrusion temperature between 230 °C and 250 °C and fed through a 0.4-mm extruder tip. A set of samples were built with the flight printer unit and flight feedstock prior to launch (the ground control samples). These samples were directly compared with the specimens printed using the flight unit on board the ISS in November and December 2014. Mechanical test specimens were built with a ±45° layup with a solid infill. Detailed information about the specimens from the ground and flight prints appear in table 1.

Table 1. Catalog of phase I prints.
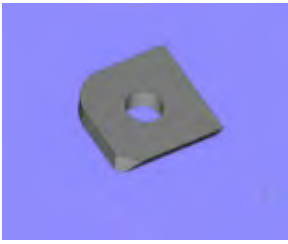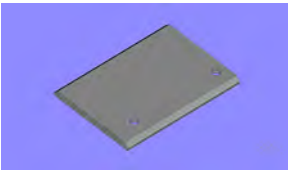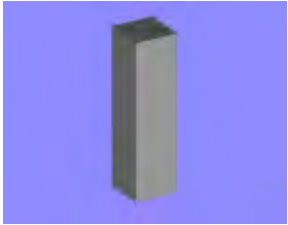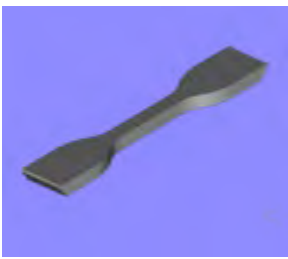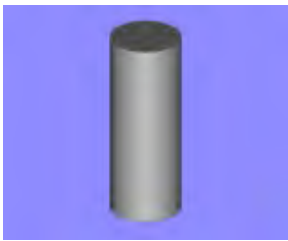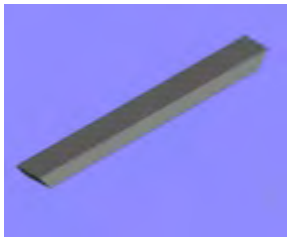
Sample Quantity	Sample Name	Image	Characteristic Dimensions (cm)	Notes
6 (5 flight, (1 ground)	Calibration coupon		Length: 3.00 Width: 3.00 Height: 0.41	This functional checkout and calibration coupon was printed to determine the calibration distance between the extruder and print plate.
2 (1 flight, 1 ground)	Extruder head casing		Length: 5.89 Width: 4.09 Height: 0.51	This is a replacement part for the 3D printer itself; it is a side plate of the extruder casing.
2 (1 flight, 1 ground)	Layer quality test specimen		Length: 1.00 Width: 1.00 Height: 3.00	This layer quality test specimen was printed to assess adhesion between layers and tolerances.
8 (4 flight, 4 ground)	Tensile coupon		Length: 11.35 Width: 1.91 Neck width: 0.61 Height: 0.41	The purpose of this coupon is to assess the tensile strength of the printed material at ±45° layup orientation.
6 (3 flight, 3 ground)	Compression coupon		Diameter: 1.27 Height: 2.54	Coupon to assess compressive strength of the printed material.
6 (3 flight, 3 ground)	Flexural coupon		Length: 8.81 Width: 0.99 Height: 0.41	Coupon to assess flexure properties of the printed material at ±45° layup orientation.

Table 1. Catalog of phase I prints (Continued).
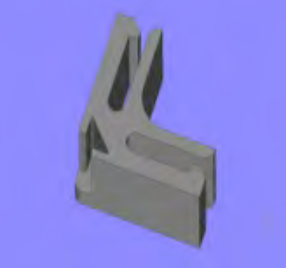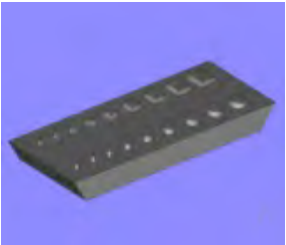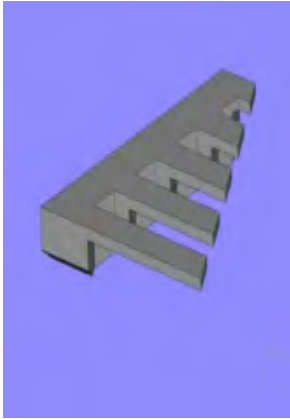
Sample Quantity	Sample Name	Image	Characteristic Dimensions (cm)	Notes
3 (2 ground, 1 flight)	Negative range coupon		Length: 7.49 Width: 2.01 Height: 0.43	This coupon will be used to assess the performance, geometric accuracy, and tolerances of the 3DP unit.
2 (1 ground, 1 flight)	Torque tool specimen		Diameter: 3.00 Height: 2.50	This coupon demonstrates the ability of 3DP to fabricate a replacement crew tool.
2 (1 ground, 1 flight)	Crowfoot specimen		Length: 4.70 Width: 3.99 Height: 1.30	This coupon demonstrates the ability of 3DP to fabricate a replacement crew tool.
2 (1 ground, 1 flight)	Structural clip component		Length: 2.69 Width: 2.10 Height: 0.90	This is a structural connector/spacer that can be utilized to assemble avionics (specifically electronics cards) on orbit.
2 (1 ground, 1 flight)	Positive range coupon		Length: 6.12 Width: 2.01 Height: 0.51	This coupon will be used to assess the performance, geometric accuracy, and tolerances of the 3DP unit for positive relief features.

Table 1. Catalog of phase I prints (Continued).

Sample Quantity	Sample Name	Image	Characteristic Dimensions (cm)	Notes
2 (1 ground, 1 flight)	Sample container		Body diameter: 4.03 Body height: 3.28 Top diameter: 4.60	This set will test the printer's capability to produce two components in the same print. Part also has interlocking threads.
2 (1 ground, 1 flight)	Microgravity structure specimen 1		Length: 2.46 Width: 2.21 Height: 0.51	This is a test of a part that would be difficult, if not impossible, to successfully 3D print in the pictured orientation due to gravity (i.e., sag, overhang, etc.). Specimen used to demonstrate how microgravity environment can be exploited to print structures that are not possible terrestrially (i.e., large overhangs without supports).
1 (ground)	Wire tie*		Length: 1.92 Width: 1.30 Height: 0.12	Part intended to assess flexibility of the material after printing.
1 (flight)	Ratchet*		Length: 11.35 Width: 3.30 Height: 2.59	This part was uplinked, illustrating how a part can be designed on Earth and manufactured in space, on demand.

*Note: Wire tie is a ground control sample and ratchet is a flight sample. As such, the wire tie does not have a flight analog and the ratchet does not have a ground analog. No direct comparison between flight and ground can be made for these parts, but their respective evaluations can be used to ascertain the overall functionality of the machine and process.

Specimen IDs and descriptions are cataloged in table 2. The 'G' prefix denotes a ground specimen and the 'F' prefix denotes a flight specimen.

Table 2. Specimen IDs.

Specimen ID(s)	Specimen Description
G001, F001A–E	Calibration coupon
G002, F002	Extruder plate
G003, F003	Layer quality specimen
G004, F004	Tensile coupon
G005, F005	Compression coupon
G006, F006	Flexure coupon
G007A, G007B, F007	Negative range specimen
G008, F008	Torque coupon
G009, F009	Crowfoot
G010, F010	Structural clip
G011, F011	Positive range specimen
G012, F012	Tensile coupon
G013, F013	Compression coupon
G014, F014	Flexure coupon
G015, F015	Tensile coupon
G016, F016	Compression coupon
G017, F017	Flexure coupon
G018, F018	Tensile coupon
G019, F019	Microgravity structure specimen
G020A	Sample container (container)
F021	Ratchet
G021	Wire tie

2.2 Tests and Test Procedures

All samples were stored individually in clearly marked and sealed plastic bags. When not undergoing testing, samples were kept in a dry place at room temperature and away from direct sunlight and moisture sources. Test conductors were required to wear latex or other suitable gloves during testing to avoid direct skin contact and potential contamination of the samples.

2.2.1 Photographic Inspection

Each ground sample, flight sample, and print tray underwent a thorough visual and photographic inspection upon receipt and unboxing of the specimens at MSFC in April 2015. During this inspection, photographs were taken from different angles and with appropriate scale representation (e.g., a standard ruler) using a digital camera (with a megapixel resolution of 8 or greater) for print-quality images. Anomalies and any suspicion of damage (which may have occurred when the print was removed from the print tray) as well as any visually apparent delamination, open voids, curling, and warping were noted.

2.2.2 Mass Measurement

A measurement of the mass using a calibrated laboratory scale accurate to 0.1 mg was repeated five times for each specimen. Density was calculated based on these measurements, and the volume was determined by structured light scanning. Mass measurement was completed in May 2015. Mass measurements are summarized in section 3.

2.2.3 Structured Light Scanning

A structured light scanning technique was used to generate a detailed dataset characterizing the surface geometric variations between the printed part for the flight and ground samples and the computer aided design (CAD) model. The scanning used an ATOS II, Triple Scan blue light-emitting diode (LED) scanner. The scanner has an accuracy of ± 12.7 µm at these volumes and the capability to capture stereoscopic images at a resolution of 5 million pixels per scan. The samples were coated in talcum powder (nonreactive with the ABS plastic) to reduce the reflectivity of the sample surfaces and provide a more accurate scan. The talcum powder grain size is ≈ 10 µm in diameter, and will have little effect on the measurements made by the scanner.

The software package for the ATOS scanner uses the stereoscopic images to capture the fringe pattern sent out from the central LED projector contained in the scanner. The software triangulates all of the surface data (using the grayscale pixels, black and white contrast from the fringe pattern) to determine the shape of the geometry. Through this process, the software generates a complete 3D model of the object being scanned. The software also provides real-time feedback to show missing surface data anywhere on the object. The missing data will be captured in subsequent scans to ensure all sides of the object are represented. The software package also has the capability to compare the model of the object generated from the scans with the original CAD model from which the print was made. This analysis reveals deviations between the nominal CAD geometry and the as-printed part. The structured light scanning analysis was performed in June and July of 2015. The data from this analysis are discussed in section 6.

2.2.4 Radiographic Testing and Computed Tomography

Three-dimensional computed tomography (3D-CT) scans of the mechanical test specimens were conducted in parallel with structured light scanning. The purpose of this analysis was to image and characterize any internal structures or material deficiencies that could affect mechanical properties. Samples were imaged using a Phoenix Nanome|x 160. To perform 3D-CT, 2D images were acquired through a 360° rotational axis; successive 2D images of the specimen (which is fixtured in the scan chamber and rotated 360°) were stitched together to construct a 3D image. Depending on the sample's geometry, resolutions as low as 8–10 µm are possible.

Two-dimensional oblique x-rays of all specimens were taken using this same instrument. The computer numerical controlled table for x-rays is calibrated to a measurement accuracy in the z-axis of 5 µm. The system has a detail detectability as low as 0.4 µm in 2D mode. Results of this testing appear in section 4.

2.2.5 Mechanical Testing

Mechanical testing commenced in August 2015 after the nondestructive evaluations (NDEs) in sections 2.2.1–2.2.4 were complete. Tensile tests followed a standard method defined in American Society of Materials Testing (ASTM) D638 and measured the tensile strength, yield strength, elastic modulus, and fracture elongation of the printed material.[5] A type I specimen would generally be chosen for this application due to the reduced stress concentration at the fillet, but the dimensions prescribed by the ASTM standard were almost too large for the printer build volume to accommodate. This limitation drove the alternate choice of the type IV specimen. The flexural test, per ASTM D790, provided the flexural stress and modulus of the printed samples.[6] The compression test, ASTM D695, was used to determine the characteristic compressive stress and modulus of the specimens.[7] Mechanical testing was completed in September 2015 and is summarized in section 3.

2.2.6 Optical Microscopy and Scanning Electron Microscopy

Optical microscope images of all specimens were taken using a Keyence VR-3200. These images reveal structural details on the surface of the parts as well as layers and regions damaged by removal from the build tray. Interlaminar regions were examined to ascertain if there was a significant difference in layer thickness for flight and ground specimens. Defects or anomalies noted in previous phases of testing were examined closely. Fracture surfaces of mechanical test coupons were also evaluated using this technique. Optical microscopy of the phase I prints was completed in September 2015 and is discussed in section 5.

Per the original test plan, scanning electron microscopy (SEM) was slated to be performed on the mechanical test coupons as well as some selected specimens using a Hitachi S-3700N instrument. Uncoated samples were to be imaged using secondary electrons in a low vacuum mode to investigate morphology and surface topography, particularly in areas of delamination. Fracture surfaces from mechanical testing and areas with evidence of over-adherence to the print tray represent key regions for evaluation. This work has not been executed at the time of this writing, but will be part of a follow-on analysis for 3DP phase I.

The overall test plan for the ground and flight specimens is summarized in table 3. Specimens which will undergo SEM are the calibration coupons, tensile specimens (fracture surfaces and paddle sections), layer quality specimens, and flexure specimens.

Table 3. Summary of specimens and tests.

Sample Name	Photographic/ Visual Inspection	Measure Mass, Calculate Density	Structured Light Scanning	Computed Tomography Scan	Mechanical Testing (ASTM Standard)	Optical
Calibration coupon	X	X	X	X		X
Extruder head casing	X	X	X			
Layer quality test specimen	X	X	X	X		X
Tensile coupon	X	X	X	X	D638	X
Compression coupon	X	X	X	X	D695	X
Flexural coupon	X	X	X	X	D790	X
Negative range coupon	X	X	X			X
Torque tool specimen	X	X	X	X		
Crowfoot specimen	X	X	X			
Structural clip component	X	X	X			
Positive range coupon	X	X	X			X
Sample container	X	X	X	X		
Microgravity structure specimen 1	X	X	X	X		X
Wire tie	X	X	X			X
Ratchet	X	X	X	X		X

The overall objectives of these tests are as follows:

- Determine whether operational capability of the printer is impacted by microgravity.
- Assess effect of microgravity on the FDM process, specifically through evaluation of material properties of parts produced via FDM in this environment.
- Characterize printer performance.

Analysis of the test results and comparison of the flight and ground prints and print trays using the methods discussed previously appear in subsequent sections of this TP. Lessons learned from the phase I print specimens (sec. 8) will inform requirements for the design of next generation space-based polymeric 3D printers.

2.3 Discussion and Additional Notes

Test plans for specimens from 3DP phase I were carefully developed to provide sufficient information to make a comparative evaluation of differences between flight and ground specimens and assess any engineering-significant microgravity effects on the FDM process. For future utilization of 3DP, test plans will be necessary to validate the performance of the part in its intended use environment and will be key to V&V activities required to certify designs and parts for usage (and subsequent inclusion in the utilization catalog, a library of preapproved parts for printing on ISS).

The anisotropy of materials produced via FDM, as well as the high specificity of the as-manufactured part to processing variables (in particular filament layup/orientation), present materials characterization challenges that are very analogous to those faced by the composites and welding communities. The possibility of testing to composite standards rather than the standards for plastics was a key point of discussion in test plan development. While additively manufactured ABS, Ultem™, etc. are anisotropic plastics, the directional dependence of the properties of these materials should not drive ISM practitioners to evaluate them using standards written specifically for composites. This philosophy is reflected in a National Institute of Standards and Technology (NIST) document that surveys material testing standards for polymeric materials; "Materials Testing Standards for Additive Manufacturing of Polymer Materials: State of the Art and Standards Applicability" summarizes established International Organization for Standardization and ASTM standards for materials testing of polymers and assesses their applicability to additively manufactured plastics.[8] In most cases, NIST recommends against testing to standards for polymer matrix composite, carbon fiber reinforced plastic, and similar classes of materials. The overall recommendation for polymers produced using additive manufacturing techniques is to apply standards for plastics with guidance (guidance in this context may mean using test specimens of different dimensions from those indicated in the standard, testing at elevated temperatures or in immersive environments, and careful consideration and characterization of anisotropy). The overall consensus from this document and from discussions which took place during the first TIM are that the ISM team should generally use standards for plastics when testing FDM-produced specimens, but modifications to the standard may be necessary.[4,8] The ISM team's current approach is to remain flexible with regard to standards implementation. At this stage in material property development activities, it is more important to test consistently and document test procedures than to follow standards that, as written, may not be best suited for the materials being evaluated. Development of standards and which existing standards are appropriate for additive manufacturing is an ongoing area of debate in the broader additive manufacturing community. There is an ASTM committee (F42) as well as a NIST group tasked with looking at these specific issues in more detail.[9] The ISM team is aware of the activities of these groups and will incorporate their recommendations for best practices as they evolve.

It is important to critically examine the test plan for the 3DP technology demonstration mission since testing and evaluation (T&E) of subsequent specimens from 3DP will likely follow a similar process flow. V&V activities for candidate parts to be included in the utilization catalog will also draw extensively from this plan. The objective of the testing for the ground and flight specimens is to characterize differences between specimens based on build environment and determine which of these differences are attributable to microgravity effects on the manufacturing process. In executing the phase I test plan, each print underwent visual and photographic inspection, mass measurement,

structured light scanning (to characterize dimensional variations between nominal CAD geometry and the as-built specimen), density evaluation (derived from mass measurements and volume calculation from structured light scanning), CT and radiographic testing (RT) (to evaluate internal geometry/layer adhesion), mechanical testing (tensile, flexural, and compression), and optical microscopy. The decision was made to limit CT evaluation to mechanical specimens with the aim of establishing linkages between any unexpected failures in destructive testing and internal material flaws. Optical microscopy was performed on fracture surfaces, but future SEM evaluation is needed to provide additional insight into failure mechanisms. While there are no major deficiencies in the phase I test plan, additional analysis of phase I specimens will be required to answer some of the open questions discussed in subsequent sections of this TP. Future 3DP specimens and functional parts with more clearly defined use scenarios, applications, and environments may also require additional tests and inspections that are not represented in the 3DP phase I test regime.

One ancillary test initiative of note is a currently funded effort at MSFC to conduct space environment effects testing for ABS plastic produced via FDM. Mechanical and ballistic impact testing of specimens exposed to the space environment in low-Earth orbit (LEO) using a space station exposure facility will assess the degree to which LEO levels of atomic oxygen (AO) and ultraviolet (UV) radiation degrade material performance. Atomic oxygen typically has a severe degradative effect on polymeric materials unless their chemical structure is modified or a coating is applied to mitigate the erosion processes initiated by AO.[10]

3. MECHANICAL TEST DATA AND DENSITY COMPARISONS

The objective of this phase of testing was to ascertain whether operation of the FDM process in microgravity has any engineering-significant impact on material quality and performance by comparing densification and mechanical properties for the ground and flight specimens.

3.1 Summary of Results of Density Comparison

Following receipt and unboxing of the flight specimens from the 3DP phase I prints at MSFC in April 2015, ground and flight specimens were weighed in the precision metrology laboratory at MSFC. Each specimen was weighed five times using a calibrated laboratory scale (Mettler analytical balance) with a capacity of 261 g and a resolution of 1×10^{-5} g. The weighing pan was enclosed in an isolation chamber. Specimen weights are summarized in table 4. They range from 0.6 g (microgravity structure specimen) to $\approx$16 g (ratchet). These measurements were used to obtain a characteristic value for the mean weight of each specimen. Uncertainty in the reported values was generally on the order of 10^{-5}.

Table 4. Average weights of 3DP specimens.

Sample Description	Sample ID	Average Mass (g)
Calibration coupon	G001	1.429
	F001A	1.363
	F001B	1.433
	F001C	1.414
	F001D	1.465
	F001E	1.405
Extruder plate	G002	7.127
	F002	6.548
Layer quality specimen	G003	2.606
	F003	2.652
Tensile 1	G004	5.013
	F004	4.942
Compression 1	G005	2.983
	F005	2.797
Flexure 1	G006	2.817
	F006	2.888
Negative range specimen	G007A	4.725
	G007B	4.760
	F007	4.680

Table 4. Average weights of 3DP specimens (Continued).

Sample Description	Sample ID	Average Mass (g)
Torque coupon	G008	10.514
	F008	10.404
Crowfoot	G009	6.815
	F009	6.777
Structural clip	G010	1.319
	F010	1.328
Positive range specimen	G011	4.113
	F011	4.106
Tensile 2	G012	5.014
	F012	5.006
Compression 2	G013	2.934
	F013	2.841
Flexure 2	G014	2.793
	F014	2.885
Tensile 3	G015	5.035
	F015	4.982
Compression 3	G016	2.884
	F016	2.788
Flexure 3	G017	2.934
	F017	2.971
Tensile 4	G018	5.017
	F018	4.870
Microgravity structure specimen	G019	0.602
	F019	0.631
Sample container (container)	G020A	9.010
	F020A	8.959
Sample container (lid)	G020B	4.532
	F020B	4.471
Wire tie	G021	1.391
Ratchet	F021	16.613

*Piece of flight extruder plate peeled off during removal from build tray.

The gravimetric density ρ was subsequently calculated for each specimen by dividing the mean mass value by the corresponding volume obtained from structured light scanning (sec. 6). The scanner has an accuracy of ±12.7 µm at the scale of the 3DP specimens. Point cloud data from the structured light scan are imported into a software program, Geomagic® Control™. Surface fill operations allow the user to create a complete surface and execute a volume calculation. This volume is representative of the as-built part and not the CAD geometry. The surface fill algorithm creates high-quality surfaces that are representative of the part geometry and is a standard procedure for structured light scanning to fill in data that are missed/not captured by the scan. Reported volumes for the specimen are tabulated in table 5 and range from 0.7 cm³ (microgravity structure specimen) to 35 cm³ (ratchet). Since the volumes represent a single calculation based on structured light scan data rather than repeated measurements, an uncertainty value is not reported.

Table 5. Volume measurements for 3DP specimens.

Sample Description	Sample ID	Volume (cm³)
Calibration coupon	G001	2.86
	F001A	2.48
	F001B	2.80
	F001C	2.82
	F001D	2.77
	F001E	2.79
Extruder plate*	G002	–
	F002	–
Layer quality specimen	G003	2.91
	F003	2.89
Tensile 1	G004	5.48
	F004	5.26
Compression 1	G005	3.13
	F005	3.05
Flexure 1	G006	3.12
	F006	3.05
Negative range specimen	G007A	5.33
	G007B	5.33
	F007	5.17
Torque coupon	G008	11.56
	F008	11.37
Crowfoot	G009	7.37
	F009	7.24
Structural clip	G010	1.46
	F010	1.47
Positive range specimen	G011	4.67
	F011	4.40

18

Table 5. Volume measurements for 3DP specimens (Continued).

Sample Description	Sample ID	Volume (cm^3)
Tensile 2	G012	5.60
	F012	5.35
Compression 2	G013	3.11
	F013	3.07
Flexure 2	G014	3.14
	F014	2.99
Tensile 3	G015	5.60
	F015	5.33
Compression 3	G016	3.12
	F016	3.08
Flexure 3	G017	3.14
	F017	3.08
Tensile 4	G018	5.52
	F018	5.20
Microgravity structure specimen**	G019	–
	F019	–
Sample container (container)	G020A	9.96
	F020A	9.82
Sample container (lid)	G020B	4.86
	F020B	4.83
Wire tie	G021	1.56
Ratchet	F021	35.30

*Structured light scanning had difficulty capturing point cloud data for the extruder specimens in the area around the lettering. Flight extruder plate also broke off during removal from print tray. Density was not calculated for these specimens in light of the likely significant discrepancy between actual and measured specimen volume.

**Microgravity structure specimen was also missing some point data. Confidence in the calculated volume is insufficient to derive a density value based on it.

Where appropriate, the density of each flight specimen was compared directly against its respective ground sample. In cases where multiple specimens of identical geometry were produced (tensile, flexure, and compression), comparative evaluation was done for the pooled specimen sets (e.g., mean density of ground tensile specimens versus mean density of flight tensile specimens). The mean density comparisons for the ground and flight specimens appear in table 6.

Table 6. Gravimetric density comparisons for 3DP ground and flight specimens.

Specimen ID(s)	Specimen Description	Average Density of Ground Specimen (g/cc)	Average Density of Flight Specimen (g/cc)	Percent Difference (With Ground as Reference)
G001, F001A–E	Calibration coupon	0.50	0.52	3.6
G003, F003	Layer quality specimen	0.89	0.92	2.7
G004, G012, G015, G018, F004, F012, F015, F018	Tensile coupons (pooled)*	0.90	0.93	3.4
G005, G013, G016, F005, F013, F016	Compression coupons (pooled)*	0.94	0.91	–2.7
G006, G014, G017, F006, F014, F017	Flexure coupons (pooled)*	0.91	0.96	5.4
G007A, G007B, F007	Negative range specimen	0.89	0.90	1.7
G008, F008	Torque coupon	0.91	0.91	0.6
G009, F009	Crowfoot	0.92	0.93	1.3
G010, F010	Structural clip	0.90	0.90	0.2
G011, F011	Positive range specimen	0.88	0.93	5.6
G020A	Sample container (container)	0.90	0.91	0.9
F021	Ratchet	–	0.47**	–
G021	Wire tie	0.89***	–	–

  *Since the data for the individual mechanical test coupons are not paired, the density comparison is based on the pooled (average) density value
    for the complete set of ground or flight tensile, compression, and flexure specimens.
  ** Flight specimen only.
  ***Ground specimen only.

Density values represent gravimetric (classical) density and do not provide any information about density variations/gradients within the part or porosity. Another density measurement for mechanical test specimens was obtained from CT data (see sec. 4), but a conversion factor between 'mean CT' and gravimetric density for ABS produced via FDM has not been developed for this material.

The following trends and observations related to the comparative evaluation of density were noted:

- Ground and flight specimens exhibit statistically significant differences (based on a t-test with $\alpha = 0.05$) in gravimetric density.

- In all but two cases (pooled flexure and positive range coupon), the percent difference in mean or median densities for the ground and flight specimens is <5%. In all cases, the percent difference in density is <10%.

- In general, flight specimens are slightly denser than ground specimens. Exceptions are the three compression coupons and the positive range specimen (in these cases, the ground specimens have a greater gravimetric density than the flight specimens).

- The densest specimens are the three flight flexure coupons. These specimens are, on average, 6.5% more dense than the analogous ground specimens.

- Density of injection-molded ABS plastic is reported as 1.046 g/cm^3. The density of the vast majority of specimens expressed as a percentage of the theoretical density thus falls in the 84% to 92% range.

- As expected, the calibration coupons and the ratchet (which have a lower infill percentage) have much smaller density values (approximately 50% and 45% of theoretical density, respectively) than the rest of the dataset.

Mechanical test specimens merit closer evaluation since material consolidation is closely linked to mechanical strength and performance. Comparison of the pooled tensile, flexure, and compression data shows that the tensile and flexure flight specimens are more dense than the analogous ground specimens. The opposite (ground specimens are more dense than flight specimens) is true for the compression specimens. Overall, the densities for mechanical test specimens seem to represent two different families of data. Density differences for mechanical test coupons are summarized in figures 2–4 and in table 7. Note that the *y*-axis scale for the bar charts does not start at the origin.
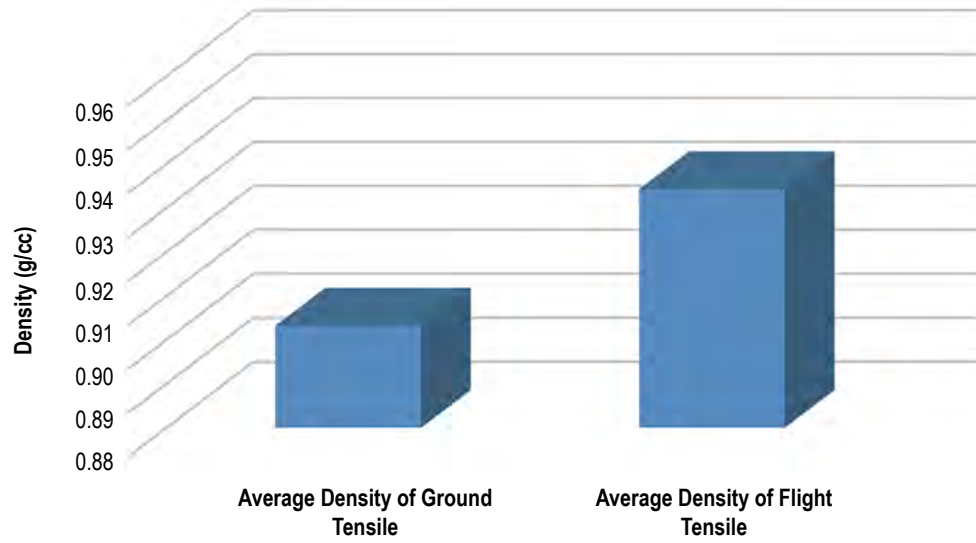
Figure 2. Comparison of average density of flight and ground tensile specimens.
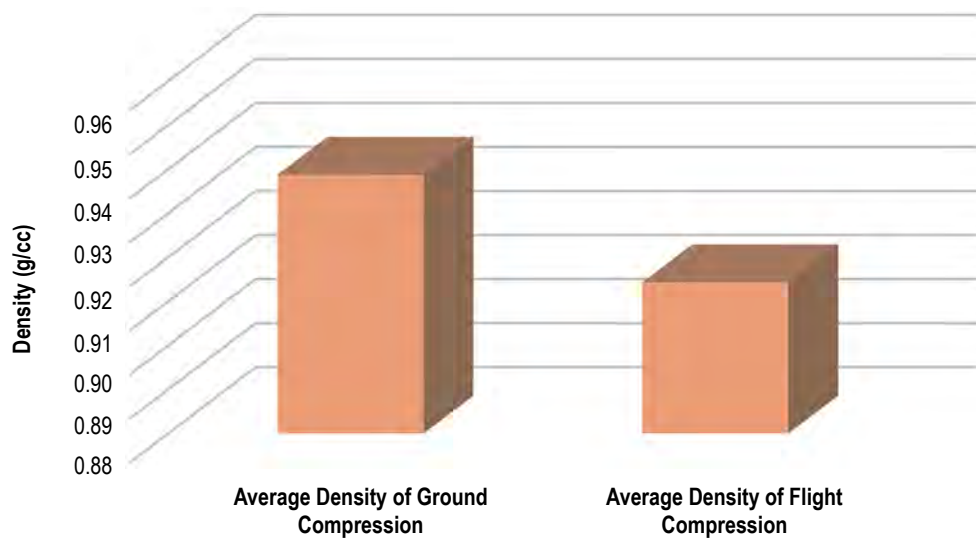
Figure 3. Comparison of average density of flight and ground compression specimens.
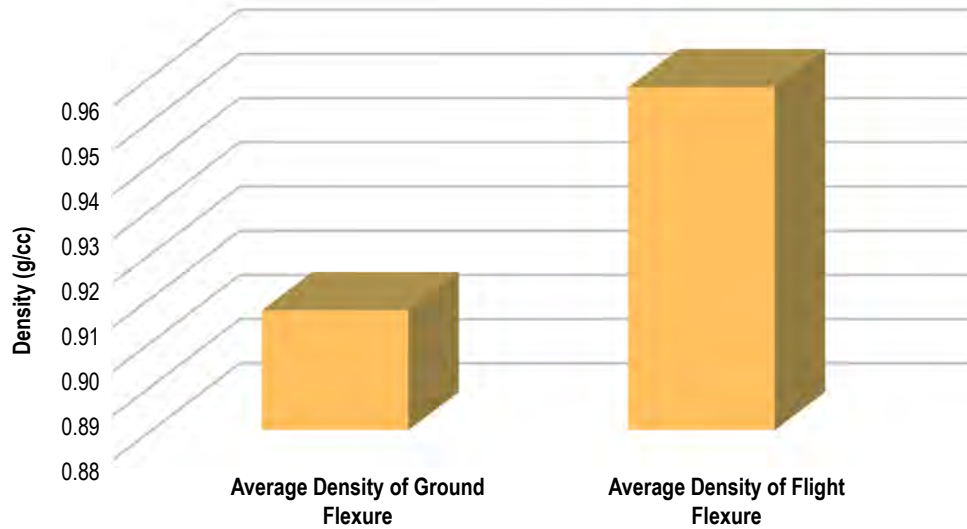
Figure 4. Comparison of average density for ground and flight flexure specimens.

Table 7. Summary of density differences for ground and flight mechanical test specimens.

Specimen Type	Percent Difference (With Ground as Reference)
Tensile	3.43
Compression	–2.60
Flexure	5.55

3.2 Summary of Results of Mechanical Testing

Flight and ground mechanical test coupons from phase I of the 3DP technology demonstration were evaluated using the capabilities of the Mechanical Testing Laboratory at MSFC. The purpose of this portion of the testing was to assess the effect of microgravity on the FDM process, specifically through comparative evaluation of material properties of specimens produced via FDM in the microgravity environment with terrestrially manufactured counterpart specimens. Table 8 summarizes the type and quantity of specimens tested.

Table 8. Summary of mechanical test specimens.

Specimen ID(s)	Specimen Description	Number of Specimens
G004, G012, G015, G018	Ground tensile coupons	4
F004, F012, F015, F018	Flight tensile coupons	4
G005, G013, G016	Ground compression coupons	3
F005, F013, F016	Flight compression coupons	3
G006, G014, G017	Ground flexure coupons	3
F006, F014, F017	Flight flexure coupons	3

3.2.1 Results of Tensile Tests

Mechanical Test Facility personnel performed eight tensile tests (four flight and four ground specimens) on ABS plastic 'dogbone' specimens under ambient (75 °F, 0 psig) conditions. Nominal dimensions for the tensile specimens were based on type IV specimens in ASTM D638-10.[5] Width of the reduced section was 0.25 in with a length of 1.3 in and a thickness of 0.13 in. A 1-in gauge length extensometer, calibrated per the B-2 classification for determining modulus of elasticity, measured tensile strain up to 100%. Tensile specimens were preloaded to a minimum of 1 lbf at 0.05 in/min, then pulled at a failure rate of 0.2 in/min. All of the equipment used during these tests was calibrated per applicable ASTM standards.

Data derived from each tensile test include:

- Ultimate tensile strength (σ_{uts}) is the load at fracture divided by the original cross-sectional area of the test specimen.

- Yield strength (σ_{ys}) is the point at which the material begins to deform plastically (per ASTM D638-10, the "first point on the stress-strain curve at which an increase in strain occurs without an increase in stress"[5]).
  – Some classes of materials exhibit behavior that makes it difficult to determine the yield stress. In these cases, yield stress may be defined as the stress that coincides with some specific amount of plastic deformation (e.g., 0.2% of the stressed length).
  – For the 3DP specimens, no yield is reported because the maximum and yield stresses are virtually coincident for ABS plastic.
- Modulus of elasticity (E) is the ratio of tensile stress to tensile strain (the slope of the line that represents the linear elastic portion of the stress-strain curve).

- Fracture elongation (%) is the ratio of the initial length of the specimen to the change in the length of the specimen measured following fracture. Elongation to failure is a measure of ductility.

An overlay of the stress-strain curves for the ground and flight tensile specimens is shown in figure 5. Table 9 provides a tabular summary of key material properties for each specimen obtained from its respective tensile test.
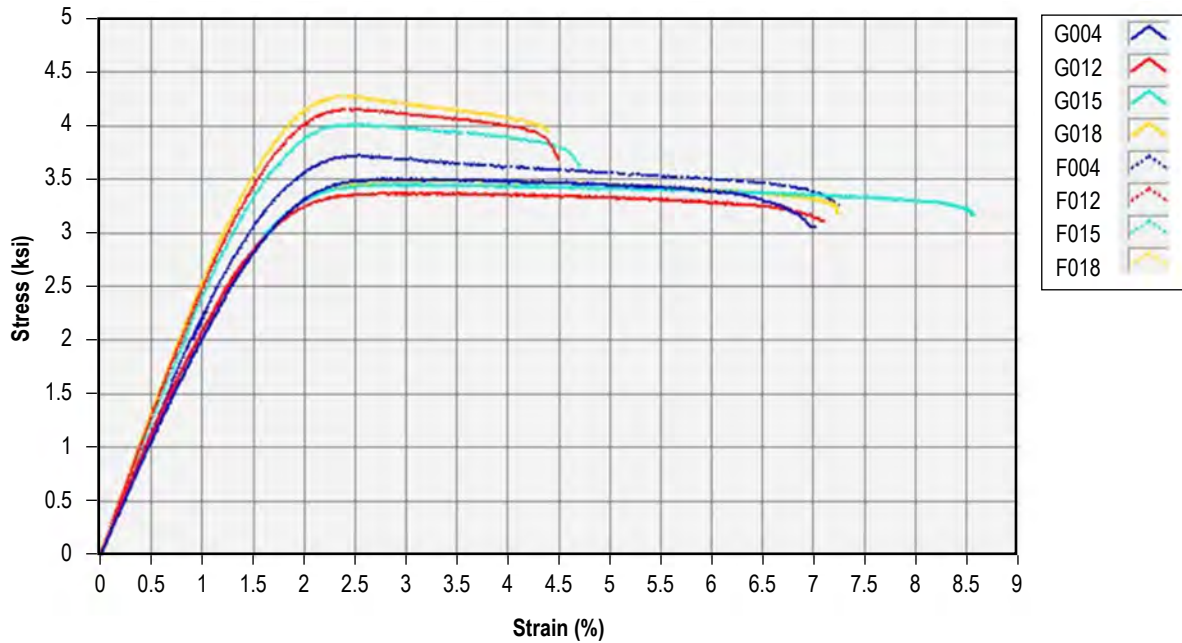
Figure 5. Stress-strain curves for ground and flight tensile specimens plotted on the same axis.

Table 9. Summary of tensile test data.

Specimen ID	Ultimate Tensile Strength (ksi)	Modulus of Elasticity (msi)	Fracture Elongation (%)
G004*	3.51	0.21	7.00
G012*	3.38	0.22	7.10
G015*	3.46	0.22	8.58
G018	3.49	0.21	7.24
F004	3.72	0.23	7.26
F012*	4.16	0.26	4.50
F015*	4.02	0.24	4.70
F018*	4.28	0.26	4.39

*Failure outside the extensometer footprint.

The comparison of material properties obtained from tensile test data from ground and flight is summarized in table 10. On average, the ultimate tensile strength of the flight specimens is 17% greater than the values measured for the ground specimens. The modulus of elasticity for flight specimens is 15% greater than the ground specimen group. The flight specimens, however, have a much lower elongation to failure than the ground specimens.

Table 10. Comparison of tensile test data for ground and flight specimens.

Property	Mean of Ground Specimens	Coefficient of Variation (%)	Mean of Flight Specimens	Coefficient of Variation (%)	Percent Difference (With Ground as Reference)
Ultimate tensile strength (ksi)	3.46	1.7	4.05	6.0	17.1
Modulus of elasticity (msi)	0.22	2.7	0.25	6.1	15.4
Fracture elongation (%)	7.48	9.9	5.21	26.3	−30.4

Comparative evaluation of tensile curves for ground and flight reveals distinct behavior for the specimen classes. While the flight specimens fail at a higher load and have a greater elastic modulus (indications that they are stronger and stiffer than the ground specimens), the percent elongation to failure for flight specimens is approximately 30%–40% less than that of the ground specimens (although some decrease in ductility is expected to accompany an increase in strength). Whether the apparent bias toward increased strength and reduced ductility is a concern will depend on the applications of the parts produced using the 3DP capability. Activities to anchor predictions of structural models with results of instrumented testing for functional parts will provide further insight into what strength and ductility is needed to ensure adequate performance of functional parts.

An important note is that several tensile specimens broke outside the extensometer footprint (see sec. 5 on optical microscopy for images tensile breaks). This was the case for the ground specimens G004, G012, and G015, as well as the flight specimens F012, F015, and F018. Breakage outside the extensometer footprint may not invalidate data if strength values are in family with other specimens in the dataset or results of additional testing. Fracture at this location is common in composites and has been observed extensively in other ground-based material characterization work for ABS. The choice of specimen design may contribute to fracture since the fillet creates a stress concentration and potential initiation point for material failure. Fracture outside the extensometer footprint does not necessarily correspond to reduced fracture elongation.

Minor extensometer slippage was also noted during testing of flight tensile specimens F012 and F018. This is corrected for by shifting the stress-strain curve so that the linear approximation of modulus passes through the origin. For F012, the curve was shifted by 0.024%, and for F018, the curve was shifted 0.019%.

3.2.2 Results of Compression Tests

Mechanical Test Facility personnel performed six compression tests (three ground specimens and three flight specimens) on ABS plastic cylinders (dimensions 0.5 in diameter by 1 in long) under ambient (75 °F, 0 psig) conditions. Nominal dimensions for the tensile specimens were based on type IV specimens in ASTM D695-10.[7] Specimens were placed between the platens of a 'birdcage' compression fixture and pulled in tension to create a compressive load on the specimen. A 1-in gauge length extensometer, calibrated to the required B-2 classification for estimating modulus of elasticity, was chosen to measure compressive strain up to 100%. Material properties based on 20% compressive strain are reported. Specimens were tested until reaching a local maximum or at least 80% compressive strain (whichever occurred first). All of the equipment used during these tests was calibrated per applicable ASTM standards.

Properties derived from the compression test include:

- Maximum stress ($\sigma_{max,20\%}$) (ksi) is the value of compressive stress that corresponds to 20% strain.

- Yield strength (σ_{ys}) (ksi) is the point at which the material begins to deform plastically (the first point on the stress-strain curve at which an increase in strain occurs without an increase in stress).
  – Yield stress is defined as the stress that coincides with some specific amount of plastic deformation (ASTM D695-10[7] does not specify a yield offset; an offset of 0.6% of the stressed length was selected).

- Compressive modulus of elasticity (E) (msi) is the ratio of the compressive stress applied to a material to the resulting compression.

Figure 6 plots the stress-strain curves derived from the compression test (up to 20% strain) for the ground and flight compression coupons on the same axis. Table 11 provides a tabular summary of key material properties for each specimen obtained from its respective compression test.
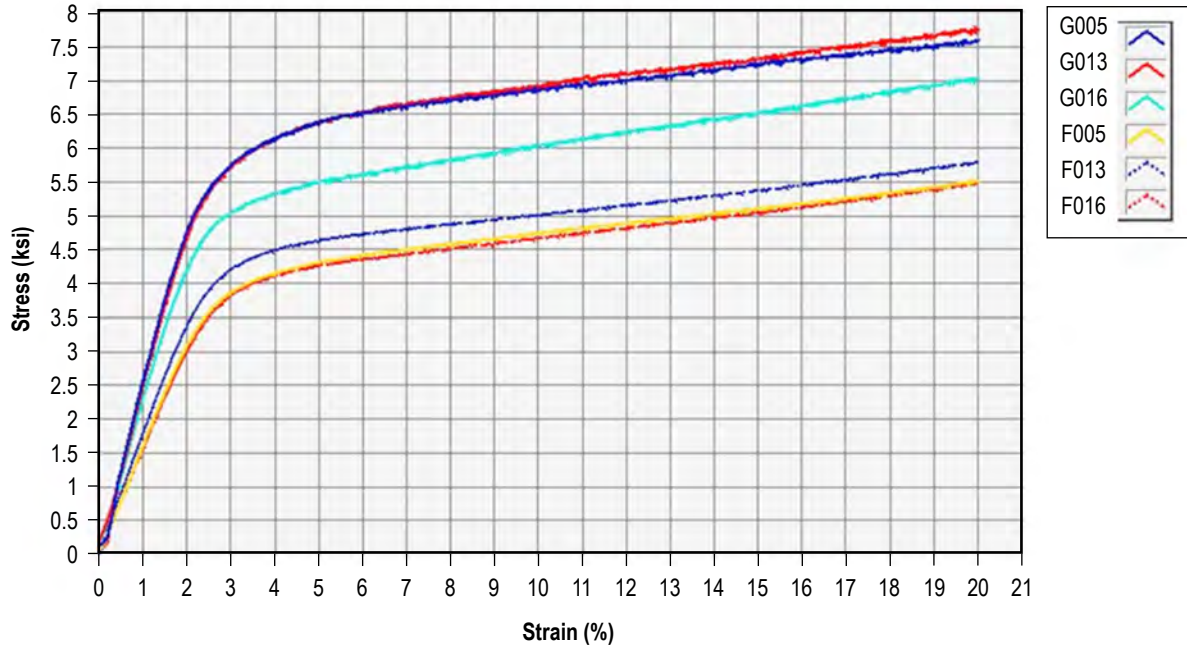
Figure 6. Stress-strain curves for ground and flight compression specimens plotted on the same axis.

Table 11. Summary of compression test data.

Specimen ID	Maximum Stress at 20% Strain (ksi)	Yield Stress (ksi)	Compressive Modulus (msi)
G005	7.58	5.67	0.25
G013	7.74	5.67	0.24
G016	7.03	4.93	0.23
F005	5.50	3.88	0.16
F013	5.78	4.19	0.18
F016	5.47	3.86	0.15

The comparison of material properties obtained from compression test data from ground and flight is summarized in table 12. In general, the flight specimens fail at a lower load and have a lower elastic modulus than the ground specimens. Comparative weakness in compression for the flight specimens may be related to their lower density. The relationship between density and mechanical properties is discussed further in section 3.3 as well as section 7 of this document.

Table 12. Comparison of compression properties for ground and flight specimens.

Property	Mean of Ground Specimens	Coefficient of Variation (%)	Mean of Flight Specimens	Coefficient of Variation (%)	Percent Difference (With Ground as Reference)
Maximum stress at 20% strain (ksi)	7.45	5.00	5.58	3.06	−25.1
Yield stress (ksi)	5.42	2.60	3.98	4.7	−36.2
Compressive modulus (msi)	0.24	4.17	0.16	9.35	−33.3

3.2.3 Results of Flexure Tests

Mechanical Test Facility personnel performed six three-point bend tests (three ground specimens and three flight specimens) under ambient (75° F, 0 psig) conditions per procedure A of ASTM D790-10.[6] Nominal dimensions for the flexure specimens were 0.4 in (width) by 0.16 in (depth). ASTM D790-10 specifies that a support span-to-depth ratio of 16:1 be used in test setup, provided "the ratio of the tensile strength to shear strength is less than 8 to 1."[6] A span of ≈2.5 in was used for these tests. The required rate of crosshead motion, per equation (1) of ASTM D790-10, for a specimen depth of 0.16 in was calculated to be 0.065 in/min. Specimens were run until failure or until ≈5% of outer surface strain was reached (whichever occurred first). None of the specimens failed within 5% outer surface strain. Flexural strength numbers are based on maximum load seen prior to test termination. All of the equipment used during these tests was calibrated per applicable ASTM standards.

Properties derived from the flexure test include:

- Flexural stress (σ_{flex}) (psi) is the stress in the material just prior to yielding during the flexure test.
- Flexural modulus (ksi) is the ratio of stress to strain in flexural deformation. The flexural modulus measures the tendency for a material to bend under load.

Figure 7 plots the stress-strain curves derived from the flexural test for the ground and flight flexure coupons on the same axis. Table 13 provides a tabular summary of key material properties for each specimen obtained from its respective flexure test.

The comparison of material properties obtained from flexural test data from ground and flight is summarized in table 14. Ultimate flexural stress and flexural modulus are, on average, approximately 20%–25% greater for the flight specimens.
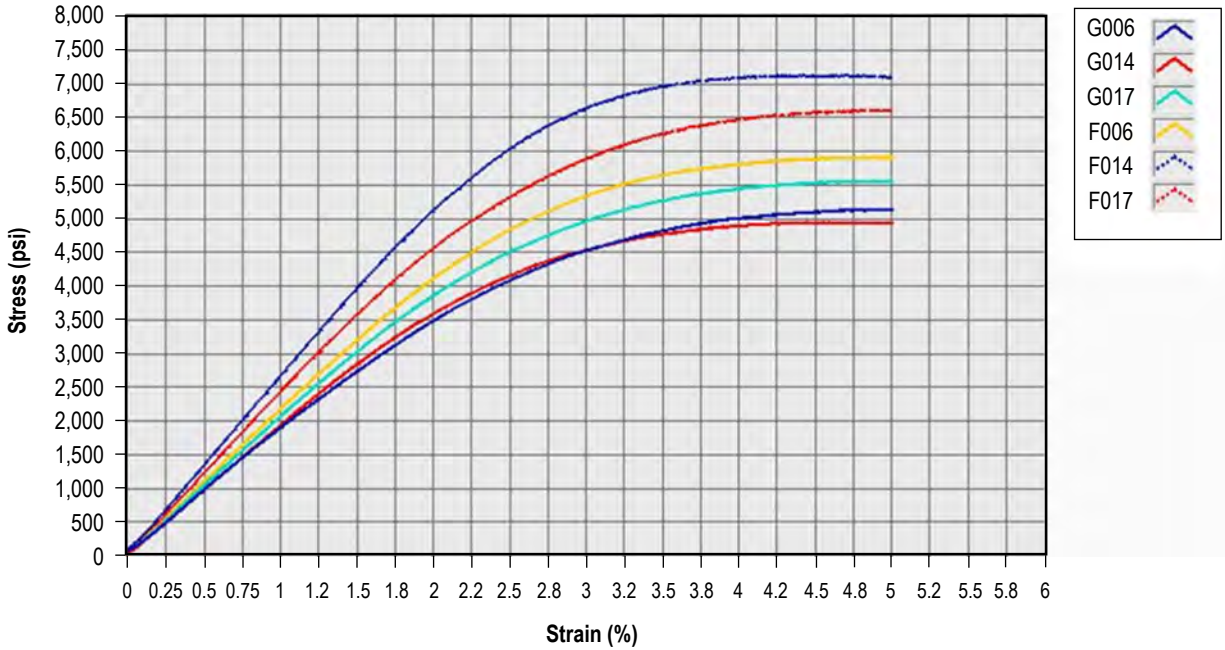
Figure 7. Stress-strain curves for ground and flight flexure specimens plotted on the same axis.

Table 13. Summary of flexure test data.

Specimen ID	Flexural Stress (psi)	Flexural Modulus (ksi)
G006	5,140	193
G014	4,940	194
G017	5,560	207
F006	5,910	218
F014	7,120	265
F017	6,600	242

Table 14. Comparison of flexural properties for ground and flight specimens.

Property	Mean of Ground Specimens	Coefficient of Variation (%)	Mean of Flight Specimens	Coefficient of Variation (%)	Percent Difference (With Ground as Reference)
Ultimate flexural stress (psi)	5,211.92	6.0	6,544.28	9.3	25.6
Flexural modulus (ksi)	197.86	3.9	241.40	9.6	22.01

3.3 Correlation Analysis: Density and Mechanical Properties

One of the key tenets of materials science is that material structure determines properties. Thus, it is not surprising that the degree of material consolidation (as measured in terms of gravimetric density) plays a key role in mechanical performance of a material. A correlation analysis was performed using the density data and the mechanical property data obtained from tensile, flexure, and compression tests to quantify the relationship between density and mechanical properties for the 3DP phase I specimens. The correlation coefficient measures the strength of linear association between two variables. Values are between –1 and 1. A positive correlation coefficient indicates that there is a direct variation between the variables; a negative correlation coefficient is associated with an inverse relationship. The R^2 value reported in table 15, known as the coefficient of determination, is the square of the correlation coefficient and indicates what proportion of the variability observed in the dependent variable can be predicted by the independent variable (in this case, density).

The results of these analyses demonstrate the trends in the density data are consistent with the trends observed in mechanical properties. A summary of coefficients of determination obtained from regression models of each mechanical property as a function of density appears in table 15. The strongest observed correlation ($R^2 = 0.88$) is between density and ultimate flexural strength. The bias of the correlation is positive; mechanical specimens with greater density are generally stronger and stiffer.

Table 15. Summary of regression analyses for density and mechanical properties.

Dependent Variable	R^2 Value for Linear Regression Model Relating Density to Dependent Variable	R^2 Value (Model With Ground Specimens Only)	R^2 Value (Model With Flight Specimens Only)
Ultimate tensile strength	0.71	0.81	0.49
Elastic modulus	0.53	0.91	0.31
Fracture elongation	0.53	0.18	0.83
Compressive strength	0.77	0.64	0.67
Compressive modulus	0.80	0.99	0.87
Ultimate flexural strength	0.88	0.999	0.80
Flexural modulus	0.79	0.83	0.75

A positive correlation between density and mechanical properties is not surprising, but the question remains as to whether subtle variations in density (differences between ground and flight specimens are generally <5%) can account for the much larger observed differences in material properties. The R^2 values for these analyses indicate that not all of the variability in the specimen property dataset is explained by variations in density. For the flexure specimens, 88% of the variability in ultimate flexural stress is explained by density variations (fig. 8). While its ability to explain variability in mechanical properties between ground and flight specimens for this dataset seems to be highly dependent on the property being measured, overall density is a reasonable predictor of mechanical performance (and as such may become a first gate metric for assessing whether a material is of acceptable quality once the relationship between density and mechanical properties is better

characterized). A sensitivity study of infill percentage (which is the build variable that can be used to control densification in the manufactured material) and resulting mechanical properties for ABS produced via FDM is needed. Even if differences in density between ground and flight specimens are sufficient to explain the differences in mechanical property data, the question remains as to what mechanism creates this density variation between ground and flight specimens in the first place. The mechanism could be microgravity effects on the FDM process, differences in operation of the hardware during the flight prints, or some other factor or combination of factors.
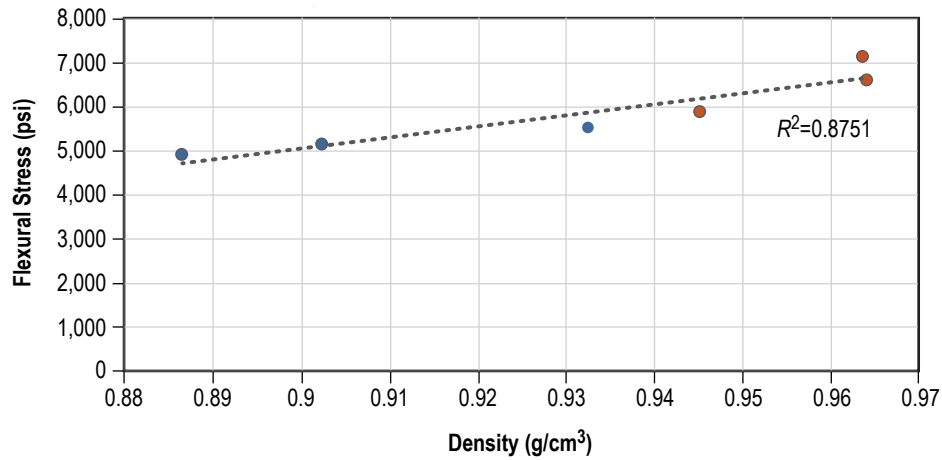
Figure 8. Regression model of density and ultimate flexural stress for ground and flight specimens.

3.4 Time Series Analysis

A time series analysis of the residuals of the mechanical property data was performed with the objective of detecting any possible changes in machine operation during the flight and ground prints that could explain variability in the dataset. This is of particular interest for the tensile specimens, where the first flight specimen printed (F004) resulted in a specimen with a stress-strain curve that more closely follows the ground specimens than the other three flight specimens.

Regression models for the combined flight and ground specimens were constructed for each mechanical property value. These models remove the effect of flight versus ground from the dataset and consider the data as a time series where the order of the print is the x-value, and the mechanical property of interest (in this case tensile strength, compressive strength, or flexural strength, depending on the specimen) is the y-value. The residuals for the regressions (defined as the difference between observed values of properties and those predicted by the regression models) were plotted on a standardized scale. These standardized (studentized) residuals contain only unexplained variability in the data. The residuals were graphed as a run chart with process control limits, and the graphs were evaluated for trends. In the case where the residual data contains only unexplained variability, no trends should be evident. Given the small size of the datasets (eight tensile specimens, six compression specimens, and six flexure specimens), the test may be too insensitive to detect problems in operation. Thus, process changes could still occur, but may be undetectable using this metric.

Figure 9 shows a process behavior chart for the ordered data. The pink line separates ground (left) from flight specimens (right), and the red bars represent upper and lower control limits. There are no obvious trends or 'pokeouts,' and the analysis does not yield any alarms based on statistical tests.
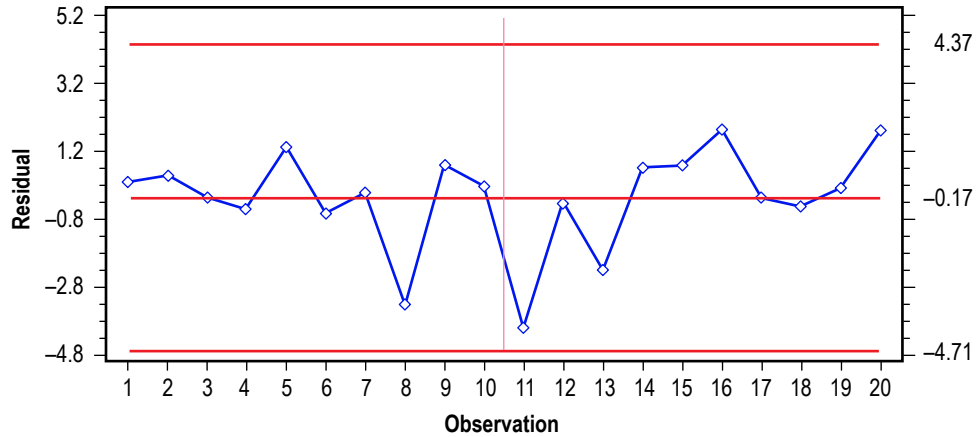
Figure 9. X chart (process behavior) for standardized residuals. Residuals from regression models predicting mechanical strengths are plotted as a function of print order. Residual analysis was restricted to mechanical test specimens.

Figure 10 shows the moving range (MR) chart for the residual analysis. This chart plots the difference between any two successive data points shown in the prior analysis (fig. 9). As with the standardized residual analysis, there are no obvious alarms and no obvious process changes detectable in the data based on the MR metric.
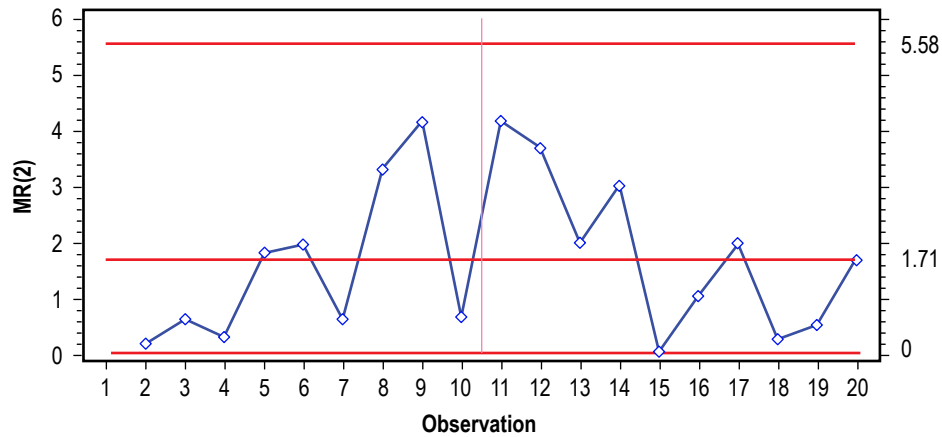
Figure 10. Moving range chart for standardized residuals analysis.

While the analyses in figures 9 and 10 do not indicate any data points that are inconsistent with nominal operating conditions for the hardware (defined based on the mean of the residuals), there are two observations which are somewhat 'unusual.' Compression specimen 3 (G016, observation 8) and tensile specimen 1 (F004, observation 11) have a standardized residual that is below –3. These specimens, while within the control limits, could skew the residuals analysis. The data were thus reanalyzed in terms of the residuals with these points removed. The standardized residuals analysis excepting compression specimen 3 and tensile specimen 1 are shown in figures 11 and 12. Both the process behavior chart and the MR chart for the reanalyzed data are unremarkable and, once again, there are no obvious process changes detectable in the data using this metric.
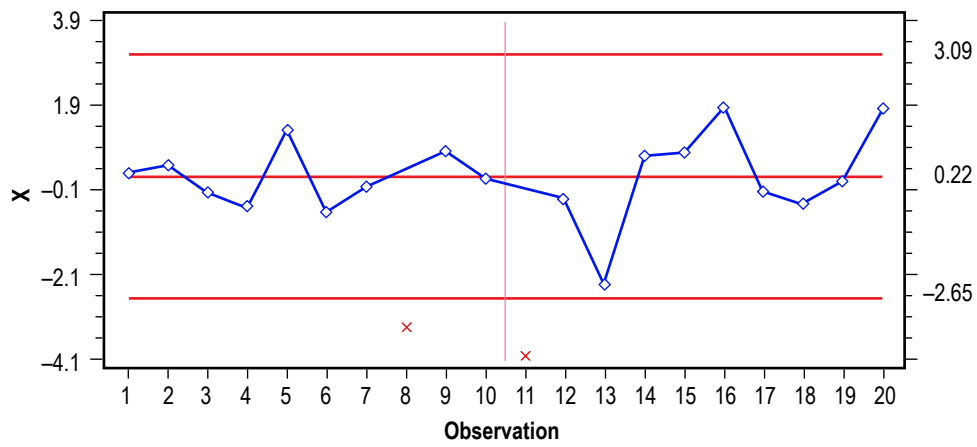
Figure 11. Residuals analysis with compression specimen 3 (denoted by red 'x' at observation 8) and flight tensile specimen 1 (denoted by a red 'x' at observation 11) removed.
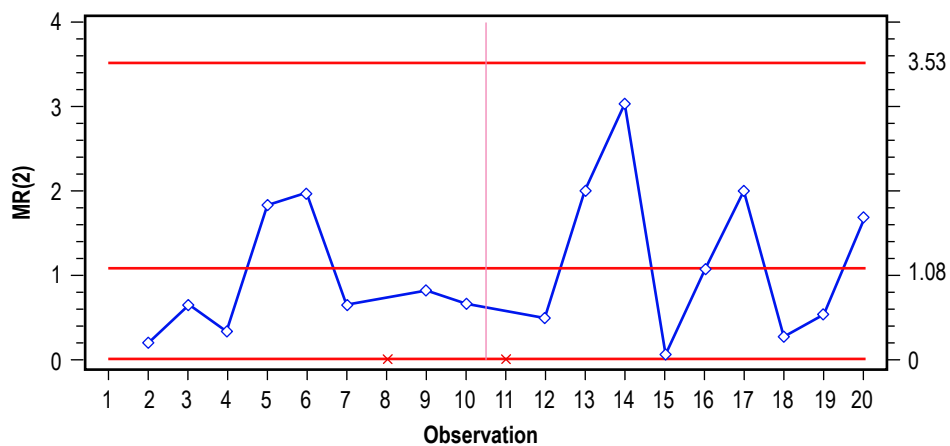
Figure 12. Moving range chart with compression specimen 3 and flight tensile specimen 1 removed.

While the overarching caveat to this analysis is that the dataset is sufficiently small enough that subtle process changes present may go undetected, overall, the analysis provides contrary evidence for hypotheses (see sec. 7) that point to abrupt changes in machine operation as an explanation for variability in the dataset. For instance, the change in the flight tensile specimen properties between specimen F004 (the first flight tensile print, which has strength and ductility in family with the ground specimens) and the three subsequent flight tensile specimens is not explained by a change in hardware operation that is detectable using this analysis technique. Residual analysis only captures operation of the machine and does not detect variation in the ordered dataset due to changes in material (either changes in chemistry due to offgassing or variation in filament diameter) or environmental conditions (humidity, temperature, etc.).

3.5 Key Findings

The analysis of the density data and the results of mechanical property testing of 3DP ground and flight specimens indicate that the two classes of specimens are significantly different (and represent two different families of data) in terms of gravimetric density, ultimate tensile strength, modulus of elasticity, fracture elongation, compressive strength, compressive modulus, flexural strength, and flexural modulus. Flight compression specimens are less dense (≈3%) than the analogous ground specimens. For tensile and flexure specimens, the flight specimens are approximately 3%–5% more dense than the ground specimens.

As expected, these trends in density closely correspond to trends in mechanical performance. Flight tensile specimens on average fail at a 17% higher load and at an elastic modulus that is ≈15% greater than the ground tensile specimens. However, the percent elongation for the flight specimens is ≈30% less than the ground specimens. Tensile specimen F004 (flight tensile 1) is more closely aligned with ground specimens in strength, modulus, and elongation than the other flight tensiles (which exhibit reduced fracture elongation). In compression, the flight specimens (which were less dense than the ground specimens) fail at 25% lower load and have a 35% lower elastic modulus relative to the ground specimens. For flexure, flight specimens have a greater flexural strength (25%) and modulus (20%) than analogous ground specimens. In general, mechanical properties for 3DP specimens are around 50% less than textbook values for injection-molded ABS. This is characteristic of ABS produced via FDM, although manufacturing process optimization can drive the material toward higher densification and better performance. For the flight and ground specimens, densities are 84%–92% of theoretical for specimens with a high infill percentage and about 50% for specimens with low infill (calibration coupons and the ratchet).

The root cause of the property variation between ground and flight specimens documented in this section is a subject of ongoing research work and may require further analysis of 3DP specimens. Aside from operation of FDM in the microgravity environment, there are a number of other variables (discussed in sec. 8) which may have contributed to these differences. Other analyses discussed in this TP (x-ray, CT, structured light scanning, and optical microscopy) provide additional insight on differences between flight and ground specimens and which hypotheses in section 7 may best explain divergence of the datasets in terms of mechanical performance. Appendix B examines the data from mechanical testing of the 3DP specimens within the context of previous ground-based material and printer characterization work undertaken by the ISM team at MSFC.

4. X-RAY AND COMPUTED TOMOGRAPHY RESULTS

4.1 Overview and Objectives

The ISM team requested that the ES43/EEE Parts Engineering and Analysis team perform 2D radiographic and 3D-CT scanning of the phase I ground and flight specimens. The system utilized for both 2D radiography and 3D-CT was a Nanome|x 160 system. The system is capable of 64,000 grayscales with a 3D-CT resolution down to 8 μm with appropriately sized samples. All flight and ground specimens underwent 2D radiography. Flight and ground mechanical coupons (tensile, flexure, and compression) were tomographically scanned. The purpose of the tomographic scanning was to identify voids and regions of possible delamination so that issues found in subsequent mechanical testing could be mapped back to any radiographic indications. In addition, the 3D-CT data were used to verify issues noted in 2D x-ray, as well as to provide a basis to delineate algorithm artifacts from true indications. This section summarizes the key findings from x-ray and CT analyses.

4.2 Two-Dimensional Radiography

All specimens were initially evaluated with 2D radiography. Figures 13 and 14 contain several examples of various specimens examined in 2D and compare the ground samples to their analogous flight samples. The radiographs of these samples were acquired at nominal accelerating voltages, currents, and imaging times typically used to image polymers such as ABS. Initially, the ISM project expressed some concerns about radiography imparting damage to the samples. However, the dosage required to damage ABS is very large and samples would have to be exposed continuously for months to impart any damage.[11] The longest time any sample was exposed to radiation during the 2D examination was 60–90 s. Subsequent to radiographic inspection and interpretation, some printing issues were identified, particularly in the area of radii and corners. The exact cause of these issues, such as platen temperature, print speeds, or software, was not evaluated at this phase of the analysis. However, issues identified are present in both the flight and ground samples, and this suggests that they are not related to microgravity effects on the FDM process. This suggests that the cause of the issue is inherent to the printing hardware or printing software and is not related to microgravity effects.
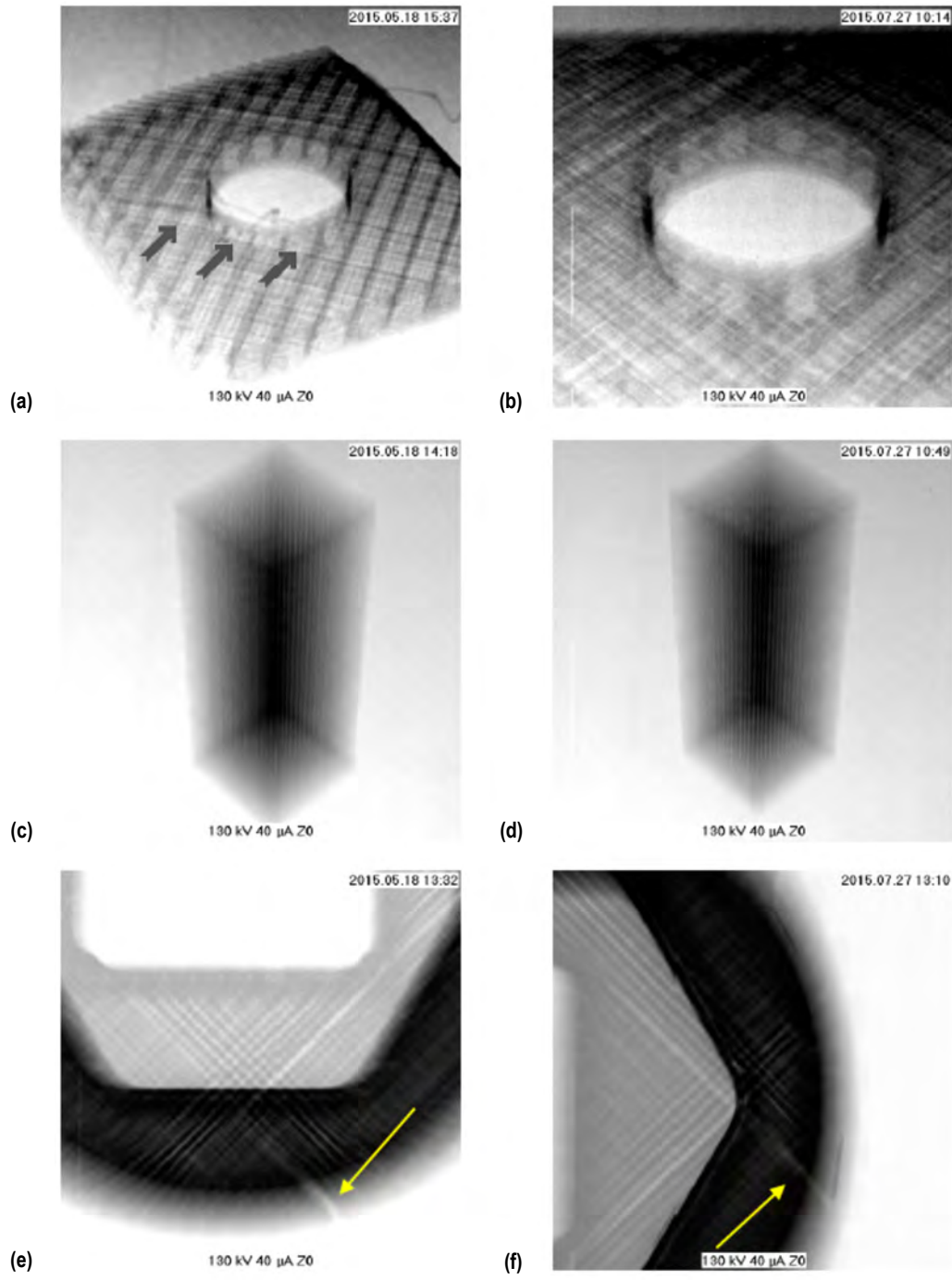
Figure 13. Radiographs showing examples of printed specimens: (a) Oblique view of a flight calibration sample. The gray arrows denote the presence of less uniform material at the hole's circumference. (b) Oblique view of a ground calibration sample. Notice in this case, the printing around the circumference is uniform. (c) Flight rectangular solid that is uniform. (d) Ground-truth rectangular solid that is also uniform. (e) Flight torque sample. There is a low-density indication present (yellow arrow). (f) Ground-truth torque sample. A similar low-density indication is present (yellow arrow).
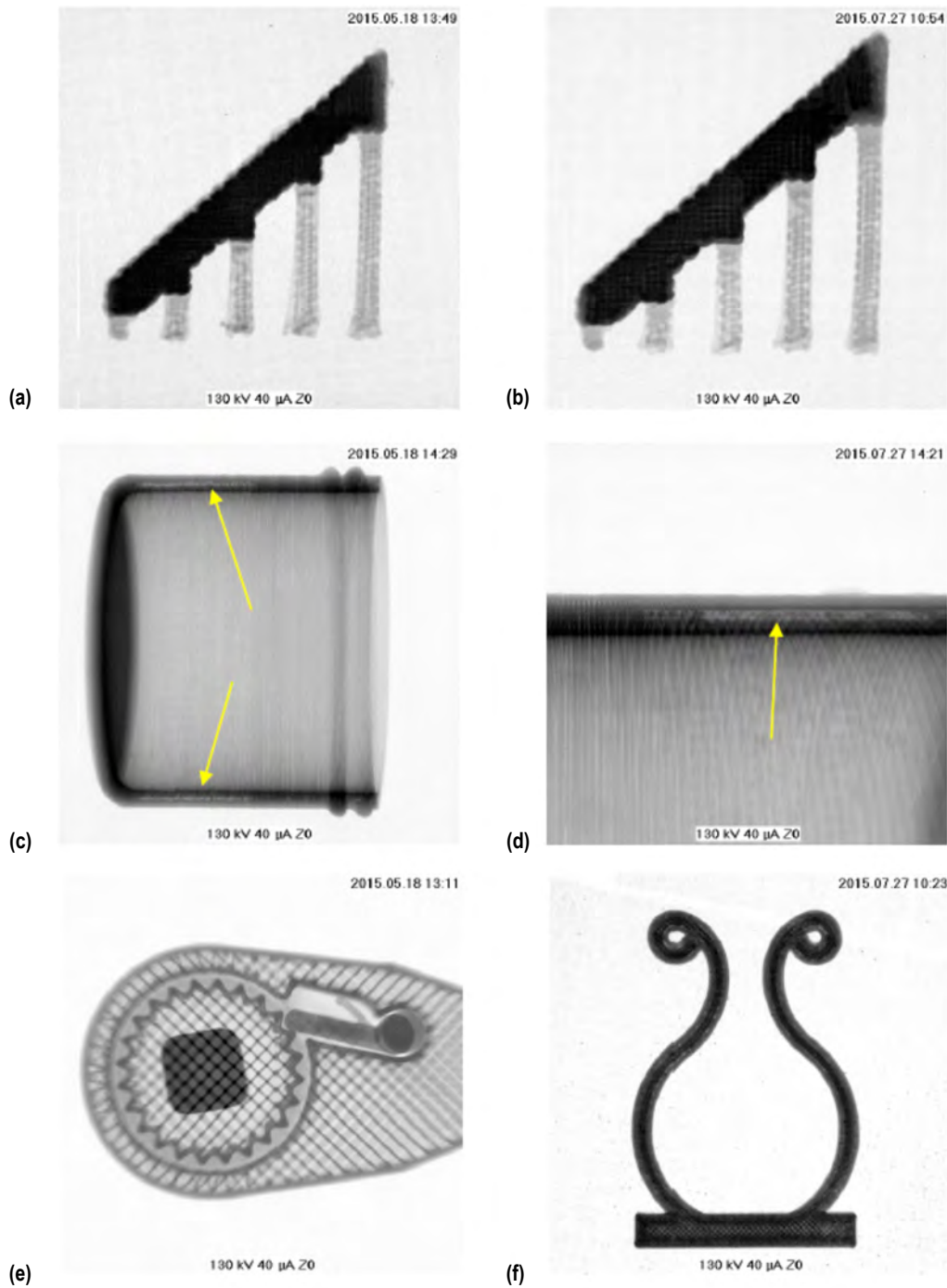
Figure 14. These radiographs show examples of printed specimens: (a) Overall view of the flight microgravity structure specimen. (b) Overall view of a ground microgravity structure sample. Both (a) and (b) are very similar. (c) Flight container that indicates lower density at the wall (yellow arrow). (d) Magnified view of a ground container that also indicates lower density at the wall (yellow arrow). Because it has occurred in both samples, this is unlikely to be a microgravity effect. (e) Mechanism of a flight ratchet. (f) The ground wire tie.

A set of tensile, compression, and flexure samples that were planned for mechanical tests were radiographed with the 2D system. This analysis was set up to facilitate identification of potential artifacts created by the 3D-CT algorithm that could be identified and ignored when analyzing the tomographs. Likewise, any anomalies identified in 2D could be verified in 3D-CT. Figures 15–17 show both flight and ground mechanical test samples. The most obvious finding from this portion of the analysis was density variations that exist in the rectangular bodies of the tensile and flexure specimens when looking along the z-axis or height. No similar variations were found when examining across the width or along the length. The z-axis density variation was typically found in ground samples as well as flight samples, which suggests that density variation was not attributable to microgravity. Indications of voids and delamination were also found, but in most cases, they were outside the area likely to fail during flexure or tensile testing. The compression samples appeared to be the most homogeneous. There were some signs of voiding just inside the outer circumference, but this was found in all flight and ground samples and extended throughout the height.
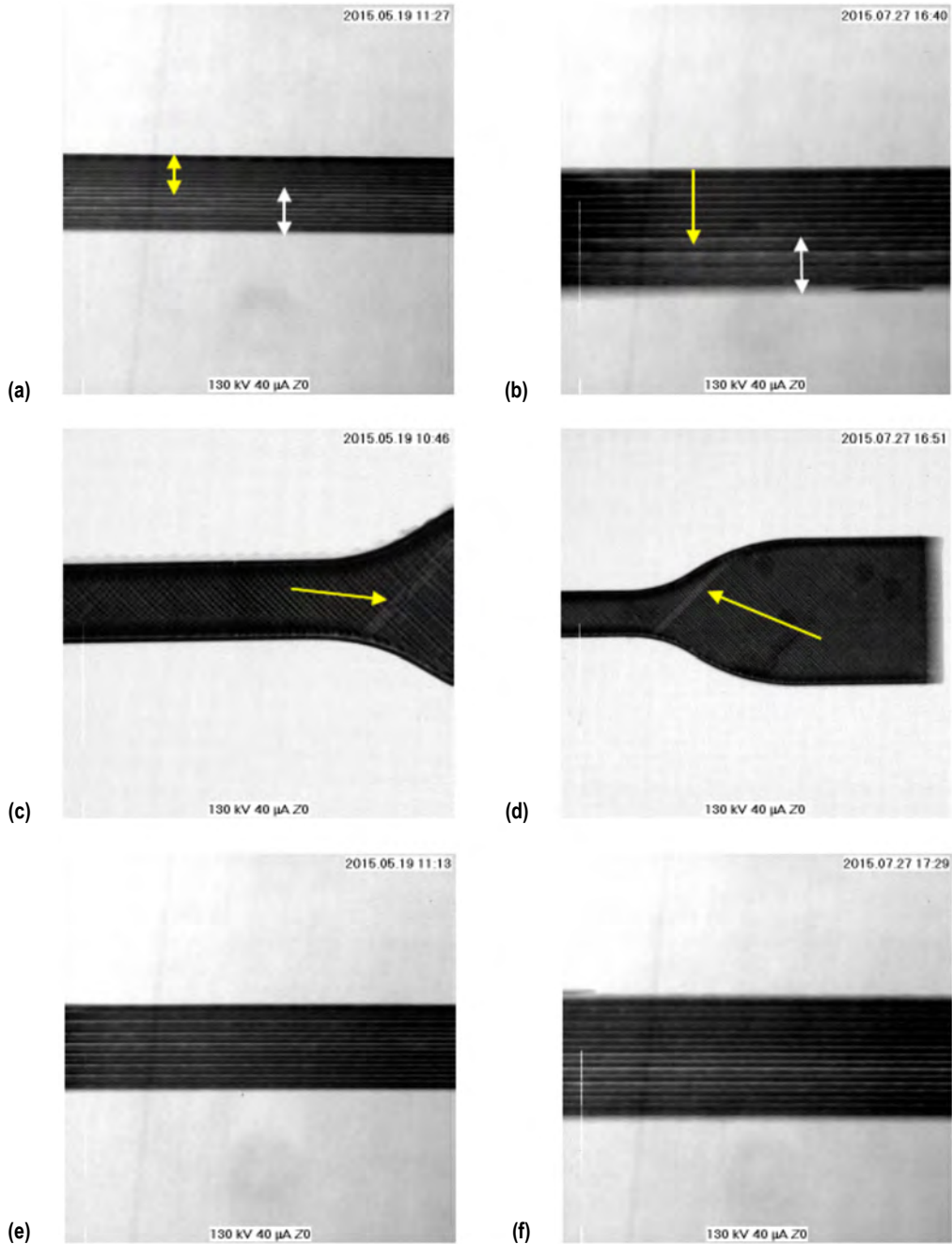
Figure 15. These radiographs show examples of tensile specimens: (a) Side view of a portion flight sample F004. There is a decrease in x-ray density from the top (yellow arrow) to the bottom (white arrow). (b) Side view of G004. The material is denser at the top (yellow arrow) than at the bottom (white arrow). (c) Portion of the flight tensile sample F012. There is a low-density indication present related to surface voiding(yellow arrow). (d) Side view of G012. The same issue in approximately the same location can be seen in the ground sample (yellow arrow). (e) Portion of the flight tensile sample F015. This image reveals a uniform x-ray density. (f) Side view of G015. The x-ray density changes from top to bottom. F018 and G018 were uniform in x-ray density.
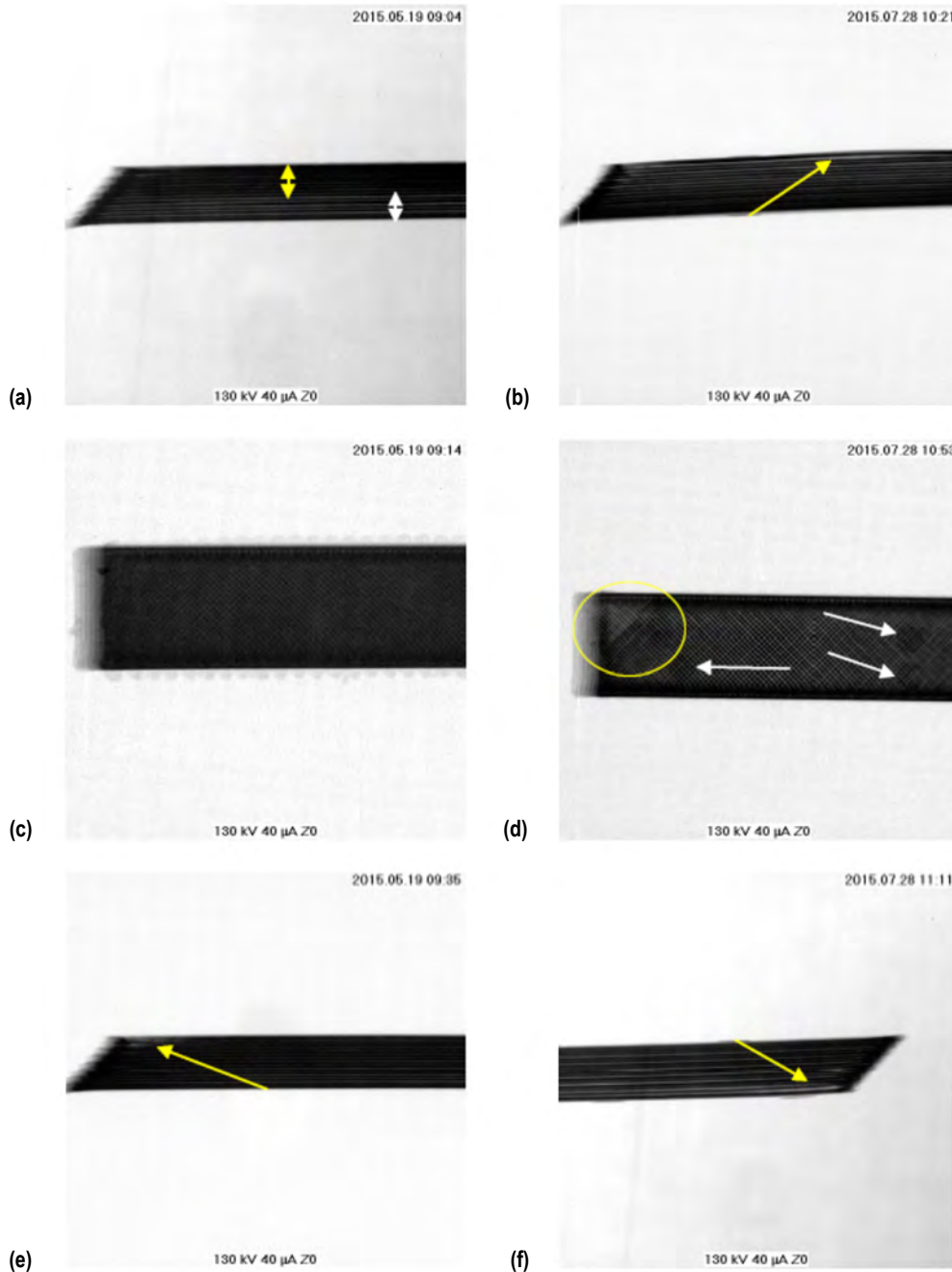
Figure 16. These radiographs show examples of flexure specimens: (a) One side of F006. The top (yellow arrow) is denser than the bottom (white arrow). (b) One side of G006. There appears to be a delamination near the surface (yellow arrow). (c) Portion of the sample F014. Printing is uniform across the width. (d) Portion of G014. There is clearly an x-ray density variation at one end (yellow oval). The dark circles are slight indentations from tabs used to fixture the part for structured light scanning (white arrows). (e) One side of F017. There is a low-density indication present related to surface voiding that runs about two layers deep (yellow arrow). (f) Side view of G017. There appears to be a delamination present (yellow arrow).
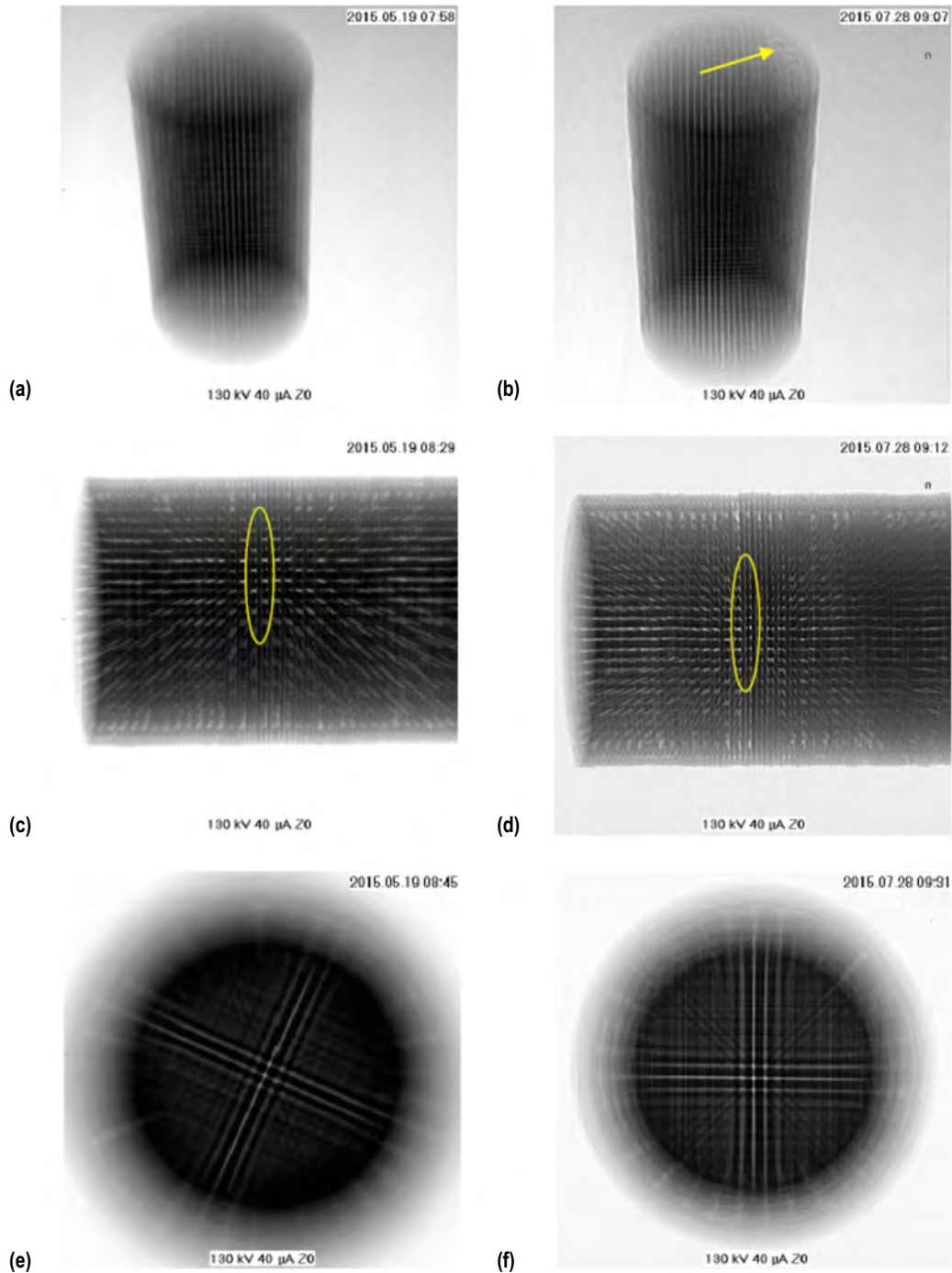
Figure 17. These radiographs show examples of compression samples: (a) Oblique view of F005. (b) Oblique view of G006. There is a low-density indication near one end (yellow arrow). (c) One side of F013. The print lines appear to be pairs along this run. (d) Side view of G006 for comparison to F013. The print lines do not appear to be pairs (yellow oval). This could be the result of G006 being slightly rotated out of phase from F013. (e) Top-down view of F016. (f) Top-down view of G016. No anomalies were noted in this view for any compression sample.

4.3 Computed Tomography

Computed tomography is a volumetric inspection method that produces images of cross sections of the inspected part. Each CT 'slice' is a visual depiction of material structure and density at a specific location in the inspected part. For example, CT slices taken on a plane parallel to the face of a cube would be square images, while CT images taken perpendicular to the long axis of a cylinder would be circular. Individual slices taken at successive steps through the volume of the inspected part can then be reconstructed into a data volume that depicts the 3D structure and density of the inspected part, and then can be manipulated to reveal internal configuration of the part.

4.3.1 Computed Tomography: Scanning

Flight and ground mechanical test coupons underwent 3D-CT scanning. Specimens were fixed using a rubber-tipped, three-pronged holder that could be affixed to the ends of each sample. The fixture applied only enough pressure to prevent slippage of the sample or other movement during scanning. Examination of each sample was performed post-testing at 10× optical magnification to ensure no damage was imparted to the contact surfaces by the fixture. A series of rapid scans were conducted to determine voltages and filters. Accelerating voltages from 100 to 140 kV, with currents selected to obtain adequate grayscales, were tested. The best images were obtained using 120 kV and 100 μA. The beam was collimated and a 0.65-mm copper filter was used. The approximate resolution reported by the instrument was as follows: 30 μm for flexure samples, 29 μm for tensile samples, and 43 μm for compression samples. The typical exposure time was 20–25 min per section. The flexure and tensile samples were scanned in two parts. Scanning regions were defined so that the most likely failure location would be captured with each scan; the region typically included the center portion of the specimen out to the largest length that was viewable. The compression samples were scanned in whole, hence the lower resolution (larger voxel size) compared to the flexure and tensile samples. Typical images acquired through CT are shown in figures 18–20 for tensile, flexure, and compression, respectively. These images are shown alongside their corresponding radiographs to illustrate that many of the indications found in 2D radiography were corroborated by 3D-CT.
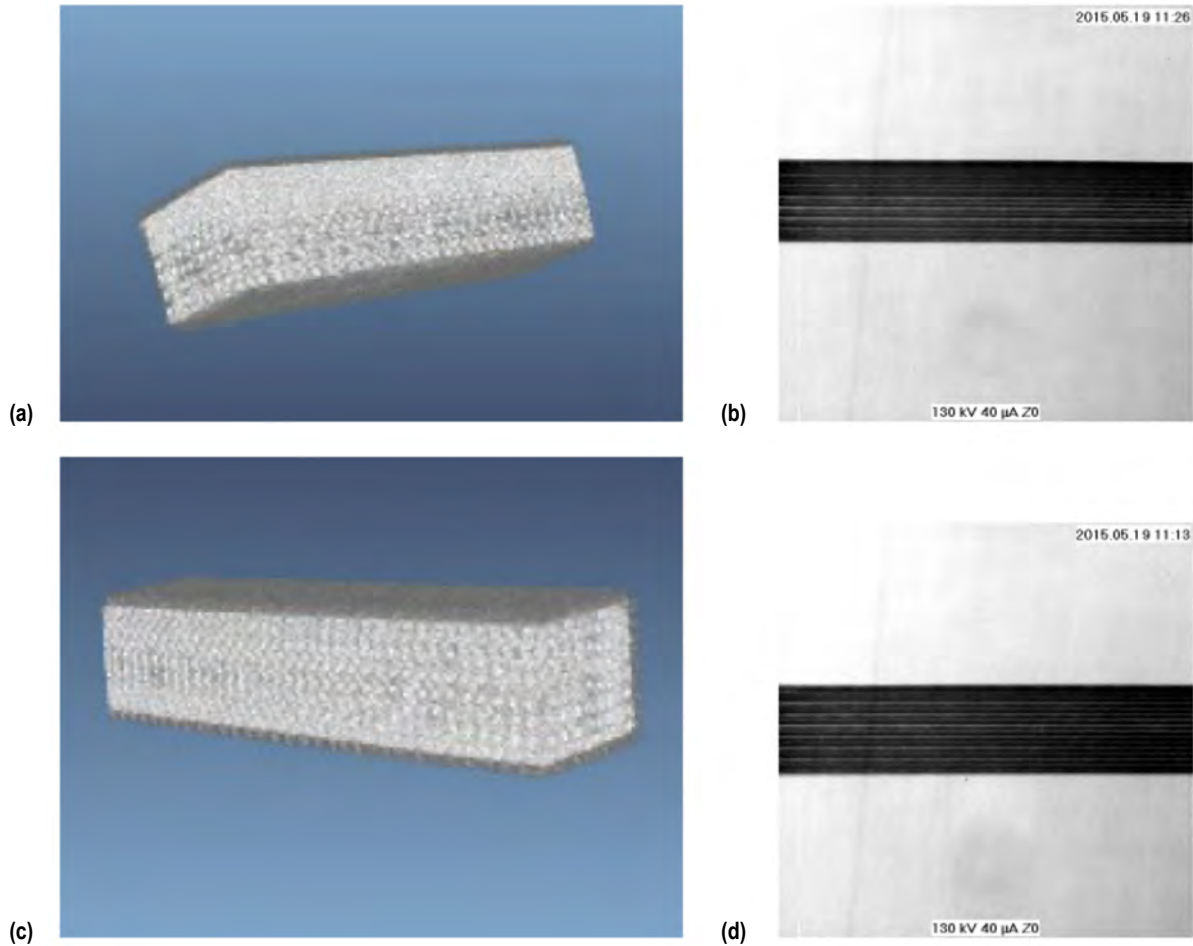
Figure 18. Examples of CT images of tensile samples: (a) Tomograph of a clipped view of F004 to show the internal construction. It has been rotated to show the same view as the 2D image. (b) Radiograph of F004. Note the x-ray density variation in this 2D image verifies what is observed in the tomograph. The density variation is clearly not an artifact of the 3D-CT algorithm. (c) Tomograph of a clipped view of F015 to show the internal construction. It has been rotated to show the same view as the 2D image. In this image, the density variation from top to bottom appears uniform. (d) Radiograph of a side view of F015 for comparison to the 3D-CT scan. Note here that the x-ray density appears uniform, verifying the 3D-CT data.

(a)

(b)
2015.05.19 09:04
130 kV 40 µA Z0

(c)

(d)
2015.07.28 10:20
130 kV 40 µA Z0
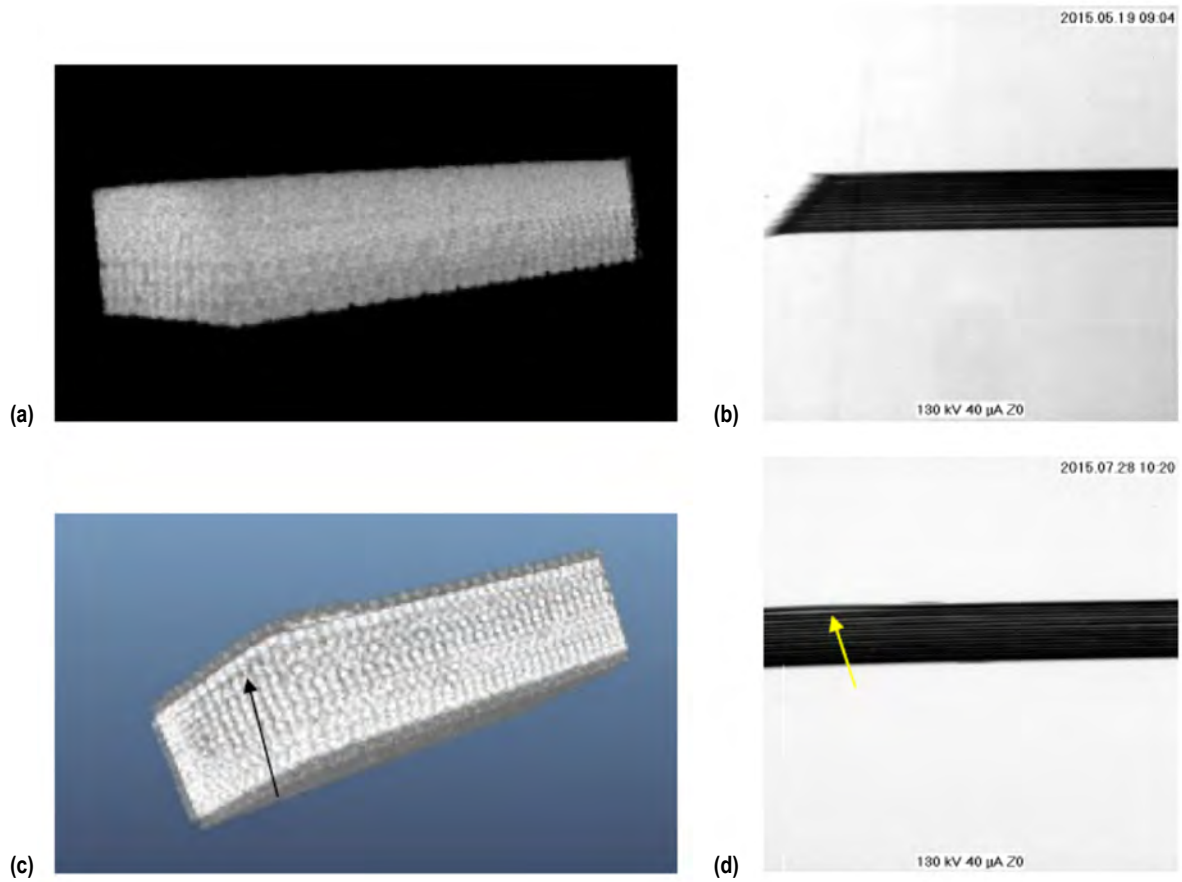
Figure 19. Examples of flexure samples: (a) Tomograph of a clipped view of F006 to show the internal construction. There is clearly an x-ray density variation from more dense at the top of the specimen (the last layers to be printed) to less dense near the bottom. (b) Radiograph of F006. This image shows the same density variation noted on CT. (c) Tomograph of a clipped view of G006 to show the internal construction. It has been rotated to show the same view as the 2D image. Not only is the density change present, but the delamination area is also visible (black arrow). (d) Radiograph of a side view of G006 for comparison to the 3D-CT scan. Note here that the x-ray density variation is similar to that observed with CT and the delamination is clearly present (yellow arrow).
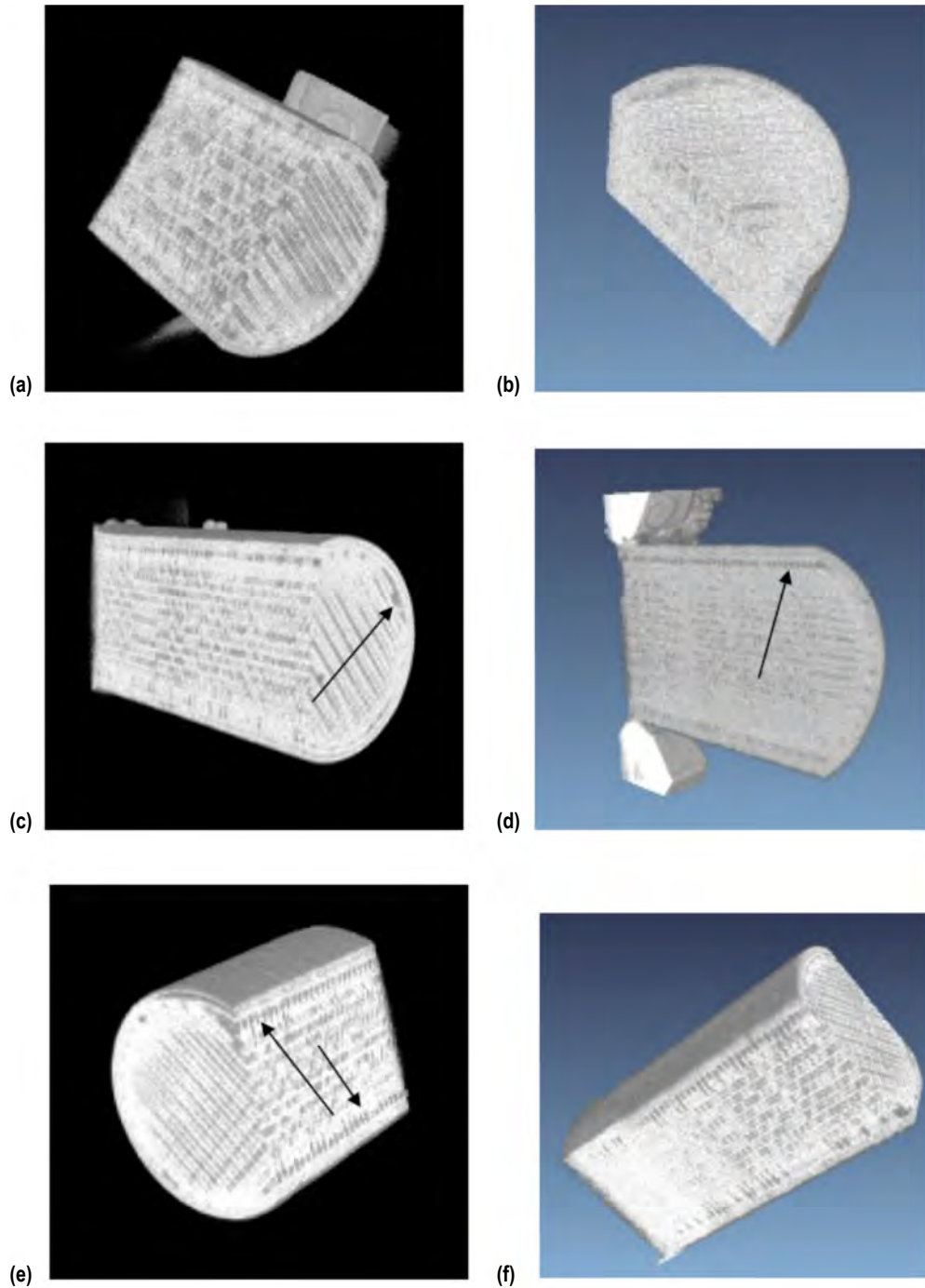
Figure 20. Examples of compression samples: (a) Tomograph of a clipped view of F005 to show the internal construction. (b) Tomograph of a clipped view of G005. (c) Tomograph of a clipped view of F013 to show the internal construction. There is a voided area near one end indicated by a black arrow (not surface related since this is an internal clip view). (d) Tomograph of a clipped view of G013 to show the internal construction. This slice verifies the lower density seen at the circumference in the 2D views of the compression articles (black arrow). (e) Tomograph of a clipped view of F016 to show the internal construction. Again, the lower density at the circumference is clear (black arrow). (f) Tomograph of a clipped view of G016.

4.3.2 Computed Tomography Analysis

Once scanning was complete, the MSFC NDE team was asked to review and analyze the CT inspection data generated by the Center's Space System Department. The NDE team worked with customers from the ISM project team as well as with the Space Systems Department to develop methods and objectives for the analysis based on understanding of the fabrication process and the initial CT data collection process. The specific objectives of this review were established as follows:

- Does the CT inspection detect voids? If so, is there a difference in the size or number of voids between the ground-built and ISM specimens?
- Do the CT data indicate differences in density between the ground-built and ISM specimens?
- Are there detectable variations in density associated with the build process, and if so, is there any difference in this effect between ground-built and ISM specimens?

The data analysis was performed using two programs: VGStudio MAX, published by Volume Graphics GmbH, and ImageJ, an open-source image analysis program sponsored by the National Institutes of Health. Initial review of the CT images of the specimen fabricated for this study showed many low-density indications (LDIs) throughout the majority of samples from both populations (ground and ISM). A typical CT slice through a rectangular area of a specimen is shown in figure 21.
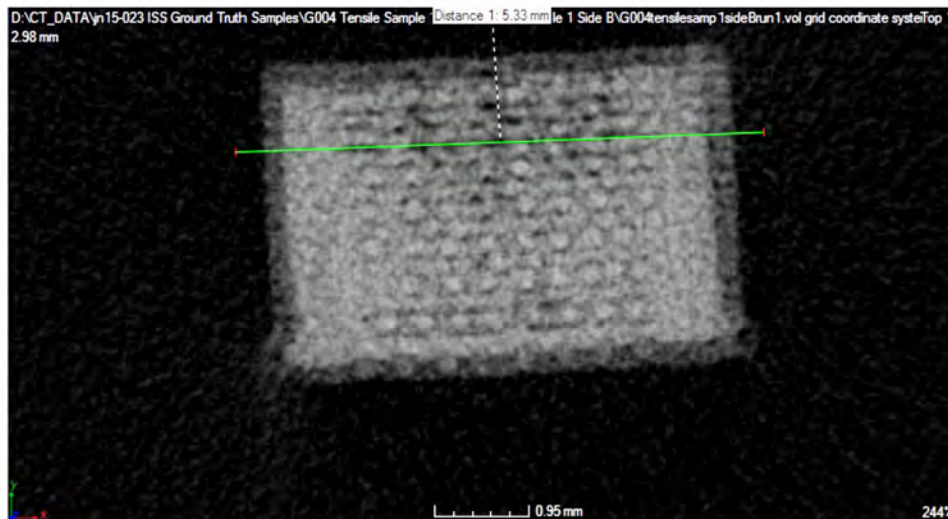
Figure 21. Example of a single CT slice through a ground-built specimen.
The dark spots within the gray rectangular cross section are LDIs.

A 3D volume constituted of the 'stack' of individual CT slices is shown, along with additional individual slices, in figure 22.
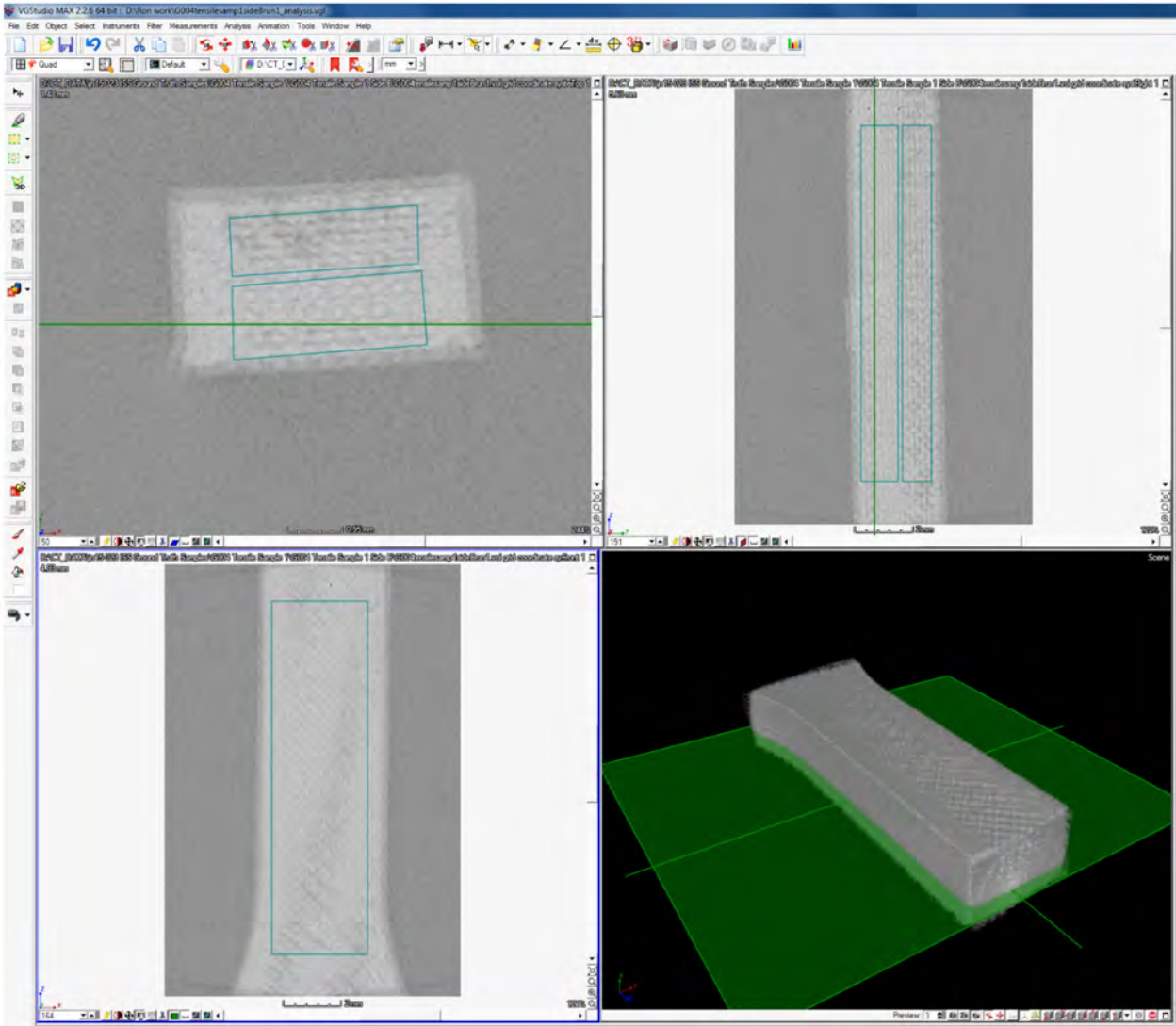
Figure 22. The 3D representation of a scanned specimen, consisting of several thousand individual CT slices, is shown in the lower-right corner. The green plane intersecting that volume depicts the location of the slice view shown in the lower-left corner.

Computed tomography is very capable of detecting open voids as well as differences in density of material either higher or lower than the nominal density of base material. In a complex 3D material such as additively manufactured composites, there are inherent variations in density resulting from the nature of the building process. In order to determine whether the LDIs detected in an inspected part are actual voids, the best practice is to simulate voids in base material using manufactured flaws (such as drilled holes) and determining how much change in CT pixel value or 'CT number' is produced by the absence of material. To date, specimens with built-in flaws have not been produced for ISM analysis, but may be part of future work. Computed tomography numbers indicate, for a given pixel in the CT image of the scanned part, the amount of x-rays absorbed by the scanned region covered by that pixel. A pixel in a CT image is commonly called a voxel, meaning that the image pixel represents a volume in the scanned part with dimensions of the image pixel in the x-axis and y-axis directions and the thickness of the CT slice in the z-axis direction. As the density of the material covered by a CT voxel decreases, so does the CT number and gray level value shown in the scan image, so lower density indications appear darker and higher density indications appear brighter compared to nominal material density. Specimens with simulated flaws were not available to serve as a precise guide to the variation of CT numbers that positively indicate voids, but some conclusions may still be drawn from the data by comparing the measured CT numbers in LDI regions to the CT number of the air surrounding the specimen, as shown in figures 23–25.

In each of the figures 23–25, the blue bounded areas are the CT numbers in air outside the component, and the green bounded areas are the CT numbers in areas inside the specimen that are of nominal density. The red arrows connect LDIs in each part to decreases in the plotted profile that indicate significant drops in CT number compared to the CT numbers in nominal areas. Definite identification of these LDIs as voids would normally be done by comparing such images to profiles across similar images with known voids. In this case, without such known voids available, it can only be stated that the magnitude of the decreases at LDI locations shown with respect to the difference between CT numbers in the air and in nominal areas strongly suggests the presence of voids in the marked regions, but does not indicate voids with certainty. A qualitative visual comparison of ground and ISM datasets did not indicate a significant difference in the number of LDIs in the ground and ISM sets.
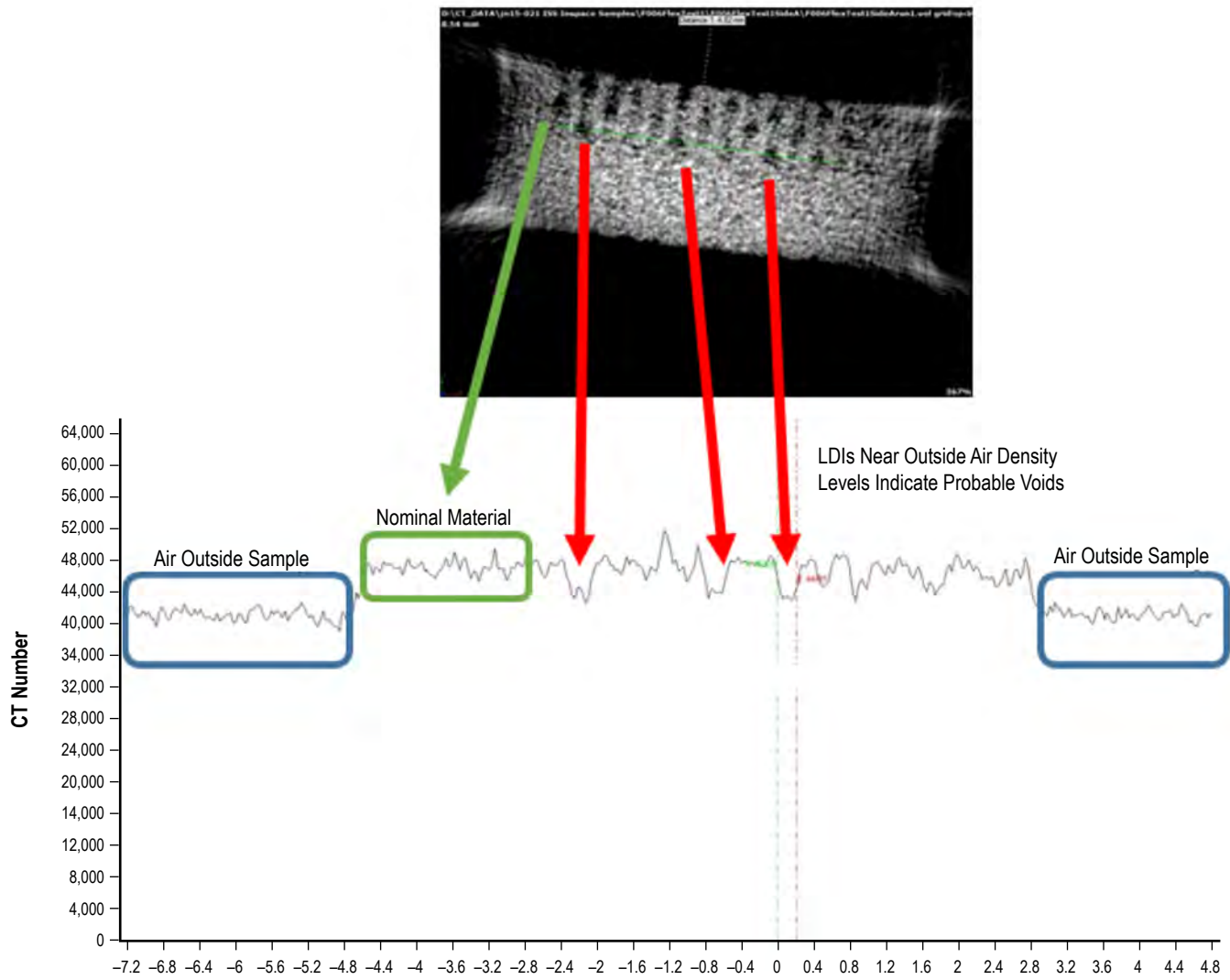
Figure 23. Computed tomography number profile for ISM specimen F006.
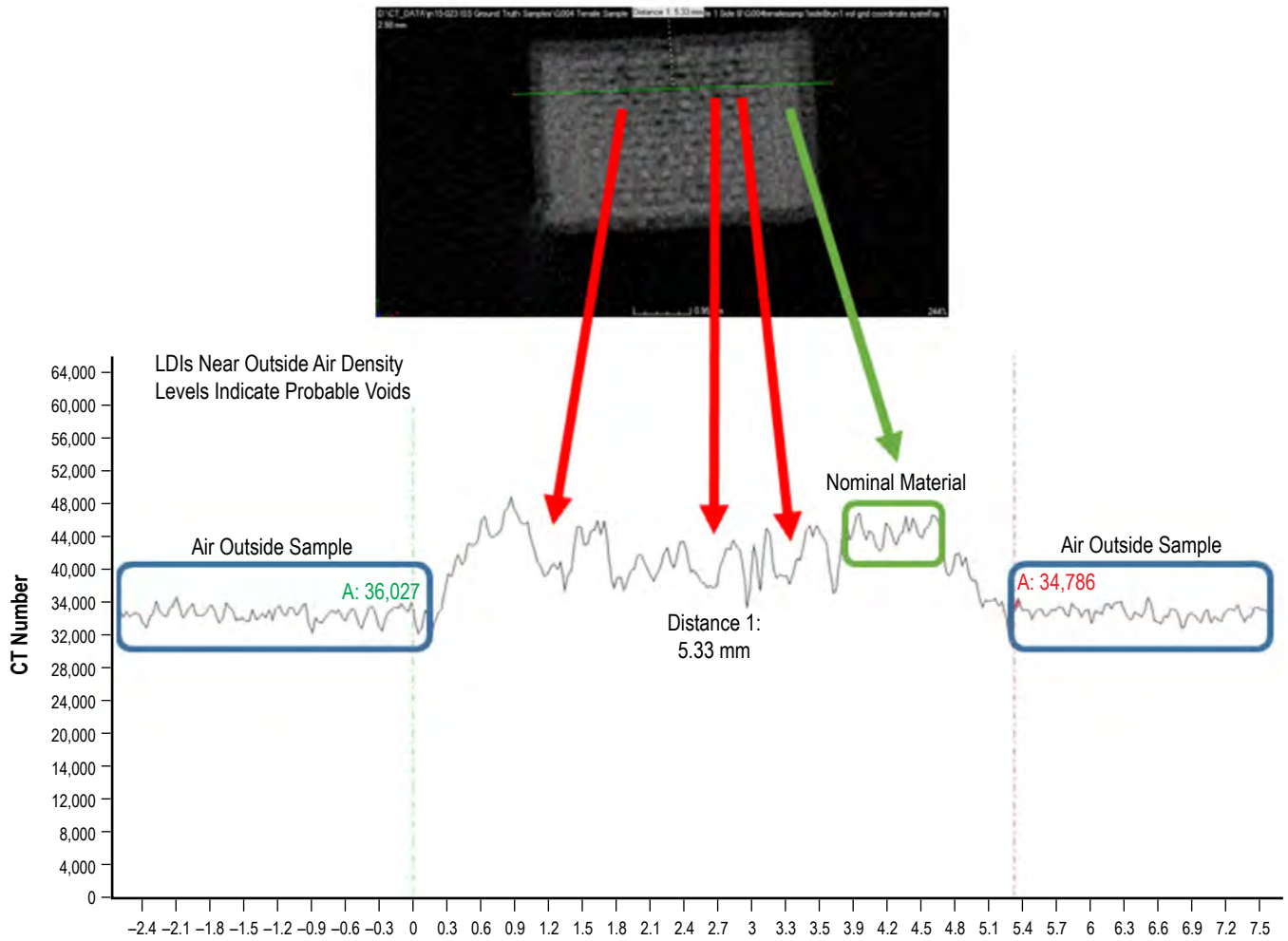
Figure 24. Computed tomography number profile for ground specimen G004.
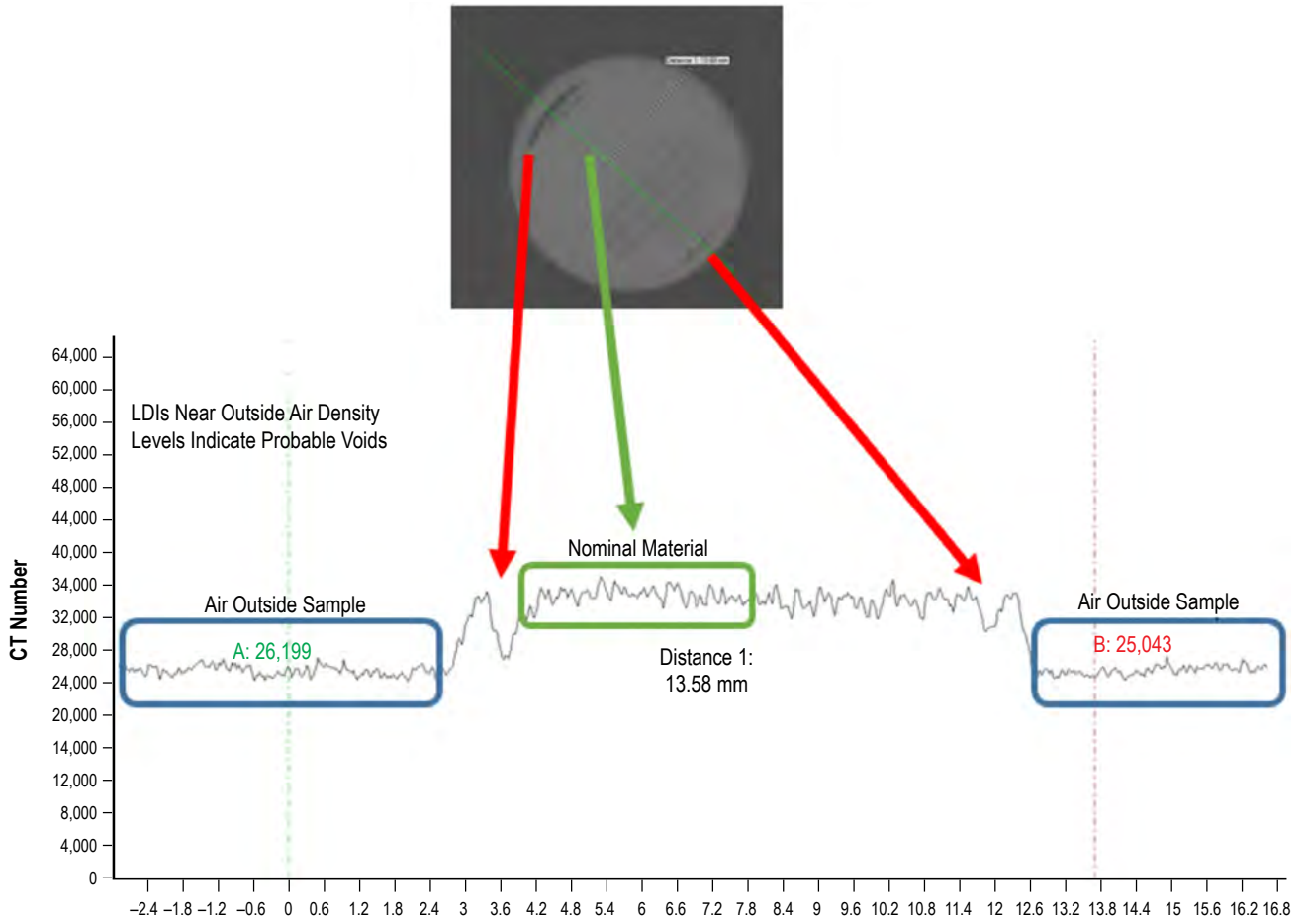
Figure 25. Computed tomography number profile for ground specimen G016.

Density variations within additive manufactured composites can be quite localized, as seen in the previous figures. In order to compare the overall densities (as determined by CT's ability to measure x-ray absorption), VGStudio's volume analyzer tool was used. An example of this tool's output is shown in figure 26.
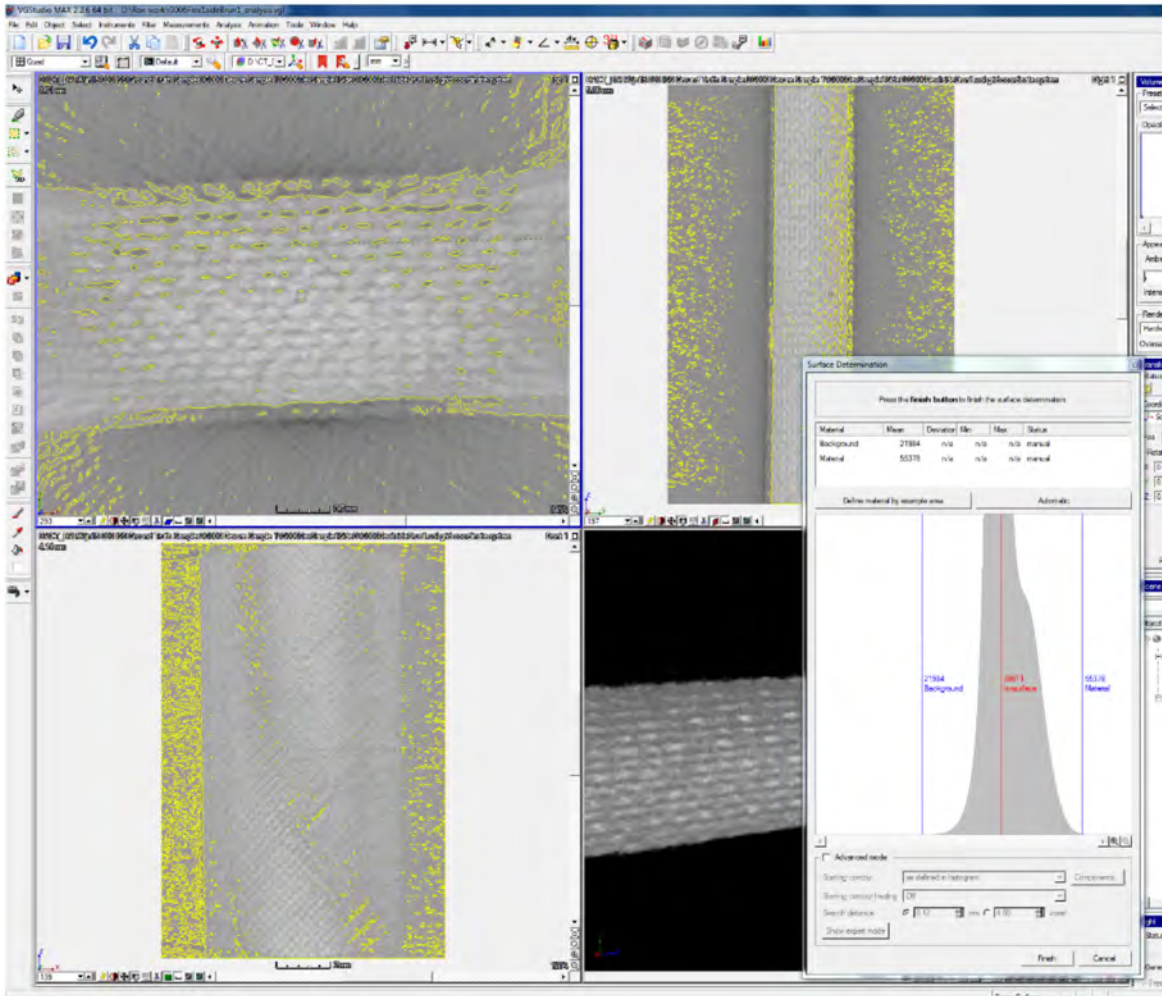
Figure 26. Screenshot of the VGStudio volume analyzer tool.

The volume analyzer works by counting the number of CT voxels within density limits set by the user in the histogram at the lower right. By setting the blue boundary lines appropriately to eliminate the lowest density voxels (air outside the part), the user can produce an approximate measure of the volume of the scanned specimen, along with a mean CT number (which represents both physical density and the x-ray absorption coefficient) for the entire volume. This is the best approximation that CT can make to classical density; that mean CT number can be correlated to physical density with properly designed samples of the material to be scanned. In this case, the mean CT number for

each scanned article was used as a representation of its density. The table of CT numbers measured for ground and ISM specimens is shown in table 16.

Table 16. Mean CT numbers for corresponding flight and ground specimens.

Part Name	Mean CT Number	Standard Deviation	Part Name	Mean CT Number	Standard Deviation
F004 side A	44,487	2,641	G004 side A	46,898	2,162
F004 side B	42,139	2,430	G004 side B	44,113	2,548
F012 side A	46,555	1,982	G012 side A	46,217	2,122
F012 side B	48,211	2,468	G012 side B	42,675	2,445
F015 side A	45,127	3,349	G015 side A	29,935	1,630
F015 side B	36,463	2,589	G015 side B	46,063	2,291
F018 side A	45,616	2,949	G018 side A	28,124	1,551
F018 side B	44,463	2,618	G018 side B	42,790	2,939

The standard deviation (SD) represents the noise inherent in (1) natural variations in the CT process due to detector noise and x-ray beam variation and (2) variations in density throughout the bulk of each scanned specimen. The usefulness of the SD as a discriminator in assessing whether ground and ISM populations have different mean CT number values is shown in figures 27 and 28.
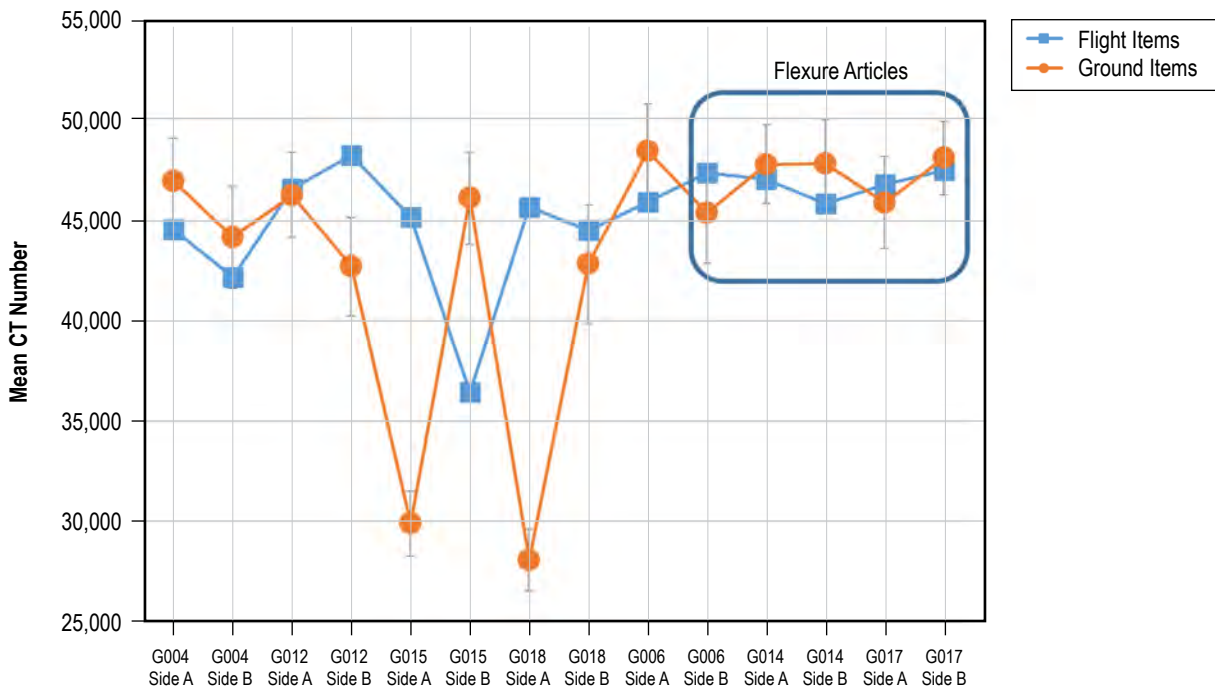
Figure 27. Graph of mean CT numbers for ground and ISM specimens; error bars represent ±1 SD. While only ground prints are indicated on the x-axis, the corresponding flight prints are plotted on the same axes in blue.
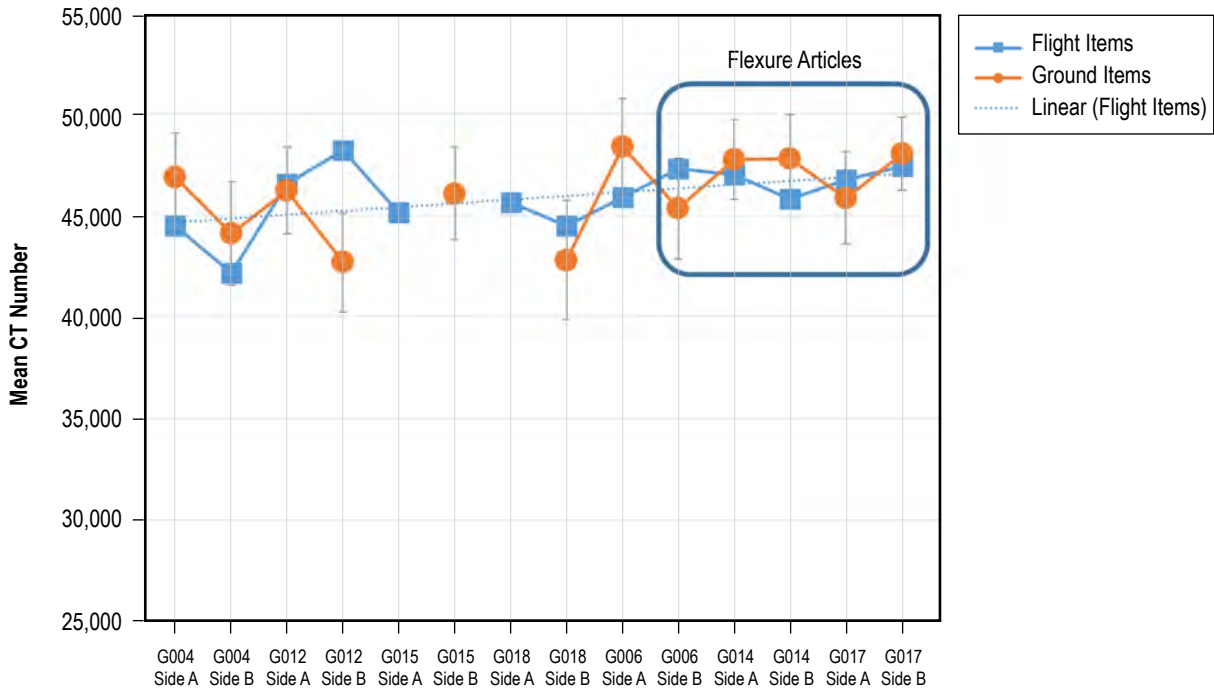
Figure 28. Graph of mean CT numbers for ground and ISM specimens; error bars represent ±1 SD. Data outliers resulting from x-ray technique variations have been removed from this dataset. While only ground prints are listed on the *x*-axis, the corresponding flight prints are printed on the same axes in blue.

Figures 27 and 28 show that the CT datasets of flexure and tensile specimens included three scans out of 16 performed (two scans each on eight test specimens, one on each end of each specimen due to limited scan area compared to specimen size) that have CT densities well outside the population of the remaining 13 datasets. Review of the raw x-ray image data used to produce the CT scans shows that in each of those three cases, the base intensity of the raw x-ray image was significantly lower than for the other 13 for unknown reasons. Figure 28 was thus generated without the three outlying datasets in order to clarify the results. Both figures 27 and 28 show that, within the boundaries of the error bars, the values of the mean CT numbers of the ground and ISM specimens do not vary from one another in a statistically significant way; there is no consistent trend of one population (ground or ISM) having a higher or lower CT number than the other. Simple statistical tests (U-test, unpaired t-test) confirmed that there was no significant correlation of mean CT numbers to ground or ISM build sets. Therefore, the mean CT number of the entire volume of each specimen was not an indicator of statistically significant CT number due to being manufactured on the ground versus ISM. More generally, CT could not determine a significant difference in bulk density between the ground and ISM sets.

Computed tomography number variations (an indicator of physical density variations) as a function of build direction of the specimens were also evaluated using VGStudio and ImageJ to produce line profiles and CT number volume analysis. In this case, the volume analysis tool was used to define subvolumes within each scanned specimen in two regions, one near the beginning of the

buildup of layers and one farther away from the beginning of build (designated as 'lower' for near the beginning of build and 'upper' for the other dataset, as shown in fig. 29). Consistent distances were maintained for this analysis.
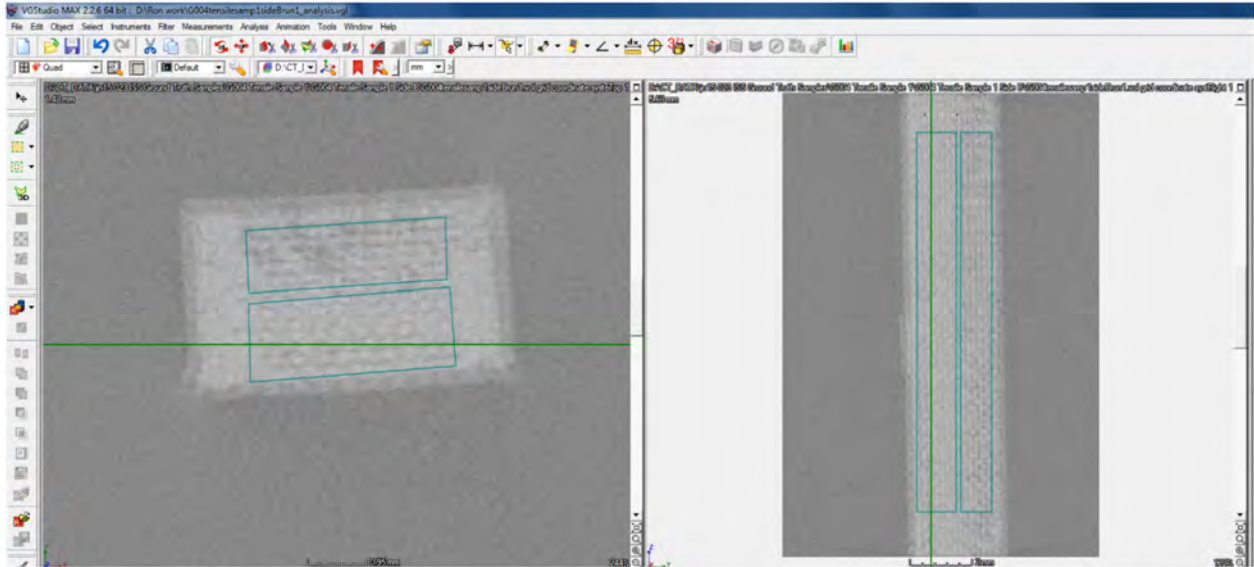
Figure 29. Screenshot of the VGStudio volume analyzer tool showing the boundaries of 'lower' and 'upper' data collection regions.

Image J was also used to measure raw x-ray attenuation through the specimens in x-ray views with the x-ray beam directed parallel to the build planes, as shown in figure 30. Density variations between the build layers are clearly visible in this view.
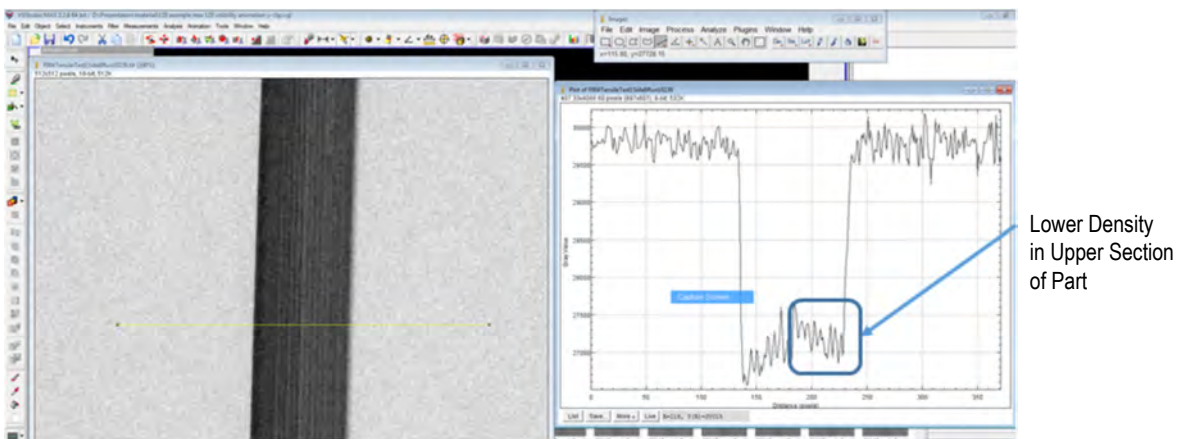
Figure 30. Profile of x-ray absorption through a specimen, with the beginning of the build on the left side of the image. The profile indicates lower density as the distance from beginning of build increases (from left to right along the yellow profile line).

Using similar methods, as with the analysis of entire scanned volumes, the upper and lower volume mean CT numbers within each specimen were tabulated; the results are shown in table 17. In every case, comparison of the difference between densities in the upper and lower sections of the samples was found to be within one SD of densities in the lower region of each sample. The SD represents the combined effects of inherent process variation in the material and inherent variation in the CT data. Variation within one SD of the more uniform lower section material is not considered statistically significant.

Table 17. Results of the comparison of upper and lower section
CT number mean values for each specimen.

Part No.	Upper	Lower	Lower SD	Percent Difference	SD abs Value (%)	Part No.	Upper	Lower	Lower SD	Percent Difference	SD abs Value (%)
F004 Side A	45,049	46,105	1,645	–2.29	3.57	G004 Side A	46,861	48,056	1,495	–2.49	3.11
F004 Side B	41,786	43,526	2,240	–4.00	5.15	G004 Side B	44,091	45,405	1,920	–2.89	4.23
F005	22,906	23,085	1,245	–0.78	5.39	G005	28,198	28,600	1,172	–1.41	4.10
F006 Side A	45,530	47,015	1,731	–3.16	3.68	G006 Side A	49,678	48,796	2,236	1.81	4.58
F006 Side B	47,036	47,794	911	–1.59	1.91	G006 Side B	43,386	45,712	3,321	–5.09	7.27
F012 Side A	47,198	47,289	1,483	–0.19	3.14	G012 Side A	46,644	47,147	1,615	–1.07	3.43
F012 Side B	49,044	49,268	1,931	–0.45	3.92	G012 Side B	42,620	43,640	2,355	–2.34	5.40
F013	19,547	19,539	293	0.04	1.50	G013	19,736	19,705	773	0.16	3.92
F014 Side A	47,428	47,905	953	–1.00	1.99	G014 Side A	48,369	48,165	1,790	0.42	3.72
F014 Side B	45,863	46,971	1,573	–2.36	3.35	G014 Side B	48,561	48,261	2,007	0.62	4.16
F015 Side A	46,860	46,904	2,143	–0.09	4.57	G015 Side A	30,279	31,053	1,005	–2.49	3.24
F015 Side B	37,061	37,362	2,555	–0.81	6.84	G015 Side B	46,314	47,364	1,584	–2.22	3.34
F016	19,118	19,340	793	–1.15	4.10	G016	33,797	34,915	1,199	–3.20	3.43
F017 Side A	47,428	47,431	1,363	–0.01	2.87	G017 Side A	46,192	46,379	2,324	–0.40	5.01
F017 Side B	47,950	47,781	1,221	0.35	2.56	G017 Side B	48,606	48,682	1,425	–0.16	2.93
F018 Side A	47,108	47,062	1,755	0.10	3.73	G018 Side A	28,921	28,652	1,280	0.94	4.47
F018 Side B	45,300	44,580	2,118	1.62	4.75	G018 Side B	43,791	43,793	2,761	0	6.30

The variation between the mean CT numbers for the upper and lower sections of each scanned item was analyzed for each sample by subtracting the upper section value from the lower section value. The lower section of each specimen was closer to the beginning of build and was considered nominal, while, in general, the CT number of the upper section was slightly lower. The difference in mean CT numbers between lower and upper regions was then compared to the SD of the CT number in the lower (nominal) section. In every case, the difference in means of the upper and lower values was less than the SD of the mean CT number in the lower section, where, as before, the SD represents the inherent variations in the material itself and in the CT inspection process. Therefore, while there was a general trend toward slightly lower mean CT numbers (and therefore densities) in the upper section, this trend was not significant compared to natural variations in the material for ground or ISM specimens.

4.4 Conclusions and Highlights

The study of CT data produced by scanning the ground and ISM specimens provides answers to the questions set forth in the objective:

• Computed tomography can detect small variations in density in additively manufactured specimens; analysis of the LDIs suggests that they are probable voids. The number and distribution of probable voids per specimen was not significantly different between ground and ISM specimen sets.

• Computed tomography did not detect a statistically significant difference in the mean CT numbers of ground-built specimens versus ISM specimens; given that identical materials and configurations were used in both build sets, it can be concluded that CT did not detect statistically significant differences in bulk density of the two specimen sets.

• Computed tomography did detect slight variations in mean CT numbers (and hence bulk density) within each scanned specimen; these variations were small, and the trend of such variations was not different for ground versus ISM build sets in a statistically significant manner.

It is evident that CT is a powerful tool for the evaluation of additively manufactured specimens and components; the known strengths of the inspection technique were demonstrated in this study. Future CT studies of ISM materials would benefit greatly from the (1) increased number of available production articles, (2) availability of test articles identical to the production articles for further optimization of x-ray and CT inspection techniques, and (3) availability of test articles with manufactured or known natural flaws that will enhance the ability to diagnose the nature of actual flaws by statistical analysis of CT inspection data from production specimens and components.

5. MICROSCOPY RESULTS

Optical microscope images of all phase I specimens were captured using the Keyence VR-3200 housed in the Mechanical Testing Laboratory at MSFC. For image acquisition, a black and white color scheme was used to maximize contrast. Plan views of the bottom and top of each specimen were obtained. For the bottom plan view, the specimen is oriented so that the layer in the x-y plane that was printed first faces upward. In the top plan view, the specimen is oriented so that the uppermost layer in the x-y plane that was the last to be printed faces upward. Side views in the x-z and y-z planes were also taken. These images, taken at 40× magnification, reveal structural features on the surface of the parts and (to the extent possible) within the specimen. Layer thickness was measured and comparisons between ground and flight specimens (or classes of specimens) were made based on this metric for analogous geometries. As noted in the x-ray/CT analysis, the lower layers are more closely clustered, so layer thickness measurements are derived from the upper portions of the specimen that represent steady state printing operation. Regions damaged by removal from the build tray are also noted. Defects or anomalies noted in previous phases of testing, regions of specimens potentially damaged in separation of the part from the build tray, and fracture surfaces of tensile specimens were also examined closely.

Tensile specimens were evaluated after the completion of tensile testing. Figure 31 compares the plan views of the tensile specimens with the 'bottom side' (layer in x-y plane that was printed first) facing upward. The location and type of break are not consistent within specimen classes. For the ground specimens, two specimens broke straight across when tested to failure, and two specimens had diagonal breaks (since these specimens have a ±45° layup pattern, 'failure follows fiber' in these instances). For the flight specimens, two of the specimens exhibit a horizontal break, while two have a diagonal fracture surface. As noted in section 3, several of the breaks were outside the extensometer footprint. For completeness, the plan view of the 'top' of the tensile specimens (specimen oriented with the layer printed last facing upward) appears in figure 32.
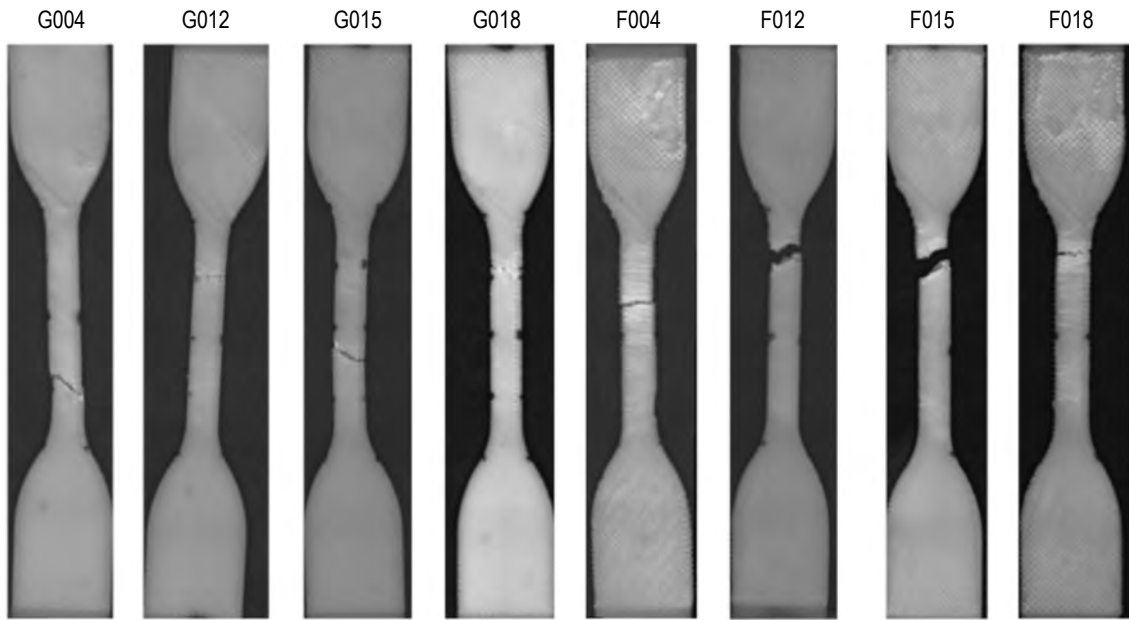
Figure 31. Plan view (bottom) of tensile specimens.
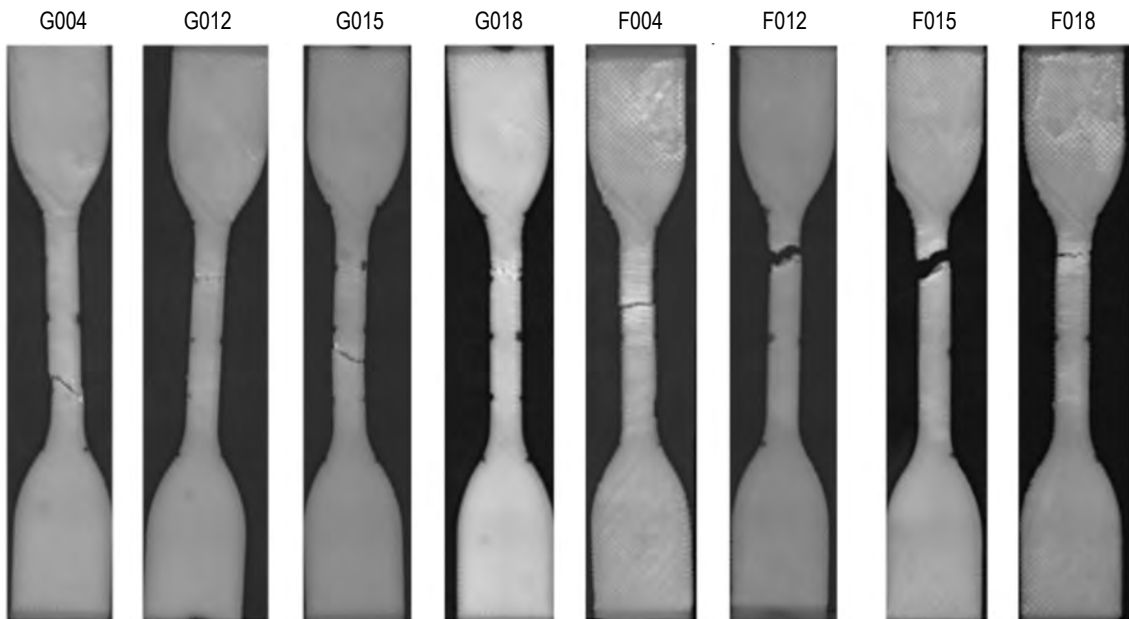
Figure 32. Plan view (top) of tensile specimens.

A closer examination of the tensile fracture surfaces appears in figure 33.

G004

F004

G012

F012

G015

F015

G018

F018
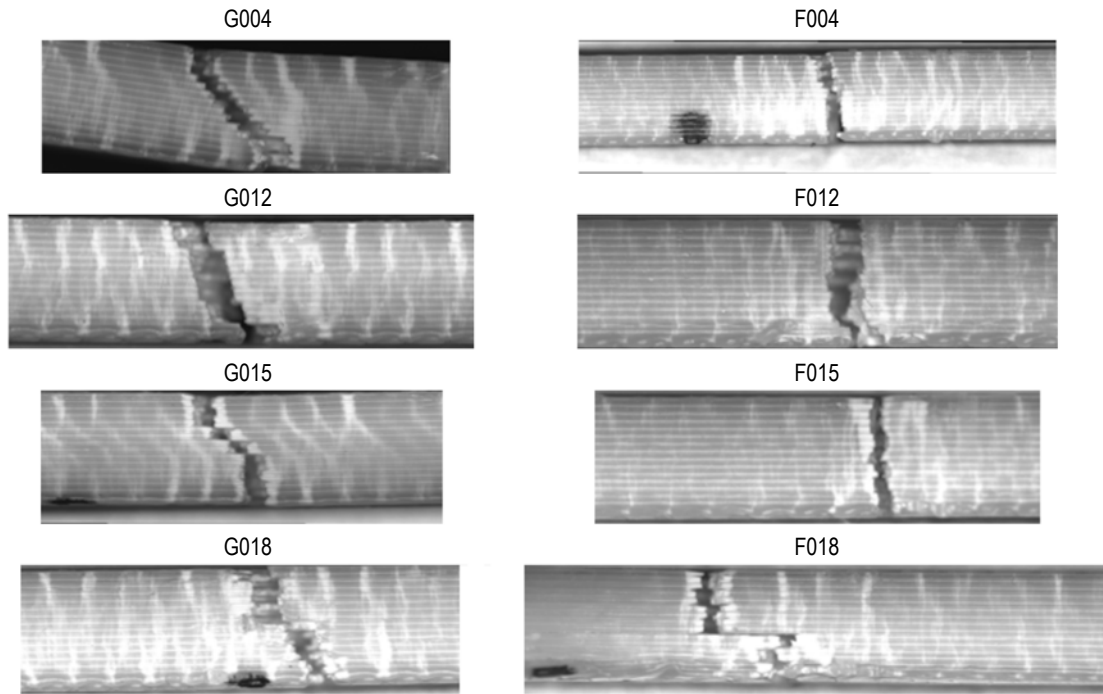
Figure 33. Close-up of tensile fractures.

Images of the fracture surfaces taken in the 'head-on' orientation (fig. 34) show denser regions in the flight specimens that are consistent with both gravimetric density measurement and x-ray/CT observations (although CT analysis concluded that the magnitude of both the density differences within the specimen and between ground and flight specimens, reported in terms of mean CT, were not statistically significant).

G004

G012

G015

G018

F004

F012

F015

F018
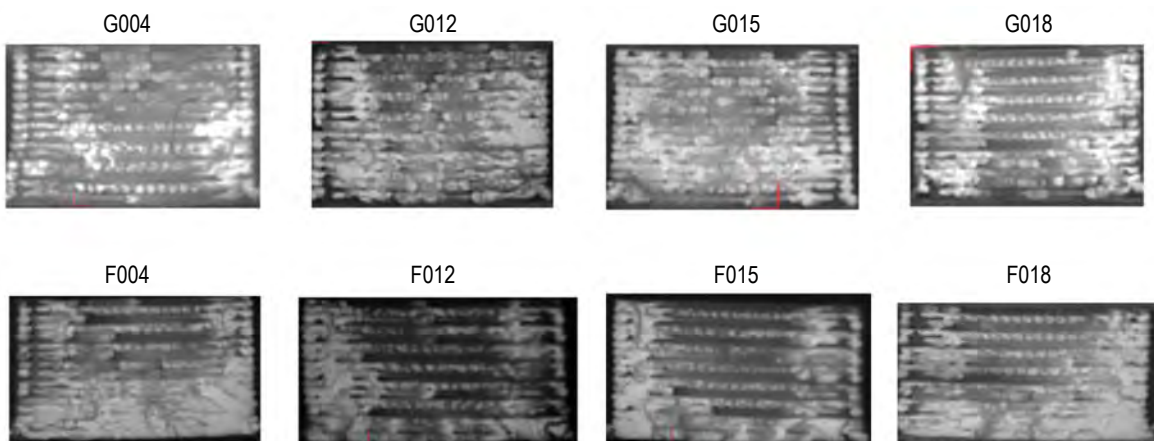
Figure 34. Images of tensile specimen fracture surfaces in the 'head-on' orientation.

Overall, the breaks in the ground tensile specimens more closely follow a diagonal (and the layup pattern) than the flight specimens. Breaks were consistently closer to the 'birthmark' (the region where material deposition begins) for the flight specimens. Stress marks were more noticeable on microscopy for the ground-based prints. The thickness of the layers in the steady state configuration (reached at halfway through the through-thickness of the specimen) were also not significantly different for ground and flight, with flight specimens exhibiting an average layer thickness of 0.008 in and ground specimens having an average layer thickness of 0.009 in.

Microscopy images of the flexure specimens appear in figure 35. As with the tensile specimens, stress marks were slightly more pronounced for the ground-based prints. Steady state layer thickness was measured as 0.01 in for the ground specimens and 0.01 in for the flight prints.
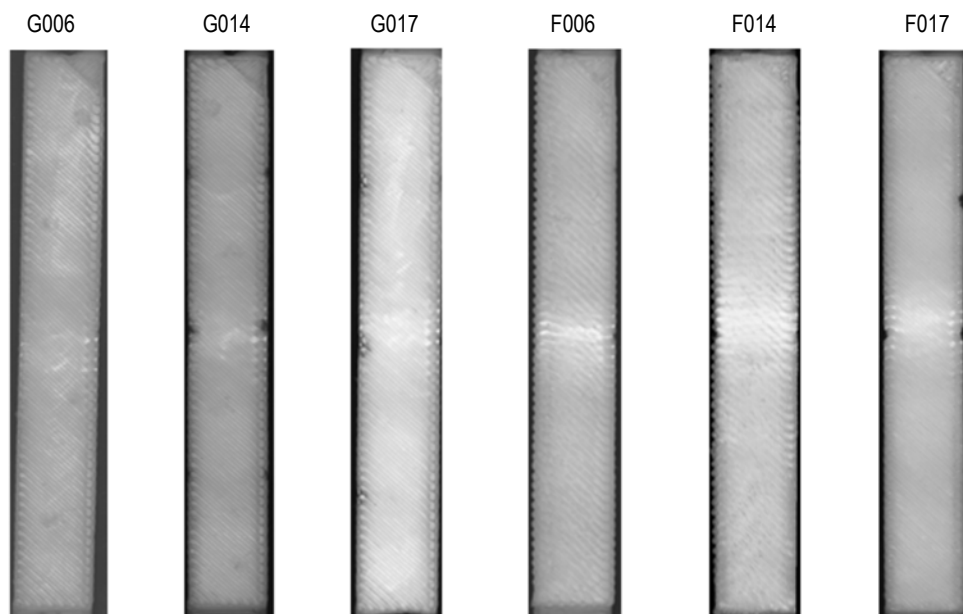
Figure 35. Plan view B of flexure specimens after mechanical testing.

Compression specimens were evaluated after mechanical testing, and microscopy images are shown in figure 36. Specimen G005 had a slightly larger 'footprint' than other specimens.

Microscopy of nonmechanical specimens also provided some insight into printer operations and adhesion. For both the ground and flight extruder plate (specimens G002 and F002), the bottom of the plate began to peel up during the print process. This effect, caused by rapid cooling of the specimen on the unheated tray, is more noticeable for the flight print. The flight extruder plate was also damaged during part removal. Figure 37 shows the top and bottom plan views of the extruder plate.
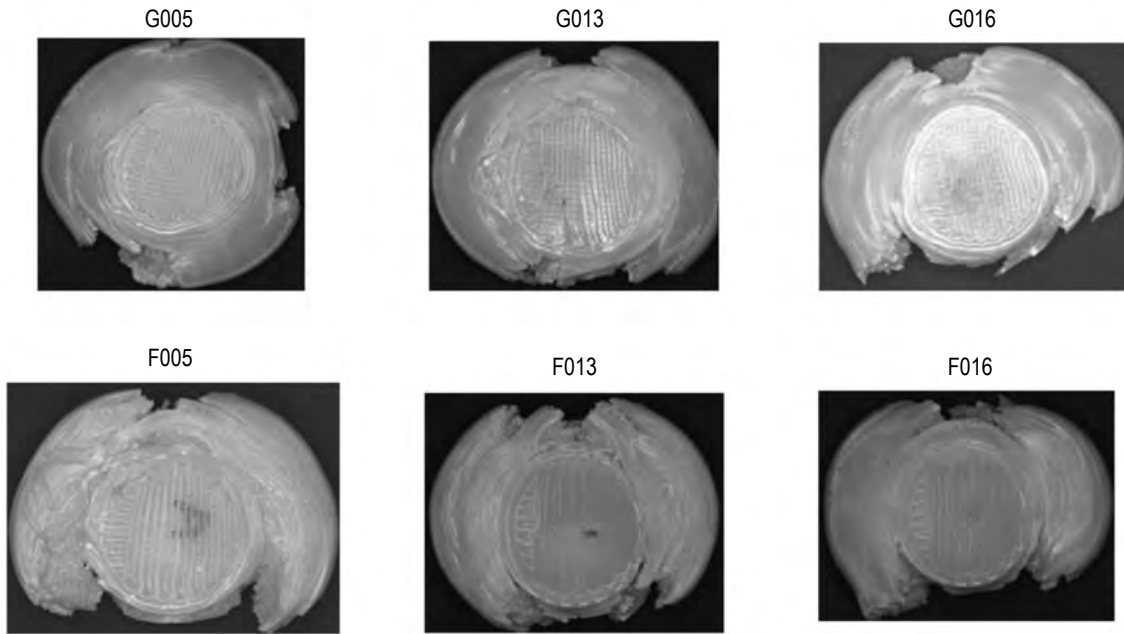
Figure 36. Microscopy images of flight and ground compression coupons after mechanical testing.
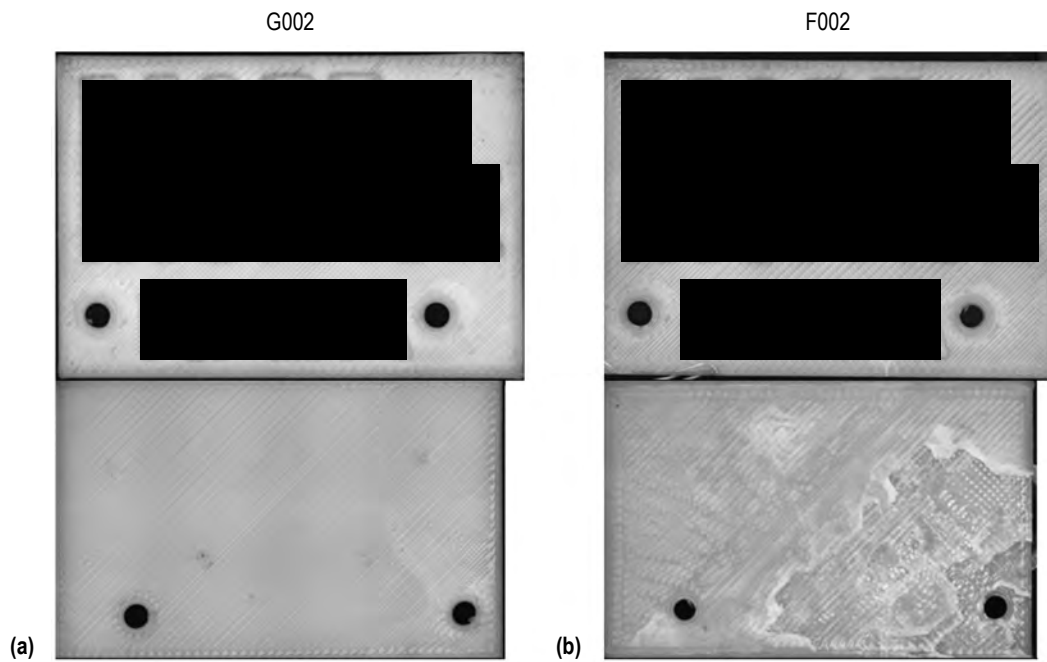
Figure 37. Plan views of top and bottom of extruder plate for both (a) ground and (b) flight.

Side views of the extruder plates (fig. 38) show the peel-up that occurred during the build process. The effect of warping on dimensional variation for this part is discussed extensively in section 6. The positive and negative range coupons (figs. 39 and 40, respectively) exhibited similar peel-up. Some of the holes on the ground specimen were not completed by the printer (apparent on the bottom plan view of specimen G007 in fig. 40).
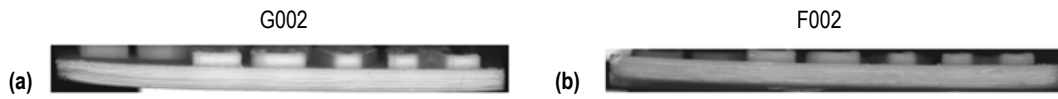
Figure 38. Side view of the extruder plate for (a) ground and (b) flight.
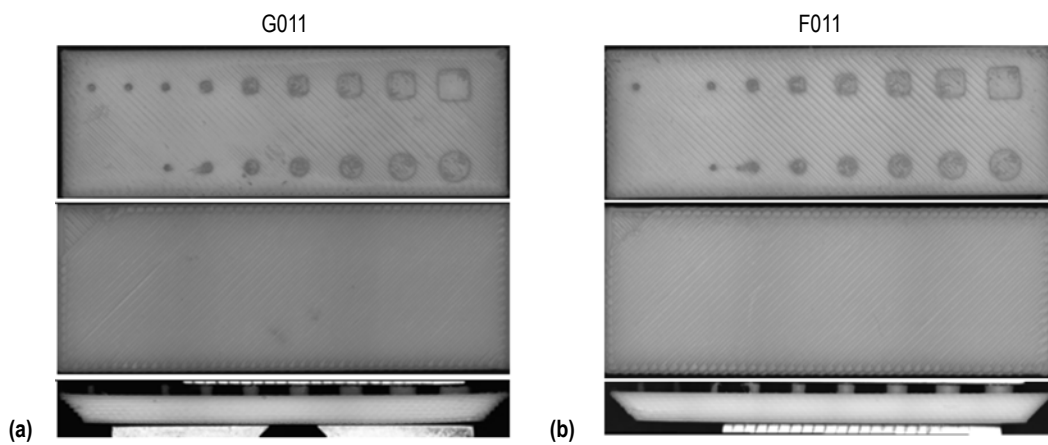
Figure 39. Plan and side views of (a) ground and (b) flight positive range coupons.
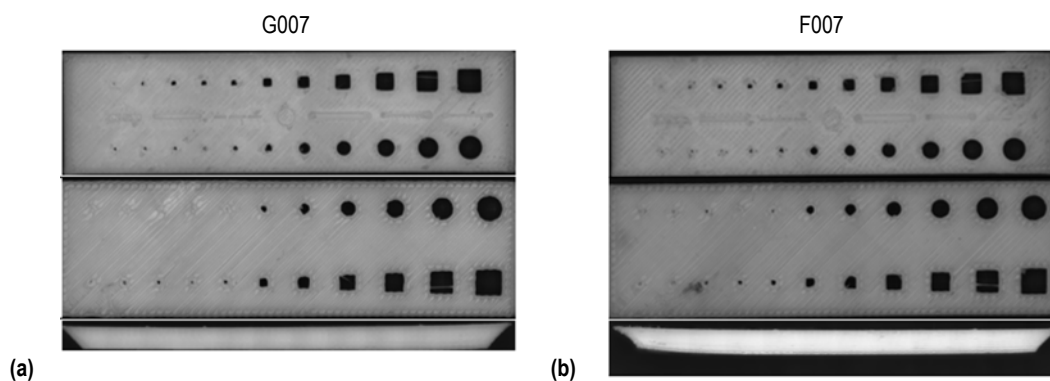
Figure 40. Plan and side views of (a) ground and (b) flight negative range coupons.

Many of the parts exhibited no apparent differences between ground- and flight-printed specimens. These include the torque coupon (fig. 41), the structural clip (fig. 42), and the microgravity structure specimen (fig. 43). For the crowfoot (fig. 44), protrusions were more pronounced on the bottom of the flight specimen and the ground specimen exhibited curling, observations which are corroborated by the findings from structured light scanning.
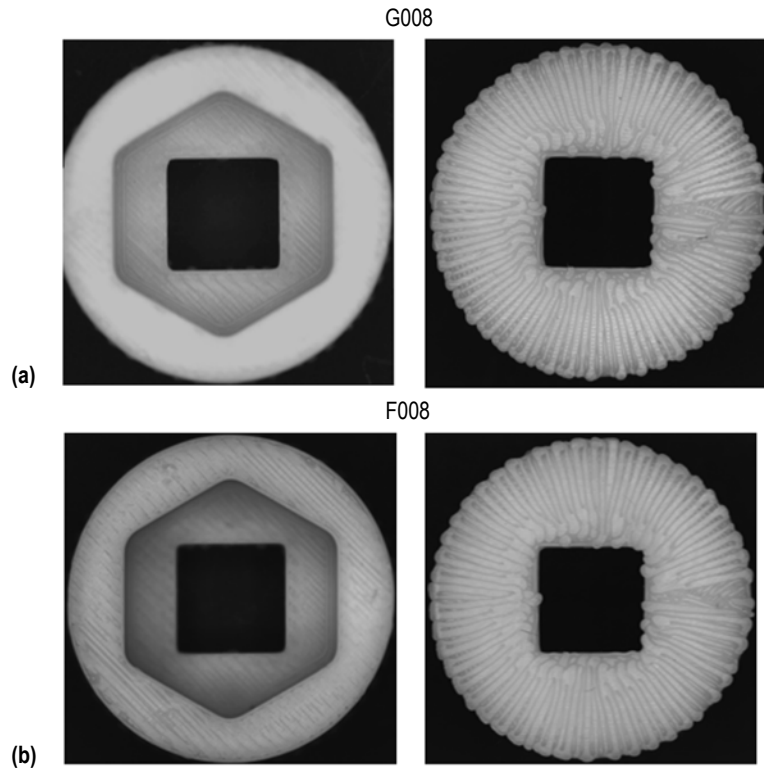
Figure 41. Comparison of plan views of (a) ground and (b) flight torque coupon.
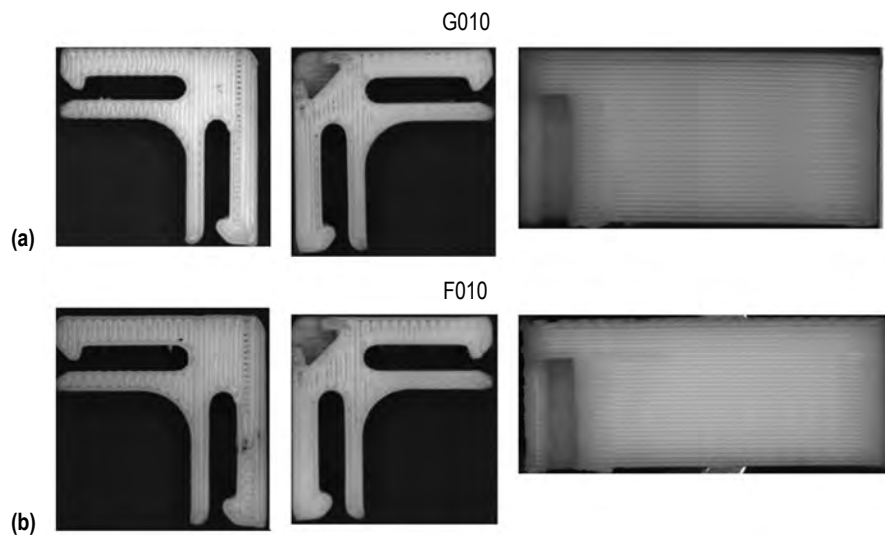
Figure 42. Comparison of (a) ground and (b) flight structural clip.

G019

(a)

F019

(b)
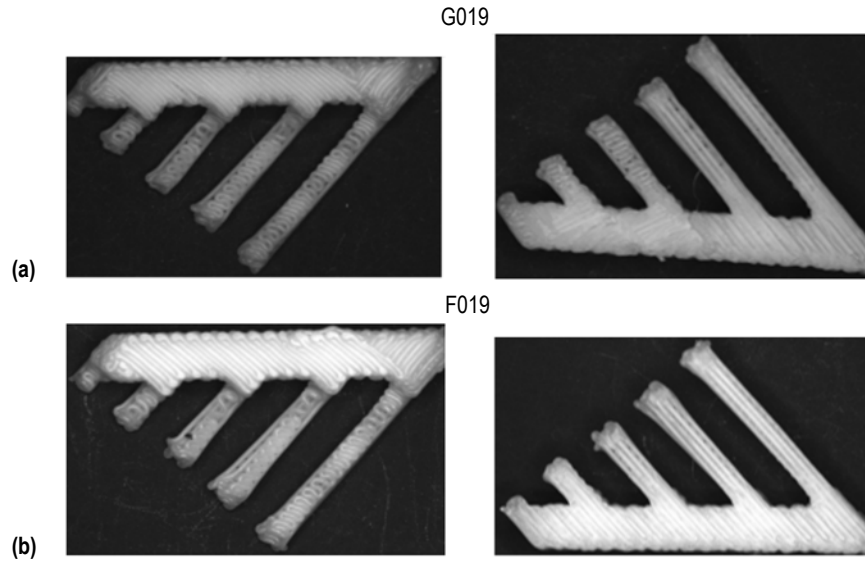
Figure 43. Comparison of (a) ground and (b) flight microgravity structure specimen.

(a)

(b)
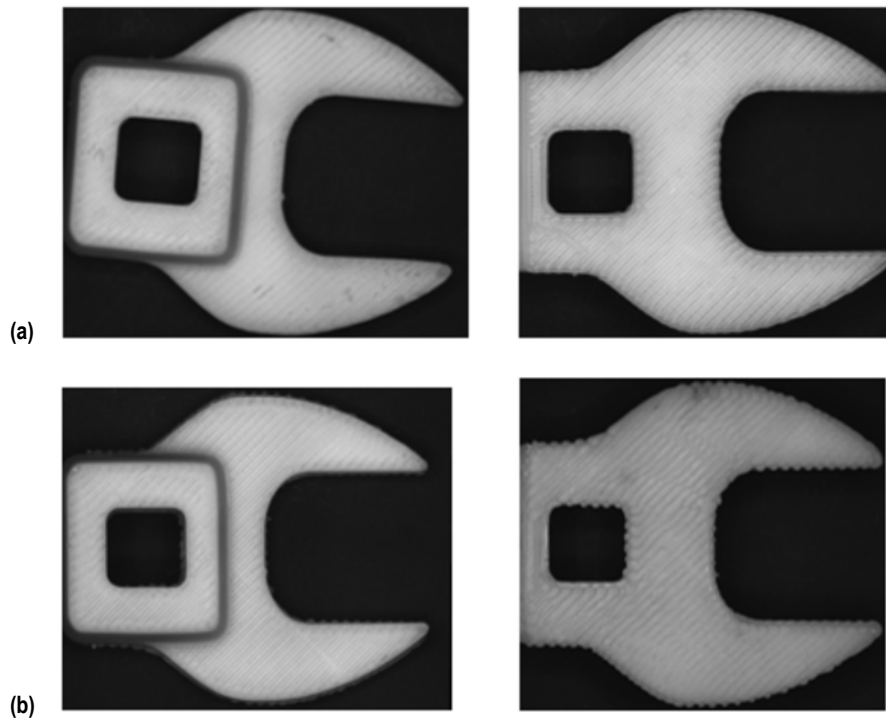
Figure 44. Comparison of (a) ground and (b) flight crowfoot specimen.

In general, microscopy results complement the findings of other, more detailed analyses. Microscopy provides a cursory examination of surface features and macroscale structural differences between flight and ground specimens. Key findings of note are extreme warping (particularly on the extruder plate), protrusions along the boundaries of specimens (evident in the crowfoot), and greater densification in the lower half of the specimens (corroborated by CT, although this density variation within the part was determined not to be statistically significant). Breaks in the tensile specimens come in two varieties: straight or aligned with the filament at a 45° angle. The location and type of break is not consistent within or across specimen classes. Breaks slightly outside the extensometer footprint may be characteristic of a type IV tensile specimen and/or ABS. These observations are discussed further in sections 4, 6, and 7, but seem to be linked to printer performance, repeatability, operations, and/or coupon design rather than microgravity effects on the FDM process.

6. STRUCTURED LIGHT SCANNING RESULTS

6.1 Scan Procedure

Structured light scanning was conducted to create a detailed dataset needed to characterize surface geometric variations between the printed part and the CAD model analogous ground and flight specimens. Point cloud data from structured light were also used to obtain a value for the volume of the closed part surface used in the gravimetric density calculation.

The scanning took place at MSFC using the ATOS II Triple Scan blue LED scanner. The scanner has an accuracy of ± 12.7 μm at these volumes and the capability to capture stereoscopic images at a resolution of 5 million pixels per scan. The samples were coated in dry talcum powder (nonreactive with the ABS plastic) to reduce the reflectivity of the sample surfaces, thereby improving scan accuracy. The talcum powder grain size is ≈10 μm in diameter, and thus had little effect on the measurements made by the scanner.

The software package that accompanies the ATOS scanner uses the stereoscopic images to capture the fringe pattern sent out from the central LED projector. The software triangulates all of the surface data (using the grayscale pixels, black and white contrast from the fringe pattern) to determine the shape of the geometry. Through this process, the software generates a complete 3D model of the object being scanned. The software also provides real-time feedback to indicate missing surface data. Missing data are captured during subsequent scans.

The software package Geomagic was used to compare the virtual objects generated from the scans with both (1) the corresponding CAD model used to make the print and (2) corresponding geometries from the ground or flight class of specimens. Geomagic indicates dimensional variations from the reference specimen (which may be the CAD model or a part from another scan). Geomagic also calculates the volume of the printed parts from the scan data and makes geometric measurements of part features (length, height, diameter, etc.).

6.2 Z-Calibration Value and Tip-to-Tray Distance

One of the key findings of structured light scanning is the effect of the tip-to-tray distance (defined as the distance between the extruder tip and the build tray that material is deposited) on dimensional variation. This distance was held constant for the ground prints, but was varied for the flight prints based on in situ assessments of printer performance made by Made In Space during operations. The tip-to-tray distance value is derived from the z-calibration value, which is commanded to the printer by the user during the print start procedure. The z-calibration value is a measurement (in millimeters) between the build surface home position and the desired location of the build surface position during printing. The z-calibration value set by the user drives the tip-to-tray distance. The relationship between z-calibration and tip-to-tray distance is illustrated in figure 45. Ideally,

the tip-to-tray distance should be 0.2 mm; however, this value cannot be directly measured with the existing 3DP hardware during flight operations since it lacks closed loop positional feedback control. The tip-to-tray distance thus must be inferred from the commanded z-calibration value (and there is no verification that actual values correspond to commanded values for flight operations). The z-calibration value will also be different for each build tray and extruder tip used since there is some geometric variation in these parts. Four build trays (designated F01 through F04) were used for the flight prints. Ground prints were completed with a single build tray (U-022).
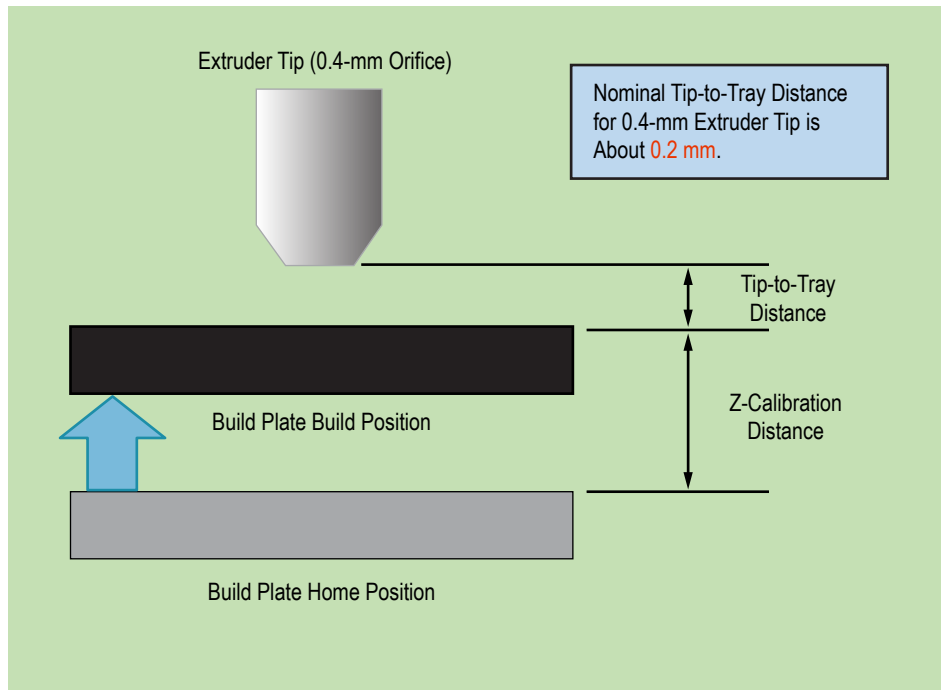
Figure 45. Relationship between z-calibration value (commanded by user) and tip-to-tray distance. For flight prints, tip-to-tray distance is not directly measurable since 3DP does not have closed loop positional feedback.

Specimens built with the extruder tip 'too far' from the build plate exhibit distinct features from those that were built with the extruder tip at a closer distance. For the set of ground control samples, a z-calibration value of 2.2 mm was used. The resultant samples consistently exhibited characteristics of having been built too far from the build surface (tip-to-tray distance >0.2 mm). Most of the ground samples (per data from structured light scanning summarized in sec. 6.3) were severely warped and showed very little protrusion along the bottom edges. However, the flight samples showed little consistent behavior with regard to the commanded z-calibration value and the resultant sample quality. Although the majority of the flight samples exhibited traits indicative of having been built too close to the build surface (tip-to-tray distance <0.2 mm), several were given z-calibration values that should have resulted in 'too close' or 'nominal' behavior. The relationships between tip-to-tray distance and dimensional variation of the parts are further explored in section 6.3.

Tables 18 and 19 tabulate the z-calibration values used for each sample during flight and ground operations, respectively. The higher z-calibration values correspond to lower tip-to-tray distances (and lower values correspond to larger tip-to-tray distances). The samples highlighted in yellow are samples that sustained damage during part removal. In the case of the highlighted flight samples, these prints over-adhered to the build surface. The highlighted ground sample in table 19 had a delamination between the first and second layers; however, overall the build exhibited behavior that leads to an off-nominal (extruder tip too far from build tray) classification.

Table 18. Z-calibration values for 3DP phase I flight operations.

Print Tray	Part No.	Part Name	Manufacturing Date	Z-Calibration Value	Assessment of Tip-to-Tray Distance Based on Part Quality
F01	F001A	Calibration coupon	11/17/2014	2.39	Too far
	F001B	Calibration coupon	11/21/2014	2.72	Nominal
	F002	Extruder plate	11/24/2014	2.84	Too close
F02	F001C	Calibration coupon	11/25/2014	2.69	Slightly too close
	F003	Layer quality specimen	12/2/2014	2.69	Slightly too close
	F004	Tensile 1	12/2/2014	2.69	Too close
F03	F001D	Calibration coupon	12/2/2014	2.79	Too close
	F005	Compression 1	12/3/2014	2.79	Slightly too close
	F006	Flexure 1	12/3/2014	2.75	Too close
	F007	Negative range specimen	12/4/2014	2.75	Too far
	F008	Torque coupon	12/4/2014	2.75	Too close
	F009	Crowfoot	12/4/2014	2.75	Too close
	F013	Compression 2	12/5/2014	2.75	Too close
	F011	Positive range specimen	12/5/2014	2.75	Slightly too far
	F012	Tensile 2	12/6/2014	2.73	Too close
	F014	Flexure 2	12/6/2014	2.75	Too close
	F015	Tensile 3	12/6/2014	2.71	Slightly too close
	F016	Compression 3	12/6/2014	2.71	Too close
	F017	Flexure 3	12/7/2014	2.71	Nominal
	F018	Tensile 4	12/8/2014	2.69	Too close
F04	F001E	Calibration coupon	12/8/2014	2.64	Too close
	F020A,B	Sample container and lid	12/8/2014	2.64	Nominal
	F010	Structural clip	12/9/2014	2.64	Nominal
	F019	Microgravity structure specimen	12/9/2014	2.64	Nominal
	F021	Ratchet	12/15/2014	2.64	Slightly too close

Table 19. Z-calibration values for 3DP phase I ground operations.

Print Tray	Part No.	Part Name	Manufacturing Date	Z-Calibration Value	Assessment of Tip-to-Tray Distance Based on Part Quality
U-022	G001	Calibration coupon	5/7/2014	2.2	Too far
	G002	Extruder plate	5/7/2014	2.2	Too far
	G003	Layer quality specimen	5/7/2014	2.2	Nominal
	G004	Tensile 1	5/7/2014	2.2	Too far
	G005	Compression 1	5/7/2014	2.2	Nominal
	G006	Flexure 1	5/7/2014	2.2	Too far
	G007A	Negative range specimen	5/7/2014	2.2	Too far
	G007B	Negative range specimen	5/7/2014	2.2	Slightly too far
	G008	Torque Coupon	5/7/2014	2.2	Nominal
	G009	Crowfoot	5/8/2014	2.2	Too far
	G010	Structural Clip	5/8/2014	2.2	Nominal
	G011	Positive range specimen	5/8/2014	2.2	Too far
	G012	Tensile 2	5/8/2014	2.2	Too far
	G013	Compression 2	5/8/2014	2.2	Nominal
	G014	Flexure 2	5/8/2014	2.2	Too far
	G015	Tensile 3	5/8/2014	2.2	Too far
	G016	Compression 3	5/8/2014	2.2	Nominal
	G017	Flexure 3	5/8/2014	2.2	Too far
	G018	Tensile 4	5/8/2014	2.2	Too far
	G019	Microgravity structure specimen	5/9/2014	2.2	Nominal
	G020A,B	Sample container and lid	5/9/2014	2.2	Slightly too far
	G021	Wire tie	5/9/2014	2.2	Nominal

Situating tables 18 and 19 within the context of structured light scanning and other analyses, there are instances that show a wide variation of resultant part quality while the z-calibration value remained constant. There are also instances where the z-calibration was lowered after building a sample of nominal quality (increasing the tip-to-tray distance) that produced a sample with characteristics commensurate with having been built too close to the build tray (e.g., sample F018). It is unclear to what extent the z-calibration (and subsequently determined tip-to-tray distance) is predictive of material quality and/or the degree of dimensional variation. Subsequent studies (discussed in sec. 9) seek to explore this relationship systematically. Variation in the z-calibration between builds during flight operations makes the dataset more difficult to analyze and compromises the ISM team's ability to draw conclusions regarding microgravity effects on the FDM process.

6.3 Key Findings

An initial analysis of the data showed that almost all of the samples from both flight and ground were significantly warped and slightly shrunken. Warping is most evident in flat parts such as the tensile, flexure, and extruder plate specimens. As noted in section 6.2, the flight samples were generally built with the extruder tip too close to the build surface, whereas the ground control samples were generally built too far from the build surface. Most of the flight samples exhibited significant protrusion along bottom edges; in particular, the first layers protruded beyond the desired contour surface. However, most of the ground samples exhibited less protrusion but pronounced warping, which is indicative of poor adhesion resulting from the extruder tip being too far from the build surface. The data do not appear to show a good, direct correlation between the commanded z-calibration value and the resultant quality of the flight samples; however, the ground samples were far more consistent. Some of the samples built on ISS were built with commanded z-calibration values that should have been lower than nominal (too far) but still resulted in the specimens' too close characteristics. Additionally, all of the circular samples (compression samples, torque coupon, and sample container) were slightly 'out of round.' By measuring the major and minor axes of the cross sections, the data show that the flight samples were more out of round than the ground samples by about 17%.

6.3.1 Warping

Warping effects noted in structured light scan data are most likely a result of 3DP having a nonheated build chamber and nonheated build surface. The uncontrolled thermal environment, coupled with ABS having a relatively high coefficient of thermal expansion, allows internal stress relief to occur prematurely (i.e., before the printed part is complete). The lower layers tend to cool and contract during the build process, causing the part to detach from the build surface. This permanently warps the part and can adversely affect the quality of the upper layers. The degree of warping is driven by the surface area of the part and the surface area-to-volume ratio. Small parts with small footprints in the *x-y* plane showed little sign of warping or shrinkage. Flat parts with larger footprints tended to warp, whereas larger parts (height ≥ plan surface area in contact with build tray) tended to shrink (or both in some cases). Incorrect z-calibration is known to exacerbate warping.

Figures 46 and 47 show the top and bottom surfaces, respectively, of a flight and ground flexure sample prior to mechanical testing. The colors correspond to the location of the scanned data points with respect to the original CAD file. Blue hues indicate that the scanned data points are below the CAD surface, whereas yellow to red hues indicate that the scanned data points lie above the CAD surface. Green indicates that the scanned data points align with the CAD surface.
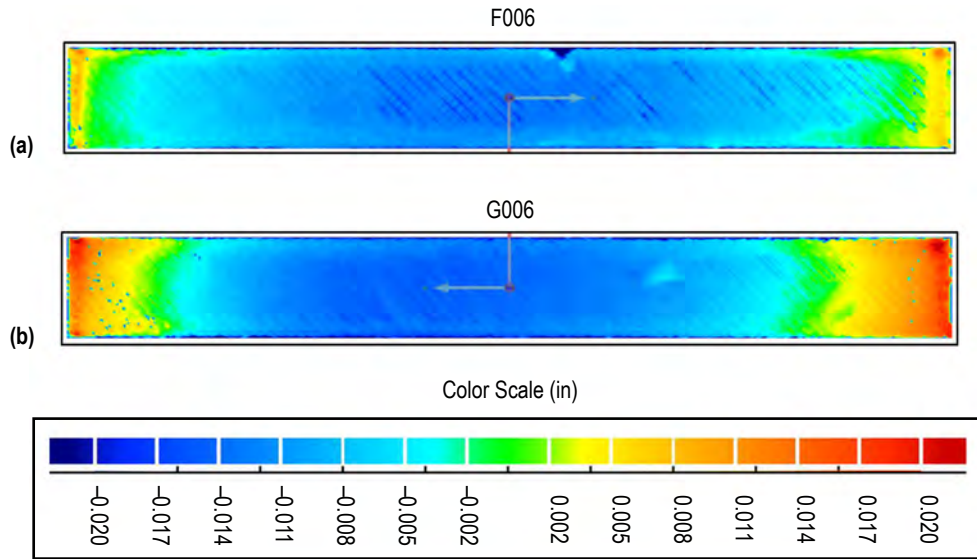
Figure 46. Comparison of (a) flight and (b) ground flexure specimens (top surface) with nominal CAD geometry.
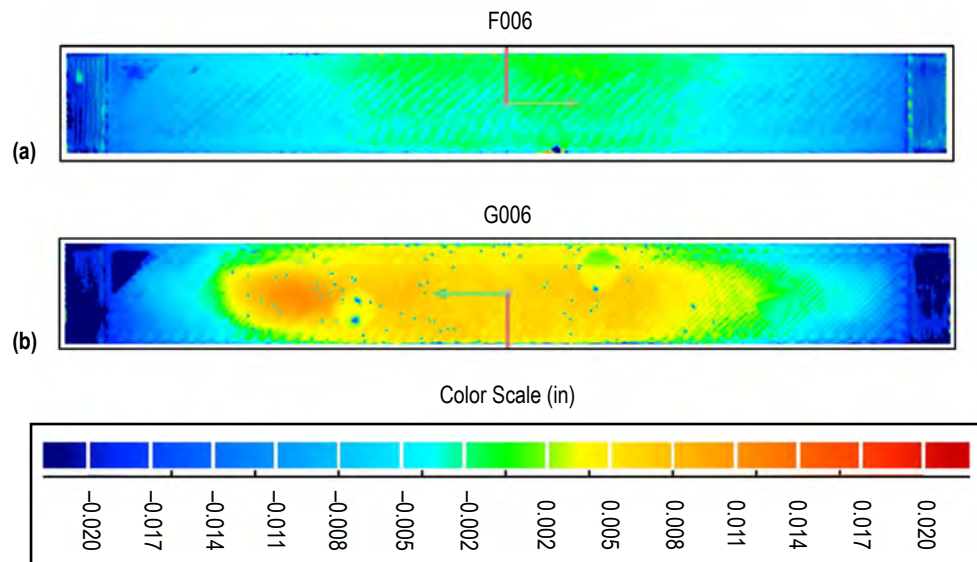
Figure 47. Comparison of (a) flight and (b) ground flexure specimens (bottom surface) with nominal CAD geometry.

Figure 48 is a whisker plot of flight and ground tensile samples. The images are obtained from 2D cutaway views of the sample. The whiskers' colors and lengths indicate where the scanned data points are in relation the CAD surfaces. The lengths of the whiskers are exaggerated by a factor of five for visibility.
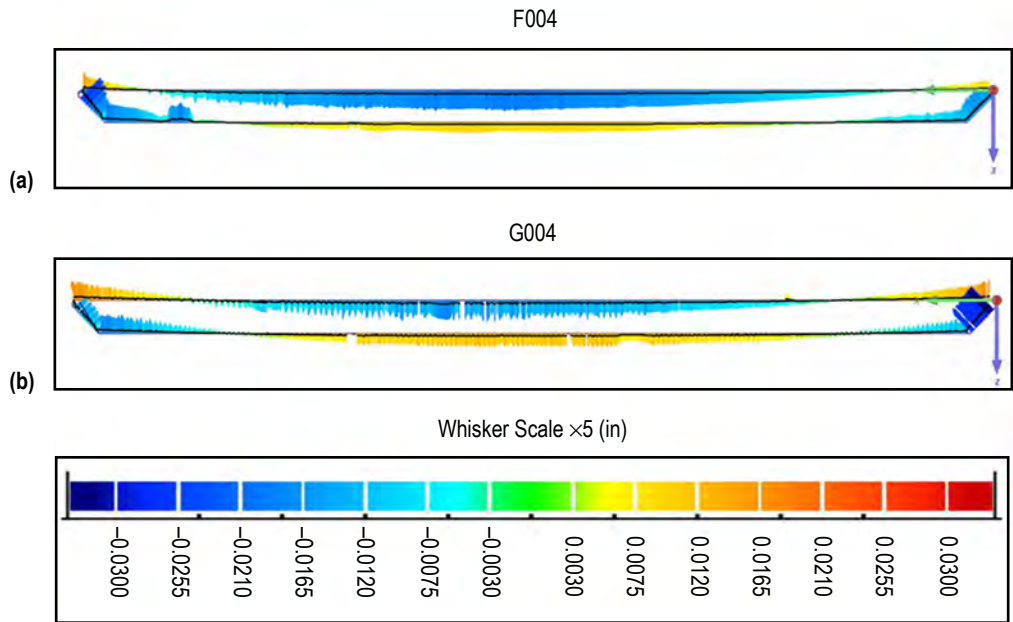
Figure 48. Whisker plot of (a) flight and (b) ground tensile specimens. Lengths of whiskers are exaggerated by a factor of five for visibility.

Figures 46–48 are representative of a general trend that the ground samples exhibit slightly more warping than the flight samples (an indication that ground specimens were built with the extruder tip too far from the build tray). This observation can also be quantified from surface measurements. Representative measurements of data points in the midsections and at the ends of the specimens were compared for ground and flight. The differences (Δ) between (1) one end of the sample and the midpoint of the sample and (2) the other end of the sample and the midpoint were averaged. The averages of the Δ values for the tensile and flexure samples are tabulated in table 20.

Table 20. Comparison of average distances between the midplane of the specimen and specimen ends for ground and flight.

Sample Type	Average Δ Flight (in)	Average Δ Ground (in)	Percent Difference
Tensile	0.0245	0.0267	8.7
Flexure	0.0170	0.0289	52.1

6.3.2 Protrusion of First Layer

Many of the samples exhibited protrusion in the vicinity of the first layers. Protrusion occurs when extruded material expands outside of the prescribed contour of the samples. These protrusions were mostly observed in the flight samples, an indication that the extruder tip was too close to the build surface for these prints. When the extruder tip is in the too close position, the bead of extruded material is wider than nominal, causing the material to protrude outside of the contour. Figures 49 and 50 clearly show these protrusions along the bottom edges of the samples. Figure 49 is a side view of a flight flexure sample. Protrusions are seen as red spots along the bottom edge. Figure 50 is a whisker plot midsection cutaway view looking down the long axis of a tensile sample. Significant protrusions can be seen along the bottom edges on either side of the tensile sample.
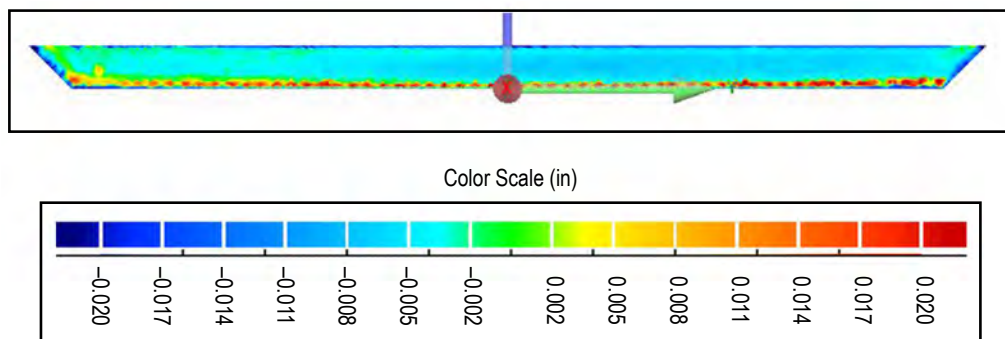
Figure 49. Protrusions detected on first layers of flight flexure specimen F014.
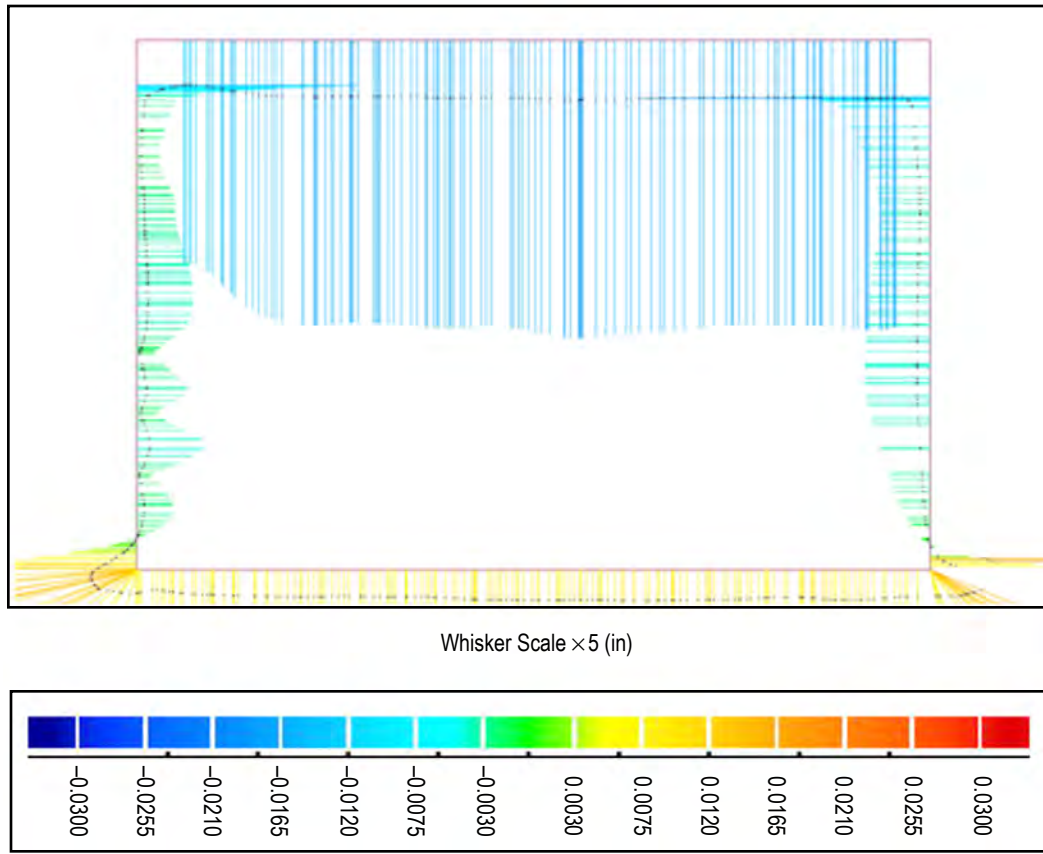
Figure 50. Midsection cutaway view of flight tensile specimen F004 showing protrusions along some edges.

6.3.3 Printer Accuracy and Circularity

Measurements of the range specimen features were extracted from Geomagic for the purposes of characterizing printer accuracy and performance. Diameters of the circular samples were collected as well to quantify roundness. These included the compression samples, torque coupon, and the sample container. The measurements were taken by highlighting the relevant areas of the scan data and then calculating appropriate feature shapes (cylinders, circles, squares, etc.) using a best fit algorithm of the selected areas.

The features of the range specimens consisted of pegs and holes of both square and circular cross sections with characteristic dimensions ranging from 0.75 to 4 mm. There were also short walls and trenches of widths ranging from 0.35 to 1.05 mm. Some of the smaller features of the range specimens were missing too much data or the data were too noisy to construct a best fit. Several of the smallest range specimen features were missing altogether due to machine and process limitations (also noted on microscopy). Table 21 catalogs the average errors of the ground and flight range specimen features as well as the associated percent errors (with respect to the dimensions specified in the CAD files). The negative values indicate that the specimen features were undersized on average.

The flight range specimens were printed more accurately than their ground counterparts. The values in table 21 for the circular features are based on averages and do not account for roundness. Similarly, the averages of length and width of the square features were used in this calculation, which do not account for the aspect ratio.

Table 21. Dimensional error in features of range coupon for ground and flight specimens.

Total Averages	Average Error Ground (mm)	Average Error Flight (mm)	Percent Error Ground (%)	Percent Error Flight (%)
All features	–0.1283	–0.1190	–10.65	–8.00
Circular features	–0.1719	–0.1625	–13.91	–7.59
Square features	–0.1346	–0.1126	–11.51	–9.63
Walls/trenches	–0.0073	–0.0379	–0.59	–3.82

A similar measurement approach was used to quantify roundness for the circular specimens (compression samples, torque coupon, and sample container). First, the circular surface was highlighted and used to calculate a best fit cylinder. The average diameter was determined based on the best fit cylinder. Figure 51 shows a compression sample with the best fit cylinder superimposed. Note the dark and light blue sections of the cylinder. The dark blue sections correspond to areas of the scanned data that were outside of the best fit cylinder, whereas the light blue portions represent points that lie inside the best fit cylinder. Additionally, each light and dark blue section has a corresponding section with the same shading on the opposite side of the cylinder, indicating that the samples' cross sections are indeed elliptical. To define the major and minor axes, two additional best fit cylinders were calculated by highlighting only the dark and light blue sections, respectively. Table 22 illustrates that the flight specimens are generally more eccentric than the ground counterparts. While both flight and ground specimens' diameters are undersized when compared to the original CAD dimensions, the flight specimens' cross-sectional areas are smaller than the ground counterparts.

The accuracy and roundness measurements holistically indicate that during flight operations the machine was more accurate (demonstrated by its ability to make smaller features relative to ground specimens), but less able to hold tolerance (larger circular features were obtained for the ground prints). The reason for this cannot be ascertained from structured light scan data alone.
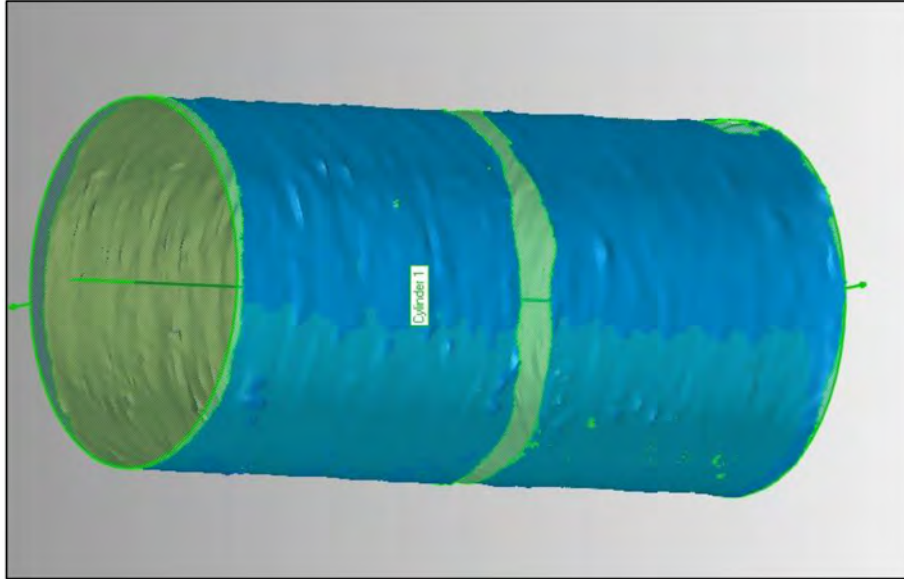
Figure 51. Compression cylinder with best fit cylinder superimposed.

Table 22. Comparison of eccentricity for ground and flight compression specimens.

Total Averages	Eccentricity	Elliptical Cross-Sectional Area (mm²)	Percent Error of Cross Section WRT CAD
Flight	0.1364	121.68	4.11
Ground	0.1153	123.03	2.96
Percent Difference	16.75%		

6.4 Conclusions

Most of the differences in geometry between flight and ground samples may be attributable to variation in the z-calibration distance (and subsequent) tip-to-tray distance between the two phases of operation. While both sets of samples were significantly warped, the excessive protrusions in the flight samples indicate that the extruder was in general too close to the build surface during flight prints. There could also be a difference in the way the polymer cools and contracts in microgravity (discussed further in sec. 7.3.1) that explains some of the geometric discrepancies observed in the phase I dataset. Differences in the cylindricity of the compression samples could potentially point to a microgravity effect on machine operations. Increased error in the moving parts of the machine, referred to as 'microgravity tolerance stackup,' is sometimes present in hardware operating in a microgravity environment. Further studies, discussed in section 9, will help to evaluate this.

7. INTEGRATED CONSIDERATION OF TEST DATA AND HYPOTHESES DEVELOPMENT

The individual analyses from mechanical and density testing, x-ray and CT, optical microscopy, and structured light scanning (detailed in secs. 3–6 of this TP) were performed in isolation. This section looks at the data in an integrated, holistic manner with the following objectives in mind:

• Assessment of the effects of microgravity on the FDM process (i.e., are any of the differences observed in flight and ground specimens in any of the phases of testing clearly attributable to operation of the FDM process in microgravity). If information from this dataset is insufficient to definitively answer the question of microgravity effects, the ISM team must identify what further analysis and testing needs to be done.

• Identification of influence variables in the 3DP dataset, which may explain observed differences in gravimetric density and mechanical properties for ground and flight specimens (also includes identification of unknowns in the 3DP dataset).

• Development of testable hypotheses to explain variability in data using root cause analysis techniques, evaluation of supporting and contraindicative data for each hypothesis, and classification of hypotheses on the basis of credibility/technical merit and likelihood of occurrence.

• Definition of a go-forward plan to further evaluate hypotheses with the greatest potential to explain property variations and elucidate what effect, if any, microgravity has on the FDM process.

7.1 Summary of Key Findings

Looking across the phases of testing and subsequent data analyses, the following key observations were noted. These findings are discussed extensively in the individual sections on testing, but are reiterated here for completeness and to anchor the development of hypotheses based on these findings.

7.1.1 Summary of Density Evaluation and Mechanical Testing

Gravimetric density, ultimate tensile strength, modulus of elasticity, fracture elongation, compressive strength, compressive modulus, flexural strength, and flexural modulus were significantly different for the ground and flight specimens. The density differences for mechanical test specimens and mechanical material property differences observed during mechanical testing are summarized in tables 23 and 24.

Table 23. Summary of density differences for 3DP
ground and flight mechanical test coupons.

Specimen Type	Percent Difference (With Respect to Ground)
Tensile	3.43
Compression	−2.60
Flexure	5.55

Table 24. Summary of mechanical material property differences.

Material Property	Percent Difference (With Respect to Ground)	Coefficient of Variation (Flight) (%)	Coefficient of Variation (Ground) (%)
Ultimate tensile strength (ksi)	17.1	6.0	1.7
Modulus of elasticity (msi)	15.4	6.1	2.7
Fracture elongation (%)	−30.4	26.3	9.9
Compressive strength (ksi)	−25.1	3.1	5.0
Compressive modulus (msi)	−33.3	9.4	4.2
Flexural strength (psi)	25.6	9.3	6.0
Flexural modulus (ksi)	22.0	9.6	3.9

Flight tensile specimens fail at a higher load and have a greater elastic modulus. On average, the percent elongation for the flight specimens is ≈30% less than the ground specimens. While not a true statistical outlier, flight tensile specimen 1 (F004) fits with the ground specimens in terms of strength, modulus, and percent elongation (fig. 5). In compression, flight specimens fail at a lower load and have a lower elastic modulus than ground specimens (fig. 6). In flexure, flight specimens have a greater flexural strength and flexural modulus than the analogous ground specimens (fig. 7).

Ground and flight specimens exhibit statistically significant differences in classical (gravimetric) density. In all but two cases, the percent difference in mean density between corresponding ground and flight specimens is <5%; for all specimens, the percent difference is <10%. In general, flight specimens are slightly denser than ground specimens. Exceptions are the three compression coupons and the positive range specimen (in these instances, the ground specimens have a greater gravimetric density). Looking at density variations for the ground and flight mechanical coupons more closely since material consolidation is generally a good predictor of mechanical performance, one finds that tensile and flexure flight specimens (which have higher strengths) are more dense than the corresponding ground specimens, but that the opposite bias holds for the compression specimens (ground specimens more dense than flight specimens). The mechanical property data follow the trends in density, as denser specimens are associated with better material properties.

7.1.2 Summary of Structured Light Scanning Results

The structured light scanning data indicated that almost all of the samples from both flight and ground were significantly warped. This warping is most pronounced in flat parts with a large surface area (i.e., the tensile, flexure, and extruder plate specimens). Flight samples were generally built with the extruder tip too close to the build surface, while ground samples were built with the extruder tip too far away from the build surface. Presumably as a result of the off-nominal tip-to-tray distance, flight samples exhibit significant protrusion along the bottom edges. Ground samples exhibit less protrusion, but have more pronounced warping. Correlation analysis of the commanded z-calibration value for the machine and the resultant quality of the part (assessed in terms of mechanical performance) does not yield a clear and consistent relationship. A controlled study where z-calibration (which determines tip-to-tray distance) is varied systematically is needed to assess the impact of this variable on material quality.

The warping observed in the specimens is hypothesized to be the result of two primary factors: (1) Internal stresses and (2) damage incurred during part removal. Nonuniform cooling of the specimen contributes to the buildup of internal stresses. The bottom layers of the specimen cool and contract while the upper layers are still being extruded. In extreme cases, the specimen will prematurely detach from the build surface, causing the upper layers to be thinner than intended. Warping is also a result of damage sustained during specimen removal, wherein an external force must be applied to remove the specimen from the rigid build surface. This applied force may permanently warp the specimen. Internal stresses and part removal have a synergistic effect; warping that occurs during separation of the part from the build tray is exacerbated by the presence of internal stresses. Warping is clearly evident in the structured light scans of the ground tensile and flight tensile specimens, shown in figure 52.
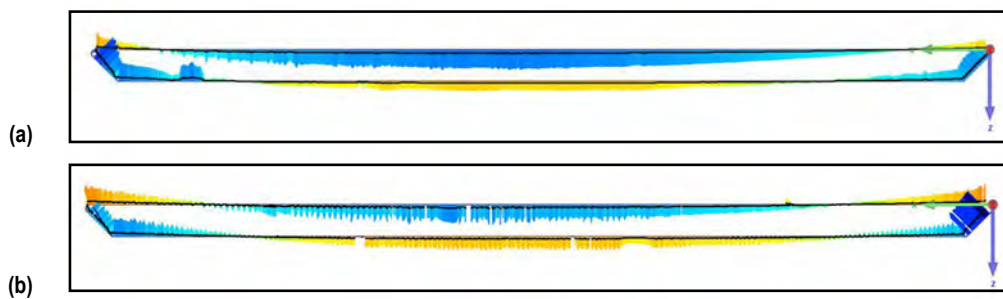
Figure 52. Structured light scan of front view of (a) ground tensile specimen G004 and (b) flight tensile specimen F004. The color scale indicates the magnitude of deviations from the nominal CAD geometry.

Some parts show evidence of warping occurring during the build process itself. This is likely attributable to poor adhesion to the build surface, as warping is more pronounced on the bottom surface (fig. 53). Reduced layer height toward the top of the part is also evident, an indication of the part's separation from the plate during the build (when the part becomes unadhered to the build surface, it reduces the tip-to-tray distance and affects a reduction in layer thickness). The increased roughness of the top surface of the part is further evidence of warping.
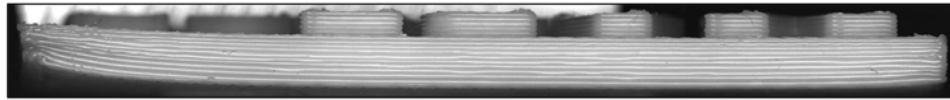
Figure 53. Left-side view of extruder plate (G002) under optical microscope. Warping on bottom surface is clearly evident and top surface experiences a reduction in layer height caused by de-adhesion of the part from the plate during the build.

Protrusions (an excess of extruded material) are another feature of note in the structured light scanning analysis. Protrusion is exacerbated by a decrease in tip-to-tray distance, as the extrusion flow rate increases when the extruder tip is off-nominal in this direction and material tends to expand outside of the desired contour boundary. The protrusions detected from structured light scanning are more pronounced in the flight specimens, an indication that the extruder tip was positioned too close to the build surface for this set of prints. Protrusions for a flight flexure specimen (F006) can be seen in figure 54. Figure 54(a) is a side view of the specimen taken during optical microscopy and figure 54(b) is the same specimen side imaged with structured light scanning (protrusions are the ridge-like features on the bottom of the specimen).

(a)

(b)
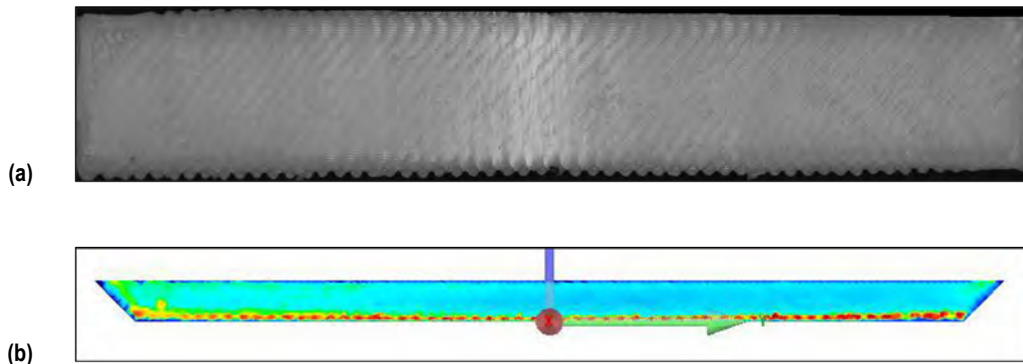
Figure 54. Protrusions on flight flexure specimen F006: (a) Side view during optical microscopy and (b) specimen side imaged with structured light scanning. The color scale indicates the magnitude of deviations from the nominal CAD geometry.

7.1.3 Summary of X-ray and Computed Tomography Results

Computed tomography of the mechanical test coupons was completed at MSFC in August 2015. Two-dimensional x-ray was also performed for all flight and ground specimens from 3DP phase I. The analysis of the scan data was performed by NDE personnel at MSFC using VGStudio 2.2. The key finding from CT analysis was that the bulk densities of the flight and ground articles (mean CT value) did not differ significantly. Density gradients in the through-thickness of specimens in the build direction were observed (the bottom half of specimens are generally more dense than the top half), but the density variation between these regions was not statistically significant. Review of the initial raw images from the CT scans (shown in fig. 55) confirm that the density of the material decreased as vertical distance from the build start point increased.
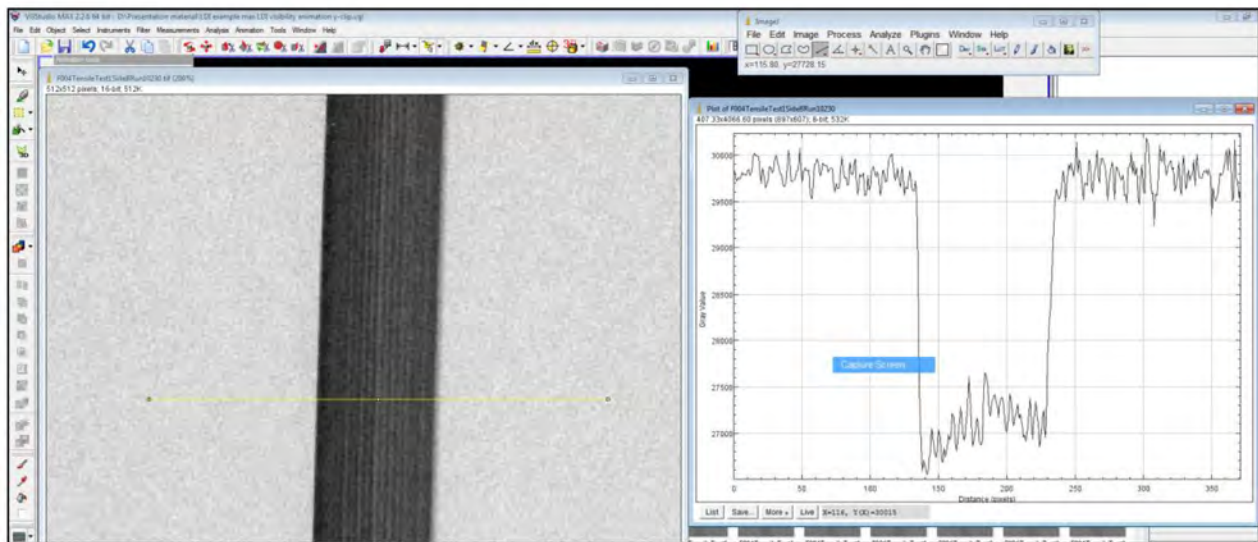
Figure 55. Raw image from CT scan of flight tensile coupon (F004) showing density differences between the upper and lower half of the specimen.

Voids were detected throughout the flight and ground articles, but porosity is characteristic of the FDM process, and no significant difference in size or frequency of voids for the flight and ground specimen sets was observed. Some LDIs detected in the specimens were profiled and compared against the density of air. An LDI with a density close to air is an indication of a probable void. Voids such as these are inherent to the filament deposition process and are most likely not related to microgravity.

Two types of voids were identified from CT and x-ray images: (1) Voids between filaments and (2) voids between infill and contour. The former (type I voids) are created by machine error in the placement of extruded filament. The latter (type II voids) are common for the FDM process and occur when the infill material does not attach to the contour material. This may also be a result of machine error, but may also be attributed to inefficient infill pattern (i.e., filling in an area with a curved contour with filament deposited in straight lines). Both types of voids were evident in flight

and ground samples and were most likely not related to microgravity, but inherent to the filament extrusion process. Significant waviness, probably caused by misalignment of the contour filament placement, was also noted on the outer surfaces of both the flight and ground samples. These features are illustrated in the 2D x-ray image of flight compression specimen F013 in figure 56. The type II void created due to inefficiency of infill pattern is commonly observed in specimens with contours (fig. 57 shows the presence of a type II void in the ground wire specimen).
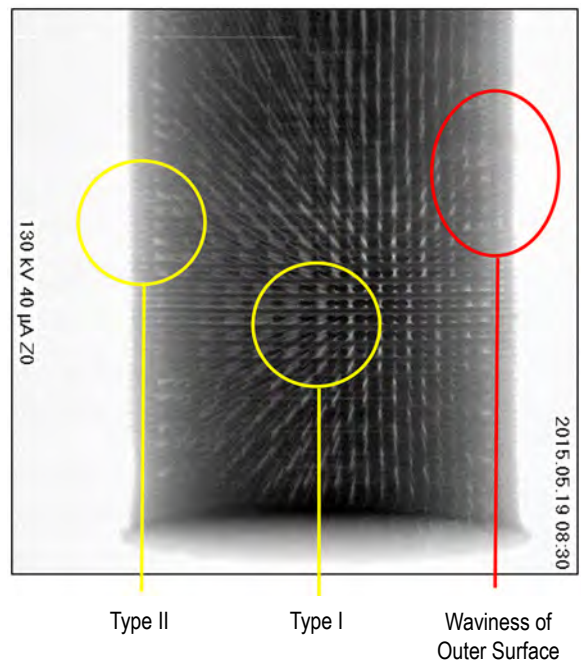
Figure 56. Two-dimensional x-ray image of compression specimen showing type I and type II voids and surface roughness.
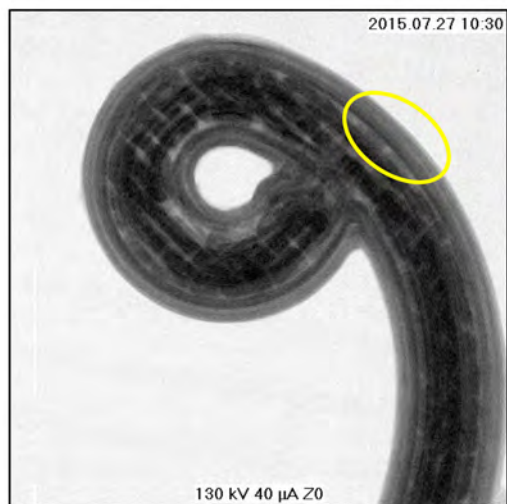
Figure 57. Type II void evident on 2D x-ray of wire tie specimen (G021).

7.1.4 Summary of Optical Microscopy

In optical microscopy, layer thickness measurements were obtained from images of 3DP specimens. Overall, no significant difference in layer thickness was observed between flight and ground specimens with this analysis. Additionally, no significant difference in layer thickness was noted between upper and lower layers, with the exception of specimens that experienced warping when the specimen separated from the plate during the build. For the extruder plate, the separation from the build plate results in the extruder tip being closer to the part being fabricated and artificially decreases thickness in layers deposited following this de-adhesion. Fracture surfaces of tensile samples (fig. 58) were also examined. Many (but not all) of the tensile specimens broke along filament lines (45°), as 'failure follows fiber.' Some possible bubbles that may be associated with filament voids were detected in two samples, including the extruder plate (fig. 59).
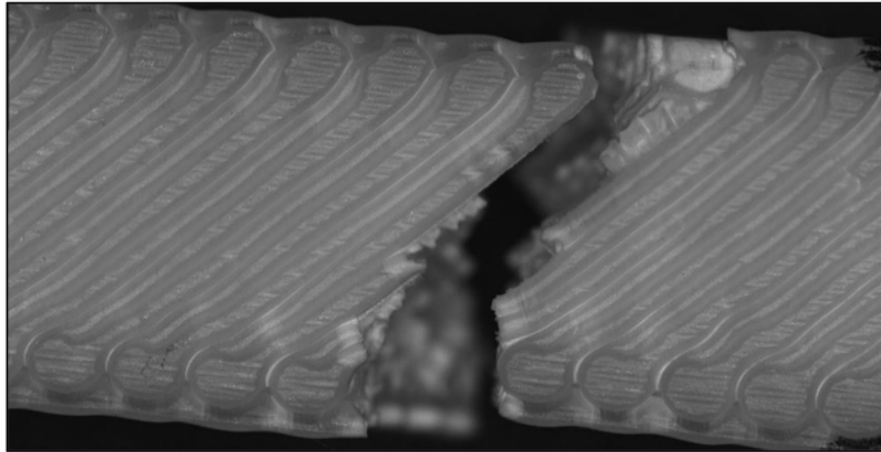
Figure 58. Fracture surface of ground tensile specimen (G015).
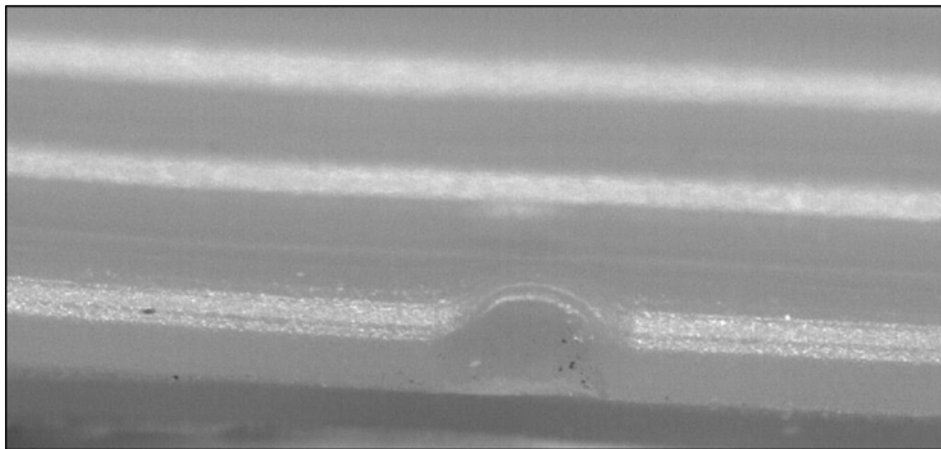
Figure 59. Possible filament void bubble in the extruder plate specimen G002.

7.2 Notes on Printer Operations

This section discusses the following aspects of printer operations that are relevant to the development of hypotheses that may explain variability in the dataset:

- Feedstock—Feedstock used to produce the ground and flight specimens was of identical material and originated from the same manufacturing lot. However, the canisters for flight and ground feedstock were different. Additionally, the flight feedstock, while still within the limits on shelf life specified by the manufacturer, was 5 to 6 months older than the ground feedstock at the time of printing.

- Changes in build tray—The build tray was changed over the course of the flight prints. Four build trays were used to produce the 21 flight specimens. Table 25 summarizes the trays and associated specimens.

- Changes in z-calibration distance—As discussed in section 6, the z-calibration distance (and subsequently, the distance between the extruder plate and the build tray, which is driven by the z-calibration setting) was changed during flight prints. This distance was held constant for ground prints. However, z-calibration is not a directly measureable metric since the 3DP hardware does not have closed loop positional feedback. A correlation analysis, predicated on the assumption that the actual and commanded z-calibration distances are equivalent, found no consistent and significant relationship between the z-calibration value (and tip-to-tray distance) and material properties. The relationship between density of the flight specimens and z-calibration distance was also very weak. For this dataset, calibration does not seem to be predictive of material consolidation or mechanical performance; however, it is difficult to draw conclusions about its true impact since it was varied nonsystematically.

Table 25. Build tray and specimens for flight prints.

Print Tray ID	Specimens
F01	Calibration coupon F001A and F001B, extruder plate
F02	Calibration coupon F001C, layer quality specimen, tensile 1
F03	All other specimens
F04	Calibration coupon F001E, sample container and lid, structural clip, microgravity structural specimen, ratchet

7.3 Exploration of Potential Influence Factors

A fishbone diagram was developed by the ISM team and Ken Johnson, a NASA statistician, to explore possible influence factors that could account for the observed variability in the 3DP dataset. The factors were broadly divided into five categories:

(1) Manpower—Factors related to human interaction with the printer hardware. This encompasses removal of the part from the build tray, differences in operators, and other as-yet-unidentified human factors.

(2) Material—This includes differences in feedstock (moisture absorption, dimensional variation, chemical composition, age, etc.) as well as radiation effects.

(3) Method—This category is comprised of variables specific to the printing process, which may be different for ground and flight or may change during the course of printer operations in a single environment: feed rate, z-calibration and tip-to-tray distance, extruder speed, print order, warpage and degree of adhesion to plate, cooling rate, densification, and specimen geometry.

(4) Machine operations—This category is closely related to (3), and there may be some overlap between the factors. Machine variables include print head temperature, printer repeatability/accuracy, hysteresis in mechanical systems, tray condition (surface roughness, cleanliness, etc.), the levelness of the plate, and forced convective cooling (presence and position of fans relative to the specimen).

(5) Environment—This includes factors related to the environment present when the specimens were printed: ambient temperature, environmental conditions (humidity and moisture, radiation, etc.), both exposure of the feedstock and the printed material, and microgravity.

The working diagram with the major factors and subdivisions appears in figure 60.
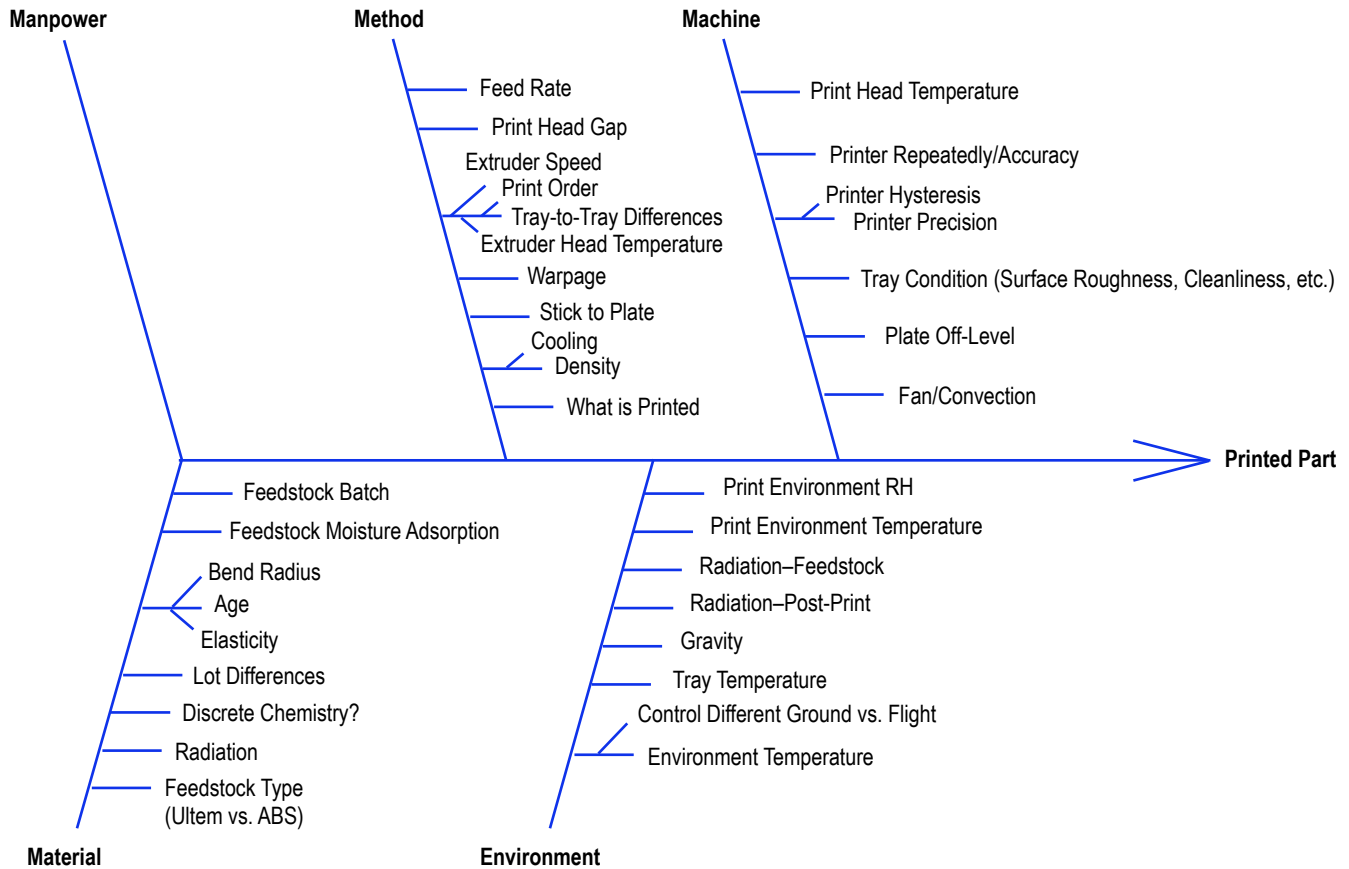
Figure 60. Fishbone diagram used to facilitate root cause analysis of variability in 3DP dataset.

Based on this working diagram, six potential influence factors were identified and prioritized for further evaluation: (1) Microgravity effects, (2) material aging (offgassing and humidity), (3) z-calibration and tip-to-tray distance, (4) test effects, (5) damage to specimens, and (6) other effects such as radiation and chemical variability of feedstock.

With each influence factor, a hypothesis (or, in some cases, hypotheses) was developed to explain the manner in which the identified factors may have contributed to the observed differences in ground and flight specimens in terms of densification, material properties, and/or dimensional variation. Supporting and detracting evidence for each hypothesis based on analysis of the 3DP dataset is discussed and open questions are identified (along with the need for additional analyses and/or experiments to generate further data related to a particular hypothesis). The influence factors and hypotheses were presented during the final session of the TIM held at MSFC (app. A) and discussed with participants, many of whom offered valuable information from their own work and research into FDM processes.

7.3.1 Microgravity Effects

7.3.1.1 Discussion. Although nothing in the test data specifically points to microgravity effects on the FDM process as a key contributor to variability (and KC-135 flights of developmental printer hardware prior to launch of the flight unit do not indicate that FDM is significantly impacted by microgravity over short time constants),[12] it is difficult to isolate microgravity effects in the current dataset due to the presence of other variables such as tip-to-tray distance that were changed nonsystematically. It is possible, however, that microgravity effects on the FDM process, which may manifest themselves as differences in cooling, adhesion of layers, tolerance stack-up of machine components in microgravity, differences in formation and distribution of material phases, etc., could result in differences in mechanical performance between flight and ground specimens. It is a well-known tenet of materials science that 'microstructure determines macrostructure' if there is some engineering-significant impact of microgravity on microstructure for ABS produced via FDM, which may be present in this dataset but is unable to be isolated due to the operational differences in processing of the flight and ground specimens.

Microgravity could potentially impact the morphology of the phase-separated domains of ABS produced via FDM. The formation of nonequilibrium phases may also be influenced by processing specimens in microgravity. Differences in the distribution of phases between ground and flight specimens have not yet been characterized, but a follow-on analysis of ground and flight specimens using atomic force microscopy (AFM) could provide insight into whether there is any significant change in phase morphology observed for flight specimens and if any detected difference is likely attributable to microgravity. This work could be performed at MSFC or NIST and has been identified as a potential additional analysis for existing ground and flight specimens.

Differences in thermal environment for the manufacture of ground and flight specimens have also not been fully characterized. The cooling rate of the printed part plays a key role in microstructural evolution and is largely determined by the specimen geometry (dimensions, surface area, and surface area-to-volume ratio). The ground specimens were printed on the flight unit for 3DP inside the ground mockup of the MSG prior to the printer's launch to ISS. The presence, position, and amount of convective cooling provided by fans and filtration systems within the MSG should thus be the same for both ground and flight prints. Buoyancy-driven convection within the part requires a thermal gradient, which is present in the ground-based prints; lower layers of the specimen cool first, and, for a time, are at a lower temperature than the upper layers, which consist of freshly deposited material. Buoyancy-driven/natural convective effects will likely be overwhelmed by forced convective cooling which is much larger in magnitude. Nonetheless, an identified difference in cooling is that natural convection will be absent in the microgravity specimens since the absence of a gravity term will drive heat transfer coefficients related to natural convective processes such as the Rayleigh number to 0. Surface tension effects dominate in microgravity, and it may be the case that the 'spreading' of the material after leaving the extruder is more pronounced for the flight prints. This is observed in soldering and electron beam welding experiments related to metals, where microgravity minimizes buoyancy and thermosolutal convection, thereby promoting a more uniform microstructure.[13] Differences in cooling due to microgravity and the dominance of surface tension during material deposition may account for the protrusions detected for the flight prints in structured light scanning data but could also be a consequence of the position of the extruder relative to the build tray for the

flight prints. Variance in build structure due to surface tension effects should also be evident on SEM analysis of ABS strands within the printed parts, another potential follow-on analysis for the 3DP specimens. Thermal modeling of the FDM process terrestrially and in microgravity represents work that is needed to better understand microgravity effects on the process. Results of this work may also provide insight into the observed density differences in the flight and ground specimens, as the cooling rate in materials processing is usually a key determiner in densification and void formation.

The other aspect of microgravity that has yet to be explored are effects on operating the machine itself in LEO. Commanded movements of the equipment could be different during operation on ISS due to microgravity-induced changes in drift, hysteresis, or other motor and system characteristics. Because the hardware does not have closed loop positional control, it is difficult to validate whether this is the case without evaluating the hardware components themselves. Tolerance stack-up (the cumulative effect of part tolerance) is a known factor in the operation of hardware on the ground, but effects can be exacerbated by operation in the absence of gravity. While the hardware underwent extensive evaluation and testing prior to launch, it is possible that operation of the machine on ISS for much longer time constants than the simulated microgravity flights could impact the function of the hardware and subsequently the performance of the parts produced using it.

7.3.1.2 Open Questions. The key open question related to microgravity effects is whether there are observable structural differences between flight and ground specimens that are attributable to microgravity. There were no consistent observable structural differences for ground and flight tensile or flexure specimens noted during CT. Optical microscopy, RT, and structured light scans of all specimens also did not identify any features that were clearly a result of processing specimens in microgravity. The larger protrusions observed for the flight specimens in structured light scanning may be a result of surface tension dominant flow processes in microgravity, but may also be an artifact of the closer tip-to-tray distance for the flight prints. Structured light scanning also revealed that cross-sectional views of flight compression specimens exhibit greater out-of-round behavior than corresponding ground specimens. (Out-of-round is defined as the deviation of compression specimen geometries from the nominal CAD geometry on the metric of circularity.) A follow-on investigation using the surface texture measurement capabilities of the tribology laboratory at MSFC is necessary to assess whether this may be a microgravity effect on the machine (and the prescribed manner in which the machine deposits material) or a consequence of the closer tip-to-tray distance for the flight prints. Since the loading of the compression specimens is in the z-direction and compression (in other materials) is typically a test that is sensitive to surface roughness, the compressive properties may be more sensitive to contour misalignment than properties in tension or flexure. A study to characterize the sensitivity of compressive properties to surface roughness for ABS produced via FDM is also needed and can be easily incorporated into other studies where compression specimens are produced. Irrespective of the cause, the increased out-of-round behavior for the flight specimens may explain their weaker performance in compression than the ground specimens.

Additionally, even if microgravity (and differences in cooling rates for flight and ground prints) has an impact on densification in the manner observed across the dataset (flight specimens are generally more dense than ground), the differences in density values for flight and ground specimens are very small (typically <5%). The sensitivity of mechanical properties of ABS produced via

FDM to changes in density has not yet been characterized by the ISM team and it is unclear whether a subtle variation in density can produce the large differences observed in mechanical properties (15% to 30%, depending on the specimen). Some information on the relationship between mechanical properties and density for ABS produced via FDM has been provided by TIM attendees and a follow-on study (which uses infill percentage to control densification) may also be needed to further evaluate this relationship. It is also unclear at the time of this writing whether differences in phase morphology in the microgravity specimens, if present, impact mechanical properties in the manner observed in the 3DP dataset.

7.3.1.3 Additional Testing and Analysis. Overall, more information on phase morphology and microstructure of 3DP specimens (ground and flight) is needed to fully assess the impact of microgravity on the FDM process and the resultant quality of manufactured material. AFM can be performed on existing ground and flight specimens to examine differences in phase morphology if desired. Additional specimens from phase II prints can also undergo this analysis. AFM can characterize differences in phase separation, phase morphology at interfaces, and the presence of nonequilibrium phases for the specimen classes.

Phase II print operations may be better poised to answer the question of microgravity effects since better manufacturing process controls (based on lessons learned from phase I operations) will be implemented. 'Locking' the manufacturing process (in particular, control of the tip-to-tray distance) will allow the ISM team to isolate the effect of microgravity on the material produced. The complexity of all comparative analyses in support of phase II work is that the ground control specimens, unlike 3DP phase I, will not be produced on the flight printer, but on the engineering test unit (ETU), a flight-like printer (and the backup flight unit for 3DP). Any ground-based prints to facilitate comparison will also not be performed in the MSG mock-up facility.

Physics-based modeling work at NASA Ames Research Center (ARC) and other research organizations can be used to assess differences in convective processes, cooling rates, and solidification for the flight and ground specimens. Construction of these models requires high-fidelity measurements of thermophysical properties for ABS as inputs. While ABS is a legacy material, properties of ABS produced via FDM are largely uncharacterized. Measurements of thermophysical properties for 3D printed ABS needed as inputs for physics-based models (e.g., specific heat at constant pressure, glass transition temperature, thermal conductivity, coefficient of thermal expansion, dynamic viscosity, and surface tension) can be performed at MSFC or at an external lab. In the interim, modeling groups supporting ISM will use cataloged values for ABS produced using conventional manufacturing techniques such as injection molding.

While some data have been provided by TIM attendees on the sensitivity of mechanical properties of ABS produced via FDM to density, a follow-on investigation using the ETU, wherein mechanical test coupons of varying infill percentage (infill represents the best manufacturing process parameter to control density of the as-built part) undergo a density evaluation (based on weighing and volume measurement from structured light scanning) and are subsequently mechanically tested, may be needed to develop the relationship between density and mechanical properties for ABS produced using this particular hardware.

A thorough literature review of polymer melts and densification in microgravity is also needed. There is a breadth of research that, while not conducted on ABS in particular, may provide transferrable insight into microgravity effects on extrusion-based processes and material solidification in microgravity, and what analyses and experiments are best suited to characterize microgravity effects in this application.

Surface texture measurement capabilities at MSFC can be leveraged to evaluate the filament misalignment observed in the compression specimens. Surface roughness and deviations in circularity can be correlated with mechanical performance of specimens in compression. However, even if there is a strong relationship between compressive strengths and dimensional deviations, the cause of the underlying out-of-round behavior must also be determined (potential causes include changes in machine tolerance in microgravity that impacts accuracy in circularity, variations in tip-to-tray distance, and microgravity effects).

7.3.2 Material Aging (Offgassing and Moisture Absorption)

Another hypothesis developed based on figure 60 was that the flight feedstock and/or printed specimens may have been exposed to a humid environment at some point during their lifecycle and absorbed moisture from the ambient air and/or simply offgassed material over time (although moisture absorption accelerates this process). ABS plastic is hygroscopic in nature and readily absorbs moisture out of humid air. Water saturation of ABS is known to degrade the material (a phenomenon called 'splaying').[14] Looking across the 3DP specimen set, there is little detectable evidence of moisture absorption in the bulk printed material. One notable exception is that a few 'bubbles' were detected in microscopy that could be filament voids, created when moisture is absorbed into the filament and results in a bubble formation in the extruded material. No bubbles were observed on microscopy for either flight or ground tensile specimens. It is possible, however, that there may be many more such bubbles internal to the samples. Computed tomography analysis does detect voids in the mechanical specimens, but these are likely voids that are inherent to the FDM process. These voids can be mitigated by optimizing manufacturing process variables to produce a 'defect free' (>96% theoretical density of bulk ABS) material.[15]

It is also unclear, given similar conditions in processing and storage of both ground and flight feedstock and printed specimens, why splaying would specifically impact the flight compression specimens and the ground tensile and flexure specimens. One noted difference in processing is that there was more idle time between builds during flight operations. If a humid environment were present (there is no indication that this was the case since the MSG is routinely used to perform very sensitive experiments and thus has a precisely regulated environment), such conditions (even if present for only a short time constant) might enable the 4 in of exposed feedstock between the filament canister and the extruder to absorb some level of moisture.

For 3DP, careful environmental controls were put in place in part to prevent moisture absorption. Feedstock is stored in a filament canister with dessicant, and printed specimens were also sealed and stored with dessicant up until ground-based testing of parts commenced. Mining the ABS characterization data discussed in appendix B, many of these specimens were built with filament that did not have dessicant in the canisters and were stored without dessicant after printing, but were

not exposed to a humid environment. Even in the absence of carefully controlled storage conditions, the specimens do not exhibit behavior that is commensurate with the flight specimens in terms of fracture elongation. Temperature and humidity on board the ISS are comparable to conditions where ground operations and testing occurred. Thus, there were no known environmental conditions the feedstock or specimens were exposed to during their lifecycle that would have provided an opportunity for moisture absorption at levels commensurate with observable material degradation. Fourier transform infrared spectroscopy (FTIR) of the 3DP specimens, in particular those with suspected filament voids, would provide additional insight into chemical differences. To further assess the effect of moisture absorption on filament quality and subsequent mechanical properties of printed specimens, the ISM team may conduct a ground-based study where feedstock and bulk specimens are exposed to varying levels of moisture for specified periods of time. Filament and printed parts would be inspected for voids using microscopy and CT analysis. Chemistry of the filament and specimens can be characterized using FTIR. Results of mechanical testing will be correlated with chemical analysis as well as the size and frequency of porosity and voids in the material (based on CT) to assess the effect of splaying on material properties. Offgassing of feedstock material over time (and its impact on mechanical properties) has not yet been characterized.

7.3.2.1 Discussion. While flight and ground prints were fabricated using identical feedstock from the same manufacturing lot, the flight feedstock was 5 to 6 months older at the time of printing than the ground feedstock. The shelf life of feedstock (as specified by the manufacturer, Maker-Bot®) is 1 year. Aging occurs naturally as a result of offgassing, but can be accelerated by moisture pickup. The 5- to 6-month delay between prints of ground and flight specimens may have allowed aging processes (and subsequently chemical evolution) of the flight feedstock to take place. Aging of the feedstock may make it more brittle, resulting in flight specimens that are stronger and stiffer than their ground counterparts. This hypothesis represents one possible explanation for the flight coupons (tensile and flexure), which fail at higher loads and have a greater elastic modulus than the corresponding ground specimens.

7.3.2.2 Open Questions. The primary evidence of feedstock aging is the enhanced strength of the flight tensile specimens and the reduced ductility (measured as percent failure to elongation) observed for three of the four flight tensile coupons. Data from mechanical testing of the compression specimens, however, show the opposite trend, as ground compression coupons are stronger and stiffer than the flight prints. It is unclear why aging effects, if indeed the cause of the observed behavior, would have impacted some specimens and not others in this manner.

Aging could also potentially explain the unusual bias (relative to the rest of the dataset, where flight specimens are more dense than ground specimens) in the density of the flight compression specimens. Loss of chemical groups in the feedstock may reduce the mass of filament, which creates a less dense specimen when extruded (but again, an explanation as to why this effect would have manifested in the flight compression specimens alone is needed). Aging may also progress differently in raw filament than in the printed samples. Since aging processes are accelerated in feedstock relative to bulk material, flight specimens may have been more susceptible to aging effects than ground specimens. Aging effects are also a function of the exposed surface area-to-volume ratio and aging that impacts the printed specimen, and would presumably be greater for specimens (such as tensile and flexure) with a large surface area. However, it is unclear why material aging

(regardless of whether it occurs as a result of natural aging or was accelerated by moisture absorption) would not have impacted tensile specimen F004 (the first flight tensile printed), which does not have a strength or percent elongation that is in consistent with the other flight specimens.

Offgassing of chemicals as a result of material aging is generally a function of time and specimen geometry. While offgassing for ABS produced via FDM has not been characterized specifically, many polymeric materials experience offgassing quickly at first and then attain a level of chemical stability thereafter unless exposed to an environment (e.g., humidity, heat) that accelerates the aging process. There is no point in the lifecycle of the flight specimens when an exposure to environments or conditions that would create such an accelerated effect is known to have been present.

7.3.2.3 Additional Testing and Analysis. A thorough literature review on mechanisms of aging in ABS and the degree to which loss of material and chemical groups impacts material properties (specifically tensile, moduli, and fracture elongation) is required. A better understanding of the time constant and conditions for which aging occurs in this material is essential to evaluate the potential effect of aging for the 3DP dataset. From interaction and discussion with TIM participants, it seems that aging of feedstock does not impact printability, but using feedstock of an age beyond the manufacturer-recommended shelf life or feedstock that has been subjected to heat cycles to simulate aging effects may result in specimens with more brittle behavior in tension. A controlled study of feedstock aging and moisture absorption is needed to quantify these effects, a research effort which is beneficial to ISM as well as the broader additive manufacturing community. Going forward, the ISM team will consider the age of the feedstock at the time of printing and the age of the printed specimen at the time of testing as a variable in subsequent data analysis.

A chemical composition analysis using FTIR can be performed on select ground and flight specimens from 3DP and compared against control samples printed with new feedstock to assess the loss of functional chemical groups due to aging and/or indications of moisture absorption. This is also a priority topic for ground-based studies, as material degradation of feedstock with age is of key interest to the broader additive manufacturing polymer community as FDM technology transitions from a rapid prototyping technique to a manufacturing technique for functional parts.

The ground-based investigation entails several tasks intended to study the effect of moisture absorption in ABS feedstock on mechanical properties of printed specimens and characterize natural aging due to offgassing. Mechanical tests will be combined with chemical analysis to determine if the moisture absorption results in a chemical reaction, breaking up the backbone of the polymer and impacting the mechanical properties. Specimens for the proposed studies will be produced using the ETU since it represents the closest configuration to the flight hardware. The ground-based investigation tasks are as follows:

(1) In task I, filaments will be exposed to moisture per ASTM D570[16] and will be taken to four different moisture (percentage) contents, ranging from 1.8% to 10% of saturation. The test data will be used to relate moisture content to tensile strength (for single filaments) and to determine the effect of moisture on polymer chemistry (characterized with FTIR).

(2) Task II will study the effect of filament extrusion during 3D printing on loss of moisture in ABS plastic. ABS feedstock will be exposed to four different moisture contents in a humidity chamber. After exposure, the filament will be extruded and the specimen weighed. The difference in weight will determine the moisture lost during the extrusion process and help to answer the question of whether moisture absorbed in the feedstock boils off during extrusion (and to what degree absorbed moisture can expect to be present in the printed part for a given humidity level).

(3) Task III will characterize the effect of feedstock moisture content on the mechanical properties of the 3D printed parts. Moisture in feedstock may boil off during the extrusion process and can lead to porosity in the part. ABS feedstock will be exposed to four different moisture contents (ranging from 1.8% to 10% of saturation) using a humidity chamber. Immediately after exposure, the filament will be extruded via FDM into tensile specimens and mechanically tested. The fractured surface of the tensile test specimens will be analyzed using SEM to characterize porosity. Prints from dry feedstock will also be tested to obtain baseline tensile strength for comparison. Results will be compared with phase I data.

(4) Task IV characterizes material loss in feedstock due to offgassing when it is maintained in a controlled environment. Equivalent sections of feedstock filament will be weighed initially prior to storage in a sealed container with desiccant. Filaments will be weighed periodically over the course of 6 months (length of study can be extended to 12 months). Single filaments will be tensile tested after weighing, and percent mass loss will be correlated with mechanical strength.

(5) Task V is similar to task IV, but seeks to understand the effect of offgassing and material loss on the properties of the printed part. Feedstock filament will be maintained in a controlled environment with desiccant and used to print five tensile specimens every week over the course of 6 months (length of study can be extended to 12 months).

(6) Task VI will study the effects of printing with older feedstock. Some data will be derived from the tip-to-tray distance study since prints will be made at the nominal calibration value with feedstock that is the same age (and has been stored in the same conditions) as the flight feedstock. If continued trending of the tensile specimens toward higher strength and ductility is observed, it may explain some of the variability in the tensile specimens between the flight and ground prints.

Some additional information on the impact of feedstock aging may be provided by specimens from phase II printer operations (although it will be difficult to decouple the potential effect of moisture absorption versus natural aging due to offgassing processes for this dataset, which is why a ground-based study is needed). If material aging does impact mechanical properties in the manner observed for the 3DP specimens, it would be expected to see further aging effects in subsequent specimens printed using the same feedstock cartridge as the phase I prints. Additionally, there is a data mining task to look for trends in other feedstock batches of similar age to the phase I 3DP flight and ground specimens. Data from a senior design project related to ISM show that ABS feedstock 12 months of age (while a different manufacturing lot from the flight specimens and printed on a nonflight-like printer) produces tensile specimens that display the reduced fracture elongation observed for three of the four 3DP flight specimens (although these data are not analogous since

storage conditions for the feedstock in question were also very different from the flight feedstock, as it was not stored in a sealed container with desiccant). While some data related to aging effects may already be available, a controlled study is required to fully assess whether aging (from the two mechanisms identified, offgassing and moisture absorption) is the source of the variability observed in the 3DP dataset.

Results of this work are relevant to the broader additive manufacturing community since phenomena related to offgassing and moisture absorption seem to be largely uncharacterized for both ABS feedstock and specimens printed via FDM. These data are likely cataloged by original equipment manufacturers of FDM machines since in many cases they also manufacture and develop specifications for feedstock. The advantage of NASA undertaking such a study (in addition to better understanding sources of variability in the phase I flight and ground prints and defining requirements for feedstock for future printers) is that the data and outcomes could be published and shared with the additive manufacturing user community.

7.3.3 Tip-to-Tray Distance

7.3.3.1 Discussion. The z-calibration value, which determines the distance of the extruder head from the build tray the extruded material is deposited on, was adjusted based on visual feedback during phase I on-orbit operations of the 3DP unit. The z-calibration distance for the ground 3DP specimens was held constant at 2.2 mm. For the flight prints, the value ranged from 2.39 to 2.84 mm. The matrix of flight prints with the corresponding z-calibration value and tip-to-tray distance indicated appears in section 6. A discussion of how the z-calibration value is defined (and the relationship between z-calibration and tip-to-tray distance) can also be found in section 6. The commanded z-calibration value and the distance between the tip of the extruder nozzle and the build tray are inversely related; a smaller z-calibration value corresponds to a larger tip-to-tray distance.

Based on data from structured light scanning, the extruder tip was positioned too close to the tray during flight prints, resulting in specimens with protrusions along the geometric boundaries. Protrusions are a hallmark of an off-nominal tip-to-tray distance in this direction. (The protrusion is a consequence of a higher volume of extrudate.[17] As indicated in sec. 3, flight specimens generally do not have a larger volume (relative to ground specimens) that would suggest the presence of higher extrudate flow rates. However, differences in cooling rates between ground and flight prints, which have not been fully explored (see sec. 7.3.1), may account for some material shrinkage.) The discrepancy in this machine setting for ground and flight specimens may explain why flight specimens are generally more dense than their ground counterparts. As previously discussed, differences in densification between specimen classes may account for the enhanced tensile strength, elastic modulus, flexural strength, and flexural modulus observed in mechanical testing of the flight prints (although the difference between densities is approximately six to seven times less than the difference in mechanical properties for specimen classes). The tip-to-tray distance hypothesis postulates that the closer position of the extruder tip to the specimen during flight prints results in denser flight specimens with better mechanical performance.

7.3.3.2 Open Questions. A correlation analysis of properties of the 3DP flight specimens (density and mechanical properties) and machine settings failed to indicate a compelling relationship between z-calibration (or tip-to-tray distance) and material quality. One limitation of the 3DP hardware is that it does not have closed loop positional control or positional feedback; thus, there is currently no way to verify on orbit that the commanded position and actual position of the build tray are equivalent. Correlation analysis is predicated on the assumption that the command and actual value of the 3DP build tray for flight prints coincide. This may not be the case if the accuracy of the machine and the function of mechanical systems (for instance, actuators) are significantly impacted by microgravity. With that caveat, parts built closer to the extruder head should be denser (and greater material consolidation is generally commensurate with increased mechanical performance), although a tip-to-tray distance that is 'too close' (believed to be the case for the flight prints) can create undesirable features such as protrusions and similar geometric boundary defects, which can function as stress risers, potentially resulting in premature mechanical failure. The hypothesis that a smaller tip-to-tray distance produces denser specimens is consistent with the flight tensile and flexure specimens, but the bias in density of the compression specimens (flight specimens are less dense than the ground specimens) does not support this premise.

Calibration may also impact part warpage and curling of the specimens, which (as discussed in sec. 6.3) can occur during printing or when the part is separated from the build plate (this difference in warpage would likely be a result of differences in cooling rate attributable to the larger volume of extrudate deposited in a layer for specimens with smaller tip-to-tray distances). Structured light scan data indicate that 3DP ground samples, where material deposition occurred farther from the tray surface, exhibit increased warping relative to the flight specimens. The discrepancy between flight and ground prints on this metric is particularly pronounced for tensile and flexure specimens, which have a large footprint/surface area that is in contact with the build tray. Increased warpage for the ground specimens (potentially an artifact of distinct thermal histories due to different calibrations) could result in degraded mechanical performance relative to the flight specimens, as warping (and bending of filament) induces microcracks in the material. This has been demonstrated in SEM images of 'warped' filament, shown in figure 61. SEM analysis was performed by Dr. Richard Grugel at MSFC. However, the relationship between the degree of warpage and mechanical properties for ABS produced via FDM has not been robustly characterized, and the extent to which differences in warpage between ground and flight specimens can account for observed variations in mechanical properties is thus unknown. The root cause of the warping for the ground mechanical specimens has also not been precisely identified. Complementary modeling work is needed to shed further light on the credibility of this hypothesis.
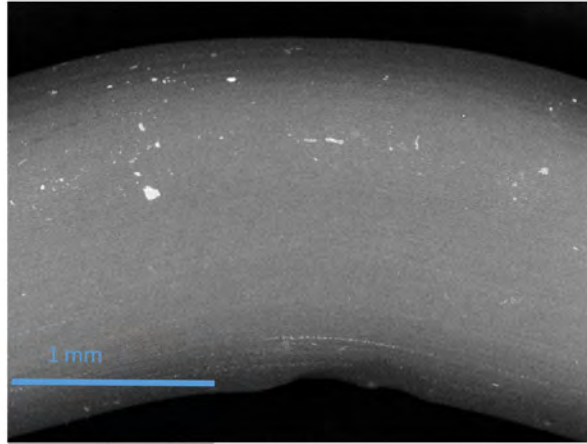
Figure 61. SEM image of bent filament. Microcracks are visible along radius of curvature. Image courtesy of Dr. Richard Grugel, MSFC.

7.3.3.3 Additional Testing and Analysis. A set of controlled, ground-based experiments using the ETU has been designed that will systematically vary the z-calibration value in increments that capture the range of values this variable was set at for the ground and flight prints. Mechanical testing and SEM analysis of these specimens will provide an empirical assessment of the strength and nature of the relationship between tip-to-tray distance and densification, mechanical properties, warpage effects, and stresses within the part. These data can be correlated with physics modeling work on ABS filament extrusion and material consolidation being conducted (in parallel with these experiments) by researchers at ARC. The ARC model predicts material consolidation and internal structure of the printed specimen based on the tip-to-tray distance (which determines the deposited volume of extrudate for a layer). Data from CT scans of specimens generated through this study will be used to validate this model or point the way toward sounder concepts that improve prediction of material quality for FDM.

Adjustment of the z-calibration value between subsequent flight prints was done in an attempt to optimize the tip-to-tray distance based on visual feedback. Changing this variable nonsytematically, however, creates noise in the dataset and makes it difficult to isolate the effect of microgravity on the FDM process, which was one objective of the technology demonstration mission. Calibration coupons (of which there were five for phase I flight operations) represent an opportunity to tune this distance to an optimum value prior to operating the printer. Future operations will employ better manufacturing process control to optimize this distance prior to commencing with prints of mechanical test coupons and other parts during on-orbit operations.

Inability to verify the calibration value is a limitation of the hardware which also complicates the evaluation of this hypothesis using the existing dataset. There is no detectable correlation between z-calibration and material properties for this dataset, but there is also no way to verify that the values specified for z-calibration correspond to the actual position of the build tray during printing. It may be possible to use a calibration plate with points at known distances to verify positional accuracy of equipment prior to operations. The uncertainty inherent in the z-calibration data further emphasizes the need for a controlled study to further characterize the impact of varying this distance on material quality.

7.3.4 Test Effects

7.3.4.1 Discussion. As mentioned in section 3, it is possible the mechanical coupon geometry and/or test setup influenced the measured mechanical properties. However, testing was done per ASTM standards for plastics, and procedures were consistent across both ground and flight specimens. Extensometer slippage was noted during testing of two flight specimens. When pronounced, extensometer slippage can result in artificially degraded values for fracture elongation. Additionally, several specimens broke outside the gauge section. Based on these observances, the strength data for the flight specimens may be more reliable than fracture elongation data (the latter leads to three of the four flight specimens to be classified as less ductile).

7.3.4.2 Open Questions. Several tensile specimens broke slightly outside the range of the extensometer. Per the ASM handbook on tensile testing and the ASTM standard testing was performed to, data from a tensile test where specimen fracture occurs in this region can be considered if the associated strength value is 'within family' (not unusually high or low) relative to similar data.[18] A break outside the gauge length is of greater concern if it occurs in the paddle regions of a tensile specimen. Failures outside the gauge section are common in composites, and data from these tests are routinely accepted so long as there is no obvious reason for exclusion. Fractures outside the bounds of the gauge length are also often seen in tests of composites which use the ASTM D638[5] type IV specimen, as the type IV has a narrower gauge section and a more pronounced fillet than other specimen types, which may exacerbate breakage in this region. Specimens with fractures outside the extensometer footprint were still included in the dataset used for analysis in section 3, but were analyzed with the knowledge that they failed in this region.

The question of failure in the indicated tensiles hinges on interpretation of the standard. If failure outside the gauge section is viewed as a binary classification (i.e., pass/fail with no consideration given to how close the break falls to the gauge boundary), then any break outside the extensometer may invalidate the test data. If failure is viewed as a continuum (i.e., evaluation takes into account how far outside the gauge the failure occurred) and is considered within the context of other data (which is the recommendation of the standard), then test results from the specimens in question may be incorporated. An additional consideration is the limited size of the dataset. If tensile specimens with fractures outside the gauge section were not considered, then data from 75% of tests of the flight specimens and 75% of the ground specimens would be discarded.

Extensometer slippage noted during testing was previously discussed in section 3. The question of whether reported values of fracture elongation in the flight specimens are attributable to extensometer slippage was raised. An extensometer slip typically manifests itself as a backwards slip on the stress-strain curve. There is no consistent amount to shift data over when extensometer slippage is observed; the correction procedure involves load matching and shifting of the data along the x-axis based on the judgment of the test conductor. Correction factors associated with minor extensometer slippage for the two flight tensile specimens are small (<1%) and are thus not substantial enough to account for the several percent difference in elongation to failure for the flight and ground specimens. While extensometer slippage will impact fracture elongation to some degree, the severity of the slippage here is minor enough that strength and modulus can still be extracted from the data with little reasonable effect.

7.3.4.3 Additional Testing and Analysis. The tensile coupon type will be evaluated as the ISM team interfaces with subject matter experts involved in standards development to provide further guidance on coupon selection. Type IV tensiles were used for 3DP flight and ground prints as well as other ground-based characterization testing for ABS produced via FDM. One key driver for continuing with the type IV is in the interest of collecting additional data that are directly comparable with prior work. The ISM team will also consider fixturing, specimen geometry, and/or test setup modifications to future tests to prevent extensometer slippage.

7.3.5 Damage to Specimens

7.3.5.1 Discussion. As noted from the analysis of structured light scanning data, some specimens incurred damage during separation from the build tray as a result of overadhesion. The 3DP unit, unlike many commercial FDM printers for polymeric materials, does not have a heated build tray. Heated platforms serve to minimize the thermal gradient between the lower and upper layers of a printed specimen, which provides for more even cooling of the part. Calibration may also come into play; adhesion was less evident for the ground prints, which may be a consequence of the larger tip-to-tray distance that reduces bonding of the first layer of the print with the tray and makes separation easier. The higher volume of extrudate deposited for a given layer under conditions where the tip-to-tray distance is smaller than desirable may also exert a greater force on the printed specimen during cooling, further contributing to warpage (this may be compensated for through adjusting the infill percentage). Other damage to the parts may have occurred during shipping, transportation, and handling, although a specific instance or opportunity for part damage during downmass or shipping has not yet been identified. During testing, a flexure specimen was clamped for structured light scanning. The indentations from the clamp are visible in the microscope image shown in figure 62.
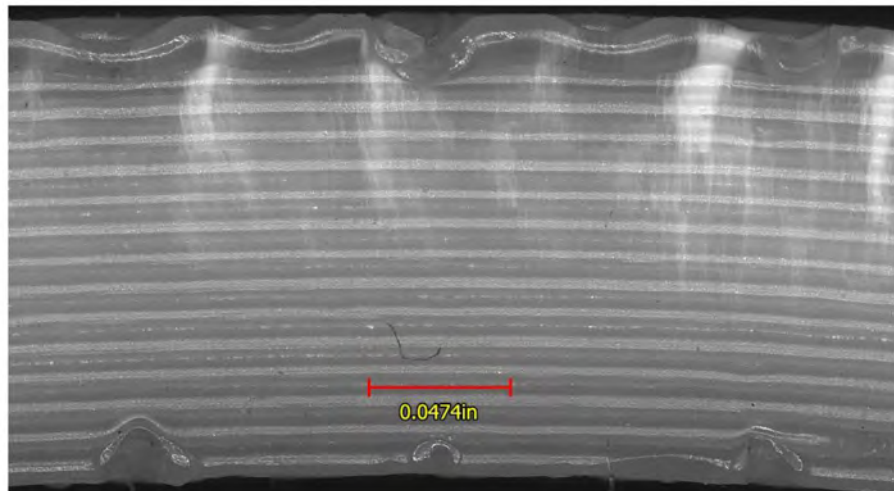
Figure 62. Slight indentations in flexure sample surface from fixturing noted on optical microscopy.

During CT, some mechanical specimens were too large to image in a single scan. The tensile and flexure specimens, whose lengths exceeded the scan envelope of the microfocus CT, necessitated two scans, with each scan imaging approximately half of the specimen along its length. To keep track of which scan corresponded to which portion of the specimen volume, one side of all tensile and flexure specimens was identified by a dot placed on the specimen using a Sharpie® marker. ABS is highly susceptible to most solvents, including two of the chemicals in Sharpie ink: diacetone alcohol and ethanol. From a chemical compatibility analysis using a material compatibility database, these chemicals have a 'minor effect' (resulting in slight permanent discoloration) on ABS. The severity of the effect and the degree to which it degrades the material is dependent on the amount of solvent present.[19] Ratings are based on a 48-hour immersion test. It is extremely unlikely that the small amount of ink applied to the ABS specimens impacted performance of the tensile and flexure specimens during mechanical testing.

7.3.5.2 Open Questions. Some of the tensile and flexure specimens do exhibit damage arising from warpage that may have occurred when the specimen was separated from the build tray via prying. Three divots were noted on flexure specimen G006 during microscopy and are likely an artifact of clamping used to position the part for structured light scanning. It is highly unlikely, based on its location, that this damage is significant enough to impact mechanical performance. Properties for specimen G006 are in family with other ground flexure specimens, which suggests that the divots did not degrade the material's resistance to bending loads.

The ink that was used to mark some specimens for CT has known material compatibility issues with ABS. However, the quantity and usage of the ink is very minor, and the markings are in the paddles of the tensile specimen and are distant from the region where fracture occurred.

7.3.5.3 Additional Testing and Analysis. Noted damage to parts and strategies to mitigate this damage in future testing work were key lessons learned from 3DP phase I. Optical microscopy should be performed on parts prior to testing (as well as post-testing) to ensure that observed features reflect the material in its as-printed state rather than changes in specimen material incurred during the testing process. Test conductors in future work will ensure that all fixturing of parts for imaging or testing does not impart damage to the part unless otherwise specified by the test. Additionally, inks needed for marking the part will be selected based on material compatibility.

7.3.6 Radiation Effects

Flight feedstock was exposed to ambient radiation during launch and on ISS prior to printing. Bulk flight specimens experienced radiation post-printing during storage on ISS and subsequent downmass. Both flight and ground mechanical specimens underwent x-ray and CT evaluation. Because the size of the tensile and flexure specimens exceeded the scan envelope, the tensile and flexure specimens were CT scanned twice. All 3DP specimens were x-rayed.

As with aging, radiation absorption rates could be different for the feedstock and the bulk material. Any radiation dose sufficiently energetic to break chemical bonds may be a contributor to material degradation (manifested as more brittle behavior) observed for some of the flight mechanical test coupons. The radiation intensities and exposure times necessary to embrittle ABS are

discussed in reference 11. The effect of radiation in ABS is initially evident at 100 kGy due to butadiene breakdown, but pronounced degradation is not detectable until exposure limits of 1,000 kGy have been reached. Specimen exposure for imaging are orders of magnitude away from doses corresponding to damage and/or material degradation. During CT scans, specimens received 90 µGy/s. Each specimen scan was 30 min. Tensile and flexure specimens had 60 min of exposure time since they required two scans. Two-dimensional imaging has much lower doses of radiation and shorter exposure times, thus the total estimated dose for a tensile or flexure specimen from imaging is 0.32 Gy, over 100,000 times less than the level at which material degradation of ABS is first observed.

The SpaceX Dragon capsule used to upmass the printer and flight feedstock and downmass the printed specimens is (like ISS) a radiation-shielded structure. Unless specimens received a much larger than expected dose of radiation during their time in space, cumulative radiation damage is unlikely as a root cause of suspected material degradation. Solar physics data from the National Space Science and Technology Center do not catalog any high levels of exposure during this time due to solar weather events. The return trajectory for Dragon is not known to pass through the South Atlantic anomaly (i.e., the region where the Van Allen radiation belt is closest to the surface of the Earth).

A further question is why radiation would impact some specimens and not others. Even if the in-space radiation levels the feedstock or specimens were exposed to during their lifecycles had been sufficient to induce material degradation/embrittlement (there is no indication that this is the case), radiation exposure would only potentially explain the mechanical behavior of the tensile and flexure specimens, since they alone are stronger and stiffer than the analogous ground specimens. Additionally, there was no differentiation in part handling, storage, or downmass that would explain why radiation would affect only specific specimens.

Some outstanding questions about radiation effects may be answered by an internally funded MSFC effort to study impacts of particle and UV radiation on ABS plastic. While this investigation will expose ABS specimens printed via FDM to in-space radiation rather than radiation levels in the crewed environment of ISS, it will provide significant information about the threshold radiation level where material degradation is first detected for this material and how radiation impacts mechanical properties. The research is highly relevant for ABS parts intended for use in the space environment. The study also includes additively manufactured metallic materials (Inconel 718).

7.3.7 Variability of Feedstock

The variation in chemical composition and/or dimension of the feedstock used to produce the flight and ground specimens along their respective lengths has not been fully evaluated (although prior to launch of the feedstock to ISS, some measurements were taken to ensure that the filament diameter was within the tolerance limits specified by the manufacturer). The quality of 3D printed parts is sensitive to the feedstock diameter, as this dimension determines the filament feed rate for the printer, which in turn determines the extrusion flow rate of the material. A basic assumption is that the filament diameter is constant. The FDM machine sets a roller speed that can provide the desired filament feed rate and flow rate necessary to ensure sufficient material consolidation and space filling.[20] If the filament diameter is less than the specified dimension, it will create a deficiency

in material flow that creates voids in the parts. Filament diameter greater than the specified dimensions would result in denser parts, but can cause the feedstock to 'jam' in the roller. No jamming or other indication of an overflow condition (potentially caused by an increase in filament diameter outside the tolerance limits specified by the manufacturer) was observed during flight or ground print operations for 3DP.

Feedstock characteristics, like powder characteristics in additive manufacturing of metallics, are a key determiner of material quality and a contributing factor to material variability. The material safety data sheet for feedstock does not specify chemical composition. Thus, the evaluation of the variability hypothesis entails three tasks: (1) Definition of the nominal distribution of chemical groups within a particular feedstock (via FTIR or procurement of manufacturer data), (2) characterization of the variation of composition at intervals along the feedstock length, and (3) correlation of chemical compositions and concentrations of sections of feedstock with properties of printed specimens produced using a specific feedstock segment. Feedstock should also be inspected to assess the size and frequency with which filament voids occur (an assessment also related to the moisture absorption hypothesis discussed in sec. 7.3.2). A ground-based study represents a way to assess the degree to which material quality depends on feedstock chemical composition, a process sensitivity which to date has not been characterized in the literature. Information from such an investigation would also inform a requirements definition for feedstock for future printers (i.e., the chemical composition, concentrations, and filament diameter range required to produce a material of acceptable quality for a range of applications).

7.4 Evaluation of Influence Factors

The influence factors discussed in section 7.3 were evaluated and ranked based on their ability to explain the variation in properties between ground and flight specimens. Comparative evaluation was based on the current dataset, experience with the FDM process, and informed engineering judgment. Factors were sorted into four categories:

(1) High credibility—A high credibility designation indicates than an influence factor is likely to explain a significant portion of the differences observed in the ground and flight specimens during testing.

(2) Medium credibility—A medium credibility designation corresponds to an influence factor that may account for some of the differences in flight and ground specimens observed during testing, but the amount of variability explained by the factor is expected to be less than that of factors placed in the high credibility capability.

(3) Low credibility—A low credibility designation describes influence factors that seem unlikely to have played a significant role in variation observed in the dataset.

(4) Uncertain—An uncertain designation indicates there is no substantive evidence from analysis of the current 3DP dataset to support or refute the hypothesis.

Table 26 summarizes the factors and their corresponding credibility ratings. Damage to specimens, radiation effects, and variability of feedstock (chemistry and dimensions) are designated as low credibility factors. Data about radiation levels present during the specimen lifecycle (on ISS and during RT) are not suggestive of radiation absorption levels near those needed to embrittle or otherwise degrade the material. Specimen damage is also rated as a low credibility factor since the only known damage to any of the specimens is the clamping marks on flexure sample G006 noted during microscopy; these shallow indentations do not appear to have impacted the mechanical performance of the specimen. Variability of feedstock diameter and changes in chemical composition of the feedstock along its length were also assessed as unlikely. Feedstock diameter at intervals along the length of the spool was measured for the flight feedstock (from the same manufacturing lot as the feedstock used for the ground prints) and verified to be within the tolerance limits specified by the manufacturer.

Table 26. Influence factors and credibility.

Uncertain	Low Credibility	Medium Credibility	High Credibility
Microgravity effects	Damage to specimens	–	Differences in z-calibration
–	Radiation effects	–	–
–	Test effects	–	Material aging (moisture absorption and offgassing)
–	Variability of feedstock	–	–

Test effects were also placed in the low credibility category. It is understood that the choice of tensile specimen type (type IV in ASTM D638[5]) may impact test outcomes. The fillet (created when the tensile specimen necks from 0.75 inches in the paddles to 0.25 inches in the gauge section) is a site of localized stress concentration, possibly resulting in reported values of material properties that are more reflective of the specimen geometry than the material quality. The same coupon geometry was used for flight and ground tensile specimens; thus, while the measured values may be less than what would be obtained with a type I tensile (which has a larger gauge section of 0.5 in), the flight and ground values should, in theory, be reduced by equal amounts as a consequence of specimen type, and relative comparisons are still valid. Application of testing standards and procedures was consistent across specimen sets. While the tensile geometry is one known factor that influences mechanical test outcomes, in general, this factor is not believed to explain any significant amount of variability in the 3DP dataset.

Microgravity effects on the FDM process and solidification in the printed specimen, which result in differences in densification and mechanical properties for the flight specimens, are also identified as an uncertain influence factor, meaning that there is a general lack of data to clearly substantiate or refute its influence at this time. As discussed in section 7.3.1, the manufacture of ABS may be impacted by microgravity to some degree, but either (1) the effect is too subtle to be detected with the testing techniques applied thus far (SEM or AFM may point more clearly toward material differences that may be a result of microgravity) or (2) the effect is detectable, but has not been attributed to microgravity because of other factors (like tip-to-tray distance) that were varied

nonsystematically. SEM analysis of 3DP specimens will identify features such as filament slump, fiber skewness and alignment, fiber thickness and shape, and characterize differences in these microstructural features between the ground and flight material that may point to a microgravity effect. Manufacturing process controls needed to isolate the effect of microgravity on the FDM process and fully evaluate the credibility of this factor to explain variability in existing and future 3DP datasets are discussed further in section 8.

Factors identified as high credibility are material aging and tip-to-tray distance. Flight feedstock was 5 to 6 months older than ground feedstock at the time of printing (and thus nearing the 1-year upper limit on shelf life specified by the manufacturer). While aging does not appear to impact printability of the feedstock, it can embrittle the material, resulting in higher strengths and lower elongation to failure in the printed specimen (the mechanical behavior observed for three of the four flight tensile specimens). Knowledge of conditions present during feedstock storage, specimen printing, specimen handling and storage, and specimen testing similarly does not indicate any point in the specimen lifecycle where the moisture present in the ambient air and/or the time the feedstock or printed part was exposed to a certain level of humidity would be a concern. However, material aging due to offgassing of feedstock over time has not been characterized. Material aging would explain the bias in strength, elastic modulus, and fracture elongation for three of the four flight tensiles and possibly the trends in flexural strength and flexural modulus for the flight flexure specimens. The compression dataset (where flight specimens are weaker than ground specimens) is difficult to explain within the context of material aging.

While no consistent correlation was detected between the z-calibration value (or the subsequently determined tip-to-tray distance) and density or mechanical properties for the flight prints, literature on manufacturing process optimization for FDM indicates that this distance is a parameter that can influence thermal flow and cooling rate, deposition rate, and interlayer configuration.[20] The need to optimize and maintain a consistent calibration distance in order to generate a structured dataset for 3DP is discussed in section 8. An investigation of the effect of tip-to-tray distance and related modeling work is a high priority of the ISM team based on interaction and discussion of hypotheses at the TIM. It is thought that variation of this operating parameter throughout the flight prints may account for a significant portion of the variability in the dataset.

The go-forward work discussed in section 9 will focus on conducting investigations that will generate additional data related to influence factors placed in the high credibility category and provide additional information needed to assess microgravity effects. An evaluation of microgravity's impact on material quality and performance for specimens produced using FDM is essential to future ISM efforts, as it defines how much of the materials characterization work needed to impart a robust predictive design and analysis capability can be ground-based. The appraisal of microgravity effects is also part of the level II requirements for ISM, which indicate that 3DP, "shall obtain data to advance the understanding of the critical design and operation parameters for the FDM process as affected by the microgravity environment." SEM analysis of the current specimen set and mechanical testing/CT/structured light scanning and microscopy/SEM of future specimens from 3DP (where manufacturing process controls are more stringent) are necessary to further evaluate microgravity effects. With regard to the high credibility factors, further work focuses on a ground-based investigation to understand and model the relationship between tip-to-tray distance and material

quality, and a controlled (also ground-based) investigation of feedstock aging and its impact on mechanical properties. Investigations into low credibility factors will be pursued as ground-based investigations as time and resources permit.

8. LESSONS LEARNED

One of the key objectives of 3DP is to use the lessons learned from operation, testing, and analysis of 3DP hardware and specimens to inform future technology demonstrations that will further prove out the processes needed to develop a robust off-world additive manufacturing capability. These lessons learned from 3DP will inform requirements development for future printers, T&E of specimens from future printer operations (both what tests are needed and the process flow for the testing regime), and definition of a phase II print matrix for 3DP that will provide key additional information needed to further evaluate the hypotheses and influence factors discussed in section 7. These future technology development efforts would not be possible without phase I of the 3DP technology demonstration mission.

Many of the following key lessons learned have been discussed previously in this TP, but are reiterated here to emphasize their significance and implications for further investments in microgravity FDM and other manufacturing processes that will be proven out using ISS as a testbed:

(1) There is a clear need for implementation of manufacturing process controls that will enable the ISM team to isolate the effect of microgravity on the FDM process. Variation of any processing parameters nonsystematically or in a manner that is otherwise unplanned for in experimental design should be minimized to the greatest extent possible. For future printer operations, the ISM team recommends that the z-calibration value (which determines the tip-to-tray distance) be 'tuned' using the calibration coupon prints. Once a nominal value has been defined based on visual feedback, printing operations should commence, and the value should not be changed thereafter unless there is a disruption in the printing process or other operational anomaly that warrants adjustment. While at this point decisions about proper calibration distance represent an engineering judgment based on visual feedback, the tip-to-tray distance study being undertaken at MSFC (sec. 9) will inform optimization of this distance based on its impact on part quality. Future printers should also provide closed loop positional feedback so that the distance between the extruder tip and the build platform (and whether the actual value deviates from the command value) can be precisely monitored during operations. To the extent possible, given the constraints on crew time and other ISS operations that must be attended to during printing, the time that specimens remain on the build tray after printing should be consistent. Uniformity in removal of parts from the build tray, packaging, and part storage is also essential to create a structured dataset from which information about microgravity effects can be extracted. Process controls will also improve repeatability and reliability of FDM, both in production of materials in microgravity and on the ground. Ground-based optimization activities outlined section 9 will characterize process sensitivities and assist with development of a locked and qualified manufacturing process with a defined operational window capable of producing parts with acceptable material characteristics. (Material characteristics needed will be defined based on the

application and intended use environment of the part, but optimization work will also provide key insight into what material properties are attainable with the 3DP unit.)

(2) A heated build tray is essential to mitigate specimen warping, reduce adhesion, and ensure symmetric cooling of the printed specimen (which will result in a more uniform microstructure). Many commercial off-the-shelf printers employ heated beds as a way to minimize the thermal gradient between the extrusion temperature and the temperature of the build tray that the material is deposited on. This thermal difference in part governs the rate of part cooling and determines the fiber solidification and molecular diffusion bonding between fibers. Generally, greater material quality (fewer voids, greater bonding between fibers, and higher densification) is achieved with a heated tray. Research into FDM process optimization by Sun et al.[21] found a positive correlation between the magnitude of the temperature difference and the size and frequency of voids in the printed specimen.

(3) As discussed in section 7.3.4 on test effects, the geometry of the tensile specimen type may contribute to a reduced ultimate tensile strength and fracture elongation due to the stress concentration at the fillet (fig. 63). The type IV specimen has a 0.75-inch width in the paddle sections, which necks to 0.25 inches in the gauge section. The type I tensile also measures 0.75 inches in the widest region, reducing to 0.5 inches in the gauge section (creating a fillet with less pronounced curvature). The choice of the type IV tensile for 3DP was driven by the shorter overall length of the specimen (type IV tensile is 4.5 inches long, while the type I tensile measures 6.5 inches). For future printers with larger build volumes, the type I tensile may be preferred to minimize the effect of specimen geometry on measured material properties. Mechanical property measurements in plastics (and composites) are more sensitive to coupon geometry since, as a material class, they are less ductile than metals (for example, many plastics and composites do not exhibit yielding behavior, and ultimate tensile strength and yield strength are virtually coincident on the stress-strain curve). The mechanical property efficiencies (the ratio of the as-built material to bulk textbook properties for ABS) might be higher for flight and ground with a type I tensile and reflective of actual material behavior rather than specimen geometry.
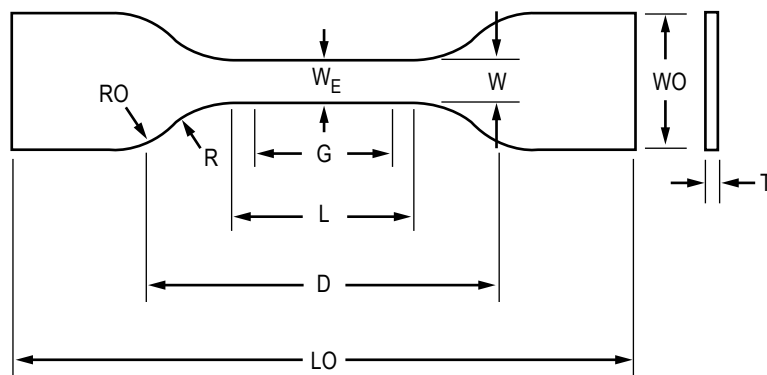

Figure 63. Type IV tensile specimen.[5]

(4) The test regime, collected data, and subsequent analyses for the 3DP phase I prints provided a wealth of information about the mechanical performance of the specimens, their internal structure, and deviations from the nominal CAD geometry. For future work, however, some modifications to existing testing/analysis as well as the addition of steps in the test process flow will be needed to provide key data related to questions discussed during the TIM. The surface roughness and cylindricity of the compression specimens needs to be evaluated prior to mechanical testing to quantitatively assess whether increased out-of-round behavior (observed in structured light scan data for the flight class of compression specimens for 3DP phase I) impacts material performance. The measurement techniques for this evaluation have recently been demonstrated by the precision metrology laboratory at MSFC using compression coupons produced by both the Stratasys® Fortus 900mc™ and a flight-like printer.

(5) SEM of the specimens was initially part of the test plan discussed in section 2. The test plan was later amended so that only tensile fracture surfaces would be evaluated with SEM to provide insight into differences in failure mechanisms for ground and flight specimens. However, interaction with subject matter experts in microgravity materials science at MSFC suggests that SEM analysis of internal specimen surfaces can reveal features such as filament slump (an effect documented in Rodriguez et al. and created by excessive cooling conditions in the printed part), evidence of material underflow or overflow conditions (which could be created by an enlargement or reduction in filament diameter or changes in tip-to-tray distance), the degree to which fibers are skewed or aligned, and differences in fiber thickness and shape (which can provide information about the temperature distribution present during cooling of the part).[15,17] Microstructural evaluation of the specimens can provide insight into potential differences in operating parameters (extrusion flow rate, nozzle correction factor, etc.) for ground and flight prints, observations that are key to assessing the effects of microgravity on machine operations. The microstructure of the specimens determines mechanical behavior; microstructural features detectable with SEM may help to explain the variation in mechanical property data for the ground and flight specimens discussed in section 3. The depth and value of information that can be obtained from SEM will make it an integral part of future 3DP specimen analysis. For future work, optical microscopy should be performed on specimens both before and after testing. Pre- and post-test evaluation enables the ISM team to distinguish between features present in the as-built part and those that are an artifact of fixturing/clamping or other material changes incurred during the testing process. This is particularly important for mechanical test coupons, as features noted in the as-built specimens on microscopy may have potential linkages to mechanical performance and failure mechanisms.

(6) Changes in management of specimens throughout the test process will also be implemented based on lessons learned from the phase I prints. While a 'first do no harm' philosophy was outlined in the test plan and applied during storage, handling, and T&E for phase I specimens, there were some deviations from procedures that should be avoided in the future. These escapements, which are not believed to have any impact on test outcomes, include (1) marking of the tensile and flexure specimens with ink and (2) suspected application of an excessive clamping force when fixturing one of the flexure specimens for structured light scanning. Clamping is generally not necessary for structured light scanning, but if required, the clamping force used to fixture the part should be maintained well below the force required to penetrate the material surface. For future specimen testing, the ISM

team will closely oversee testing procedures to ensure that fixturing of specimens for imaging or testing does not impart damage to the part unless otherwise specified by the test. (Specimens must be cut and polished as preparation for SEM analysis. Mechanical testing, where specimens are placed under load and tested to a specified load limit or failure, is also an exception.)

9. FUTURE WORK

Future work was prioritized and defined based on the credibility ranking of influence factors discussed in section 7. Future work consists of further analysis of 3DP phase I specimens, ground-based investigations conducted on flight-like printers to generate additional data relevant to influence factors in the high credibility and uncertain categories, and analysis of specimens from flight-based investigations conducted as part of phase II 3DP operations. At the time of this writing, 3DP phase II operations may occur in the spring of 2016, but could slip further due to payload reprioritization for the MSG, the space station facility from which the 3DP hardware operates.

Potential further work to better understand the 3DP phase I dataset is listed below in order of priority:

- SEM of 3DP phase I specimens—SEM of calibration coupons and tensile and flexural mechanical test coupons from the 3DP phase I prints is a priority analysis. SEM can identify features (such as filament slumping, filament skewness or alignment, and changes in filament shape and diameter), which, by virtue of their presence or prevalence in one class of specimens over another, could be indicators of microgravity effects on the FDM process. SEM will also provide insight into failure mechanisms and features in the internal structure of the part, which may have linkages to mechanical performance, SEM analysis provides data relevant to assessment of the following potential influence factors: tip-to-tray distance, microgravity effects (both on the FDM process and machine operations), moisture absorption (since SEM can detect splaying), and feedstock variability (changes in fiber width outside the expected may indicate an overflow or underflow condition created by a change in feedstock filament diameter). Chemical concentrations could also be obtained during SEM analysis with the energy dispersive x-ray spectroscopy (EDS) module.

- FTIR of 3DP phase I specimen—FTIR analysis will provide information about the chemical composition of the feedstock, the variability of chemical composition of feedstock along its length, and the chemical composition of the printed specimens. FTIR indicates the functional groups present in the specimens and (when the FTIR equipment has a mechanism to maintain pressure on the sample when mounted for analysis) their concentrations. FTIR will provide information relevant to evaluation of the following influence factors: offgassing/moisture absorption and feedstock variability.

- Investigation on the effect of tip-to-tray distance—Using the ETU, the flight-like unit for 3DP, the ISM team will print a matrix of tensile coupons, layer quality specimens, and compression coupons where the tip-to-tray distance is systematically varied from its nominal position. The range of the tip-to-tray distances considered will envelop the commanded variation in this value for the flight prints. Printed specimens will be evaluated through mechanical testing, structured light scanning, x-ray/CT, and SEM to assess the impact of tip-to-tray distance on dimensional variation (including frequency of protrusions, deviation from circularity for the compression specimens, and degree of warping/curling), mechanical properties, densification, and internal structure.

The physics-based modeling group at ARC has developed a model to characterize the impact of the tip-to-tray distance on the structure of specimens printed via FDM. The ground-based experimental investigation using the ETU will provide empirical data for model validation or point the way toward sounder modeling concepts that more accurately reflect material behavior during printing.

- Investigate effects of filament misalignment on compressive properties—Based on structured light scanning data, the flight compression specimens were found to deviate slightly more from the nominal CAD geometry than the ground specimens. It was hypothesized that the greater out-of-round behavior for the flight specimens may contribute to their reduced mechanical performance relative to the ground specimens, which exhibit less dimensional variation in the *x-y* plane. In addition to the root cause of this behavior (which could be a microgravity effect on machine operations), the relationship between circularity/cylindricity and compressive properties needs to be understood. The precision metrology laboratory at MSFC has demonstrated several techniques that can be used to assess cylindricity and surface roughness for compression specimens. Stylus profilometry using the Talyrond from Taylor Hobson® constructs a map of the compression cylinder by building up a series of straight-line axial profile traces around the specimen circumference. This analysis provides an assessment of cylindricity that complements the structured light scanning data. Stylus profilometry as well as a noncontact technique, laser scanning confocal microscopy, can be used to characterize surface roughness. Surface roughness and contour misalignment assessments performed prior to mechanical testing will be correlated with compressive properties. In the literature on compression testing of materials ranging from wood to concrete, compression seems to be a test that is very sensitive to surface aberrations and/or geometric irregularities. Variations in cylindricity and surface roughness for compression specimens may explain the reduced performance of the flight specimens on this metric in the 3DP dataset and help the ISM team better understand how geometric slicing and filament deposition for these particular specimens can be optimized to produce a best-quality material. This characterization can also be incorporated into other studies that produce compression specimens.

- Sensitivity of mechanical properties to densification—One of the outstanding questions of the TIM was whether subtle variations in density (recall that flight and ground specimens had density differences of only around 5%, although the density bias of the compression specimen set was inconsistent with the other data compared) can translate into the much larger (15%–30%) observed differences in mechanical properties. The ISM team derives a sensitivity curve for density and mechanical properties by systematically varying the infill percentage of the printed specimen, measuring density, and correlating density of a specimen with the corresponding properties measured during mechanical testing. Printed specimens of various infill percentages will be weighed, structure light scanned, and mechanically tested using the same procedures outlined in the 3DP test plan. Gravimetric density is derived by ratioing the mass with the volume measured during structured light scanning analysis and can be correlated with results of mechanical testing to generate a curve that predicts mechanical properties as a function of density. This curve would enable the ISM team to assess the magnitude of the effect of a small change in density on mechanical properties and better understand the relationships between infill, density, and mechanical performance of ABS specimens printed with FDM. This investigation can help explain the 3DP dataset, but it is also of interest to the broader industry as FDM transitions from a process used to build prototypes to a manufacturing technique for functional parts.

- Material aging—This investigation, outlined in section 7.3.2, would consider the effect of both offgassing and moisture absorption on properties of feedstock and the printed part. Recreating or mimicking the potential effect of feedstock aging due to offgassing and/or moisture absorption for the flight prints is difficult since it is unclear (other than the fact that flight feedstock was 6 months older than ground feedstock at the time of printing) what exposures or other environmental variables (in feedstock storage, printing, or shipping/handling of printed parts) may have contributed to aging effects. What is proposed here is a general study with the goal of determining what behaviors or trends in data from these analyses are similar to the datasets for 3DP and can thus be extrapolated as a possible explanation for the observed variability between the ground and flight specimens. Outcomes of the full study as discussed in section 7.3.2 include:

    - Correlation between moisture absorption in filament feedstock and tensile strength and polymer chemistry.

    - Understanding of moisture lost in filament during the extrusion process, answering the question, if x% of moisture is present in the initial filament, how much boils off during extrusion?

    - Determines to what degree absorbed moisture will be present in the extruded filament for a given humidity level.

    - Correlation of moisture absorption in feedstock with mechanical properties and moisture present in printed part.

    - Characterization of mass loss and chemical evolution over time in feedstock filament due to offgassing.

    - Correlation with feedstock mechanical performance.

    - Correlation of feedstock mass loss due to offgassing with mechanical performance of the printed part.

    - Characterization of selected phase I specimens using FTIR to understand chemical differences in flight and ground specimens, which may be attributable to offgassing or moisture absorption.

    - On-orbit evaluation of aging effects based on analysis of phase II prints.

- Thermal modeling to evaluate differences in convective processes (with the printed specimens) and solidification for FDM specimens produced in microgravity—The objective of this work, which could be undertaken by the thermal modeling group at MSFC or the physics-based modeling group at ARC, is to predict the temperature distribution of the printed part based on process parameters which influence thermal environment and cooling rate. The results of thermal analysis work will inform process changes for future printer operations to produce specimens with optimal material quality.

- AFM of 3DP phase I specimens—The purpose of this analysis is to characterize differences in phase morphology (presence and distribution of material phases) between ground and flight specimens. As discussed in section 7.3.1, changes in localized temperature profiles at the weld line (layer) interfaces during printing can result in the formation of nonequilibrium phases, which in turn impacts mechanical performance (fig. 64). Phase morphologies that are unique to flight specimens may shed light on microgravity effects on the FDM process. This work could be done at MSFC or in partnership with NIST, who also proposed the investigation as part of a materials science request for information (RFI) related to 3DP.
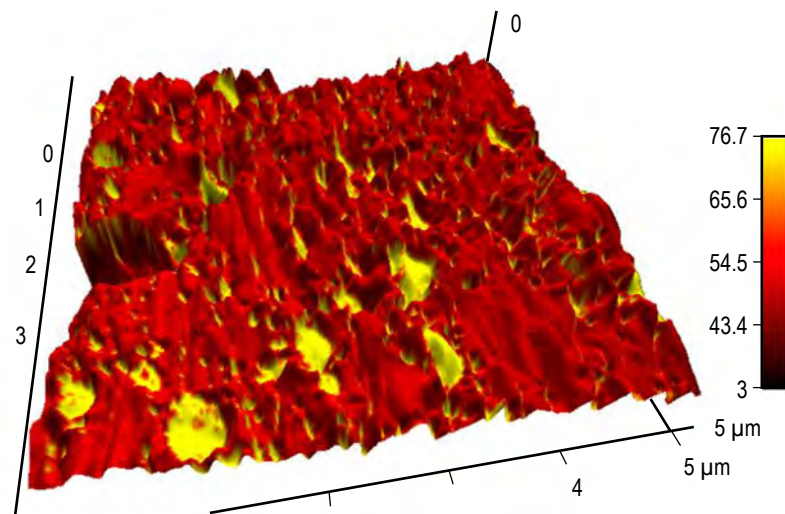
Figure 64. AFM micrograph of FDM-printed ABS showing phase morphology. Yellow is the butadiene phase, and red is the more ridge continuous phase. Image provided by NIST.

At the time of this writing, the Mechanical Test Laboratory has demonstrated the FTIR capability for this application and has performed an analysis of selected specimens from the ground and flight prints. This work will be summarized in a subsequent report, but no chemical differences were detected between the classes of ground and flight specimens analyzed thus far. Tensile specimens, the calibration coupons, and the layer quality specimens from 3DP phase I are undergoing SEM evaluation, and the analysis to date (which will also be summarized in volume II) suggests that structural variations in the parts resulting from processing differences in ground and flight prints explain the variations in mechanical properties within class and between class (ground vs. flight) for the tensile specimens. A tip-to-tray distance study is currently being executed. A systematic study of the impact of material aging on tensile strength and moduli has been designed. Some data on the relationship between density and mechanical properties for FDM parts have been provided by TIM attendees and a senior design project related to ISM. A study of the effect of filament misalignment on compressive properties has been incorporated into the tip-to-tray study and will be subsequently published in volume II.

The scope of the flight-based investigation for further analysis is currently limited to the phase II prints. Phase II will consist of 42 specimens and will include additional tensile, compression, and flexure specimens as well as functional parts. With improved manufacturing process controls, phase II prints will serve to do the following:

(1) Isolate the effect of microgravity on the FDM process. Testing and analysis of 3DP phase II specimens will provide greater insight into whether the variability in the 3DP dataset is accounted for by microgravity effects or is an artifact of changes in tip-to-tray distance, material aging, or another influence factor.

(2) Provide additional data relative to the material aging hypothesis. The initial prints of phase II specimens will be performed with feedstock that is already loaded into 3DP and has been on station since the arrival of the 3DP hardware in September 2014. At the time phase II prints occur, this feedstock will be well beyond the recommended shelf life specified by the manufacturer. By comparing data from mechanical testing (and possibly chemical composition analysis) from ground and flight 3DP phase I specimens and flight phase II specimens, the ISM team can assess whether continued trending toward embrittlement of the material occurs with use of older feedstock (which might manifest as phase II specimens with tensile strengths that are greater than 3DP phase I prints but have even lower fracture elongations).

(3) Provide greater statistical sampling for mechanical property data. The sample size for mechanical specimens from 3DP phase I is small (a total of eight tensile, six compression, and six flexure, with half of each sample set originating from the flight prints and the other half from the ground prints). Additional data obtained from mechanical testing of phase II tensile, compression, and flexure specimens will provide insight into whether trends, biases, and characteristic mechanical properties reported based on phase I testing are consistent with further flight operation of the printer. Whether confirmatory or disparate from the original dataset, phase II prints may lend additional clarity to causes of variability in the phase I data and which concepts/hypotheses are best poised to explain property differences between flight and ground specimens.

The ability of the investigations discussed to (1) provide information related to the influence factors identified in section 7 and (2) potentially explain variability in the phase I 3DP dataset are the key considerations in task prioritization by the ISM team. Time and resources are also constraints in the definition of follow-on tasks. At this juncture, SEM analysis of selected 3DP phase I specimens, an empirical and analytical investigation of the impact of tip-to-tray distance on material quality, and a material aging study are considered the highest priority work. While all of the identified tasks will provide valuable data, the ISM team has made an effort to determine which investigations are of the greatest engineering significance and are most likely to yield information that will help the ISM team to satisfy the requirements of the 3DP technology demonstration, optimize 3DP operations to improve material quality, understand the variability in the 3DP phase I dataset, and inform requirements for future printers. It is believed that these highest priority investigations will return the information needed to assess influence factors for the 3DP dataset and advance understanding and utilization of FDM for ISM.

APPENDIX A—SUMMARY OF TECHNICAL INTERCHANGE MEETING TO OUTBRIEF RESULTS OF PHASE I PRINTS

The purpose of the two-day TIM held at MSFC on December 2 and 3, 2015, was to (1) outbrief the results of the testing of the first phase of prints from this project and (2) leverage shared experiences and collective knowledge in advanced manufacturing and materials development to better understand the dataset. The meeting brought together experts from NASA, other government organizations, industry, and academia.

Affiliations of participants in this meeting included NIST, Army Research Laboratory, MSFC, ARC, University of Virginia, University of Dayton Research Institute, University of Houston, Made In Space, and Naval Sea Systems Command.

The TIM consisted of an overview session followed by more focused presentations addressing specific test results and aspects of the data as well as related special topics. Detailed information about the content of each presentation and subsequent discussion are provided in sections 2–8 of this TP.

A.1 Day 1: December 2, 2015

The meeting began with an overview of the ISM project given by project manager Niki Werkheiser. The objective, requirements, and success criteria for the 3DP technology demonstration mission were presented. Other ISM activities, including the phase II prints using the current ISS printer (3DP) (which will take place in 2016), ground-based materials characterization activities and the material property database for 3DP, future solicitations for external ISM, SBIR-sponsored work on a feedstock recycling capability, and STEM outreach activities related to 3DP were also discussed. The overview emphasized that ISM seeks to develop on-demand manufacturing capabilities that will enhance crew safety, support sustainable operations for exploration, and many activities beyond 3DP.

A summary of a precursor TIM, focused on development of baseline material properties for ISM and defining materials characterization activities to support ISM, was presented by Tracie Prater, Ph.D., from MSFC. The meeting took place at MSFC in July 2015 and had nearly 60 participants from NASA, other government agencies, industry, and academia. The summary report from this meeting has been published as a NASA Technical Memorandum and can be accessed through the NASA Technical Reports Server.[4]

Quincy Bean, the principal investigator for the 3DP technology demonstration mission, presented a summary of the test plan and test procedures for the phase I prints. The specimens underwent multiple phases of testing at MSFC from May through September 2015. The objective of the testing was to enable comparative evaluation of ground specimens (printed using the flight printer

prior to launch) and analogous flight specimens of identical geometry that were printed on board ISS. All ground and flight specimens were photographed, weighed using precision metrology capabilities in EM10, x-rayed, and scanned using structured light scanning to create 3D rendering of parts that could be compared to the nominal CAD geometry. Mechanical test coupons (compression, flexure, and tensile) were CT scanned prior to mechanical testing. All specimens were also examined using an optical microscope in EM10; for the mechanical test specimens, this evaluation was conducted after destructive testing was complete. This presentation also covered the baseline requirements for the 3DP technology demonstration. Niki Werkheiser reiterated the key question that the ISM project seeks to answer with this technology demonstration: Are differences in part performance attributable to microgravity? During discussion, another question was posed: If differences are observed, how would they affect overall performance, and can part design compensate? Some attendees felt that more fundamental scientific research needs to be performed in order to fully answer the question, while others felt that the focus should be on microgravity differences that are determined to be of engineering significance (i.e., focus on large effects that would affect overall part performance).

During the early afternoon, invited presentations were given. Dr. Ed Garboczi from NIST presented information on additive manufacturing research that NIST is involved in. NIST has been conducting round robin studies with the industry and working toward the development of additive manufacturing standards for both polymers and metallics. Most of NIST's additive manufacturing efforts have been focused on additive manufacturing of metals; however, they have recently begun studying polymeric additive manufacturing (i.e., FDM). They have determined that structural failure of FDM parts tends to originate at weld line interfaces and have performed AFM to measure nanomechanical properties. It was suggested that AFM may be sensitive enough to detect subtle microstructural differences between parts printed terrestrially and in the microgravity environment.

Following the first TIM, an informal RFI was sent out to the materials science community (but primarily focused on participants in the polymers session of the MaterialsLAB ISS workshop for microgravity materials science research) to solicit ideas for potential uses of the printer to conduct materials science research. Three responses were received. The experimental concepts were presented at this TIM by the investigators who proposed the work:

(1) Dr. Jacinta Conrad from the University of Houston spoke about an investigation to determine the feasibility of 3D printing nanoparticle-reinforced composites in microgravity. These nanoparticles add material functionality (e.g., enhance thermal or electrical conductivity) and result in higher strength parts that expand the range of material uses. The microgravity environment may enable printing of higher solid loadings of nanoparticles and finer spanning features, which in turn will improve the properties of printed structures.

(2) Dr. Thomas Forbes from NIST proposed using 3DP to enable real-time sampling and particle sizing and offline chemical composition measurement of ultrafine aerosols emitted during the thermal extrusion process. The study aims to provide information on the size and concentration of emitted ultrafine particles, as well as the chemical composition of vapors and deposited particles that are byproducts of the printing process and would help to address environmental health and safety concerns that may be associated with operating the FDM process in a crewed habitat.

(3) Dr. Ed Garboczi presented an investigation from Drs. Ryan Killgore and Ryan Wagner on using AFM to assess microgravity effects on phase-separated domains of ABS produced by FDM.

Dr. Tracie Prater presented the gravimetric density and mechanical property data for the flight and ground control samples. Gravimetric density values were calculated based on specimen weights obtained using a precision balance in EM10, and volumes were derived based on structured light scan data. In general, flight specimens are slightly more dense than ground specimens. Exceptions to this are the compression coupons and the positive range specimen, which were less dense than their ground counterparts. The masses of the samples had only slight differences. Each class of mechanical test performed (tensile, compression, and flexure) yielded two clear families of data for flight and ground specimens. Data from tensile tests indicate that the flight samples were on average stronger and stiffer than the ground samples; however, the fracture elongation of the flight specimens was reduced relative to the ground specimens. Flight tensile sample F004 (the first specimen printed) could fit in either family (flight or ground) in terms of strength and stiffness, but had a fracture elongation that is statistically in family with the ground dataset. For the flexure specimens, the flight specimens had an ultimate strength and modulus that were significantly greater than the analogous ground parts. The compression specimens showed the opposite trend; for this class of specimens, the flight samples were weaker than the ground samples. This trending correlates well to the density data, as denser parts have better mechanical performance. While variations in density between ground and flight specimens may explain observed differences in mechanical material properties, the question as to what mechanism is responsible for the difference in density remains unanswered. During discussion of mechanical property data, it was noted that variation in feedstock filament diameter imparts a change in part density. Filament diameter variations can change the volumetric flow rate of extruded material from the nozzle, which can then result in thinner extrudate beads, which in turn will lower the overall part density or create a weak spot/failure initiation point. The importance of extrusion flow rate to part quality is documented in papers by Rodiguez et al. from the University of Notre Dame.[15,17] Mike Snyder (Made In Space) said that feedstock filament used for flight and ground operations was inspected, but diameter was not precisely measured. The filament was inspected to verify that it was within the acceptable diameter range allowed by the 3D printer.

A.2 Day 2: December 3, 2015

Dr. Ron Beshears presented the CT data. The images from the CT scans show an abrupt step change in density that occurs about halfway through the thickness of many of the specimens. These density variations were mostly observed in the flight samples. Densities were calculated from the CT data as a CT number. This value cannot be converted to standard density units using the current dataset, but a conversion factor can be obtained for future analyses by scanning a witness sample of the same material with a known density. The differences in CT number between flight and ground samples in general follow the same trend as the gravimetric density measurements (i.e., flight denser than ground). However, the mean CT differences were not considered statistically significant. Density for the top and bottom sections of the parts were also compared. The CT numbers were usually higher for the bottom half of the specimen (i.e., the first half to be printed) than the top; however, the differences were again not considered significant.

Erick Ordonez presented the microscopy data. Examination of the tensile samples' fracture surfaces showed that many of the samples' bottom few layers were smeared together more than the top layers. This corresponds to the findings from the CT data, which indicates that the lower half of the specimens are denser than the top halves.

Quincy Bean presented the structured light scan data. The scan data show that almost all of the samples were warped or shrunken slightly. Most of the flight samples exhibited protrusions along the bottom edges, which is indicative of the part being built with the extruder tip too close to the print tray. If the tip is too close, then the extrudate bead width will widen, resulting in protrusion in the bottom layers beyond where the part edges should lie. The ground samples in general were more warped than the flight samples. Warpage is generally an indication of poor adhesion to the build surface and may have been caused by the extruder tip being too far away from the build surface for the ground prints. Structured light scanning also showed that the compression samples overall are slightly out of round, but that the ground specimens exhibit less dimensional variation from the CAD model than the flight specimens. During discussion, a question was posed as to whether small differences in part geometry/tolerance would result in large differences in mechanical properties. The extruder tip being too close to the build surface may explain the higher densities and strengths in the flight tensile and flexure samples, but does not account for the weaker and less dense flight compression coupons. The differences in the mechanical properties of the compression samples may be explained by tolerance differences; however, more data need to be obtained to understand what relationship, if any, exists between out-of-round behavior (perhaps quantified in terms of surface roughness) and compressive properties.

The integrated data presentation reviewed the results of the phases of testing discussed during the TIM: mass and density, mechanical testing, structured light scanning, x-ray and CT, and optical microscopy. A fishbone diagram constructed by statistician Ken Johnson and the ISM team to identify process influence factors was discussed. Testable hypotheses developed based on this diagram that could potentially explain observed differences in mechanical properties for flight and ground specimens were presented individually. These included microgravity effects, material aging/offgassing, changes in z-calibration and the tip-to-tray distance, test effects (i.e., mechanical coupon geometry and/or test setup influenced measured mechanical properties), exposure of feedstock and/or printed part to humidity, moisture absorption, radiation effects, and chemical variation in feedstock. Supporting and refuting evidence for each hypothesis (based on the 3DP dataset) was discussed. Open questions related to each hypothesis were identified as well as a plan for further analysis. Lessons learned from operations of 3DP and subsequent testing of the ground and flight specimens were also summarized. The presentation concluded with an executive summary, highlighting successes of the project, remaining questions, and a go-forward plan based on evaluation of the credibility of hypotheses, open questions, and task prioritization. Many participants in this session of the meeting offered valuable feedback based on their own work with the FDM process and ABS that will inform the team as it moves forward. Inputs included sensitivity of ultimate tensile strength to subtle changes in density for ABS produced via FDM, investigating the relationship between specimen hardness and modulus and ductility, effects of moisture absorption on ABS, and specific evaluations (SEM and AFM) that could provide insight into microgravity effects. Discussion

from the TIM will guide additional analysis of flight and ground specimens with the related objectives of detecting signatures of microgravity effects on the FDM process and explaining differences in density and mechanical properties between ground and flight specimens. Test plans, procedures, and analysis tools may also be amended to provide the best possible dataset for future test specimens. The phase II print matrix was evaluated and revised based on feedback received from materials experts to generate specimens that can potentially answer open questions identified during the TIM and pave the way toward full utilization of 3DP and ISM capabilities.

APPENDIX B—COMPARISON OF 3DP DATA WITH PREVIOUS GROUND-BASED MATERIALS CHARACTERIZATION WORK

Because the properties between the flight and ground prints are disparate and clearly represent two families of data, it is worthwhile to examine the flight and ground dataset within the context of other, previous ground-based materials characterization work for ABS produced via FDM to look for commonalities in properties and manufacturing conditions that could help to explain the observed variation in the 3DP dataset. Although the datasets from the materials characterization studies are certainly not directly comparable with the 3DP specimens because of wide-ranging differences in printers, feedstocks, thermal conditions, machine operations, etc., they do provide some insight into whether the observed property values for 3DP are within the bounds of other ground-based specimens (and general process variability, although the sources of the variability for the ground-based characterization work and the 3DP specimens may be, admittedly, very different).

Currently, there are four other datasets that can be considered:

(1) The SS series, produced on the FDM Titan™ (made by Stratasys) with ABS P400 white feedstock.
(2) The GN series, produced on the ground test unit (GTU) for 3DP with ABS natural feedstock.
(3) The EF series, produced on the ETU for 3DP with ABS natural feedstock.
(4) The LF series, produced on a flight-like printer and delivered to NASA by Made In Space (ABS natural feedstock).

Table 27 summarizes the data series, the make and model of the machines the specimens were produced on, feedstock information, and storage conditions for the specimens. Specimens from the GTU (GN series), ETU (EF series), and the LF series were produced on flight-like printers. The least relevant dataset from the perspective of evaluating the test results of the 3DP specimens is the SS series, since it was produced on a Stratasys machine and used a different feedstock (ABS P400 white) than all other specimen sets (which used ABS natural). The SS, GN, EF, and LF series specimens were also not stored with desiccant, and for GN and EF, no desiccant was in the feedstock cartridge, potentially rendering specimens from these sets more susceptible to environmental effects and moisture absorption than the 3DP specimen set (where storage conditions were more carefully controlled). All specimens (with the exception of the SS series) were made with the same G-code (slice) files as the 3DP specimens; however, the build parameters for the SS series were set such that the filament placement emulates the original G-code as closely as possible. All samples used the same filament orientation (±45°) for layup.

Table 27. Summary of data series for ABS plastic produced via FDM.

Sample Series	Machine		Feedstock				Sample Storage
	Make	Model	Supplier	Material	Lot	Desiccant in Cartridge	
SS	Stratasys	FDM Titan	Stratasys	ABS P400 white	3083	Yes	Sealed bag, no desiccant
GN	Made In Space	GTU	Makerbot	ABS natural	69674	No	Sealed bag, no desiccant
EF	Made In Space	ETU	Makerbot	ABS natural	69674	No	Sealed bag, no desiccant
LF	Made In Space	Unknown, flight-like	Makerbot	ABS natural	69674	Unknown	Sealed bag, no desiccant
G	Made In Space	Flight unit	Makerbot	ABS natural	69674	Yes	Sealed bag with desiccant
F	Made In Space	Flight unit	Makerbot	ABS natural	69674	Yes	Sealed bag with desiccant

The SS, GN, and LF series consist of 45 specimens (15 tensile, 15 compression, and 15 flexure). Batches of five specimens each were tested at three temperatures (–20 °C, room temperature, and 90 °C). For comparison with the 3DP dataset, results from these series were restricted to room temperature tests.

Some additional specifics and fabrication notes on the data series are summarized as follows:

• For the SS series, all 15 samples of each type (tensile, flexure, and compression) were fabricated simultaneously in a single build.

• For the GN, EF, and LF series, specimens were built one at a time.

• The GN series had a damaged build tray, and a Lexan™ sheet (1-mm-thick polycarbonate) was affixed to the build surface. During each build, the Lexan sheet would bow up from the build surface, moving the build surface closer to the extruder tip than nominal. As a result, all GN samples were built too close to the extruder tip. Specimens exhibited protrusions along the bottom edges.

• The GN series had a different thermal environment than the 3DP series owing to the presence of the Lexan sheet on the build tray, but the commonality between the flight specimens and the GN series is that both were built with the extruder tip positioned too close to the build tray. A more complete discussion of tip-to-tray distance and its impact on the resulting material in terms of dimensional variation appears in section 6. The relationship between tip-to-tray distance and mechanical properties has not been characterized, but will be investigated as part of a follow-on investigation (further discussed in sec. 6).

• For the EF series, specimens were inspected for quality control after fabrication. Samples that exhibited significant warping or protrusions were rejected.

In comparing the datasets, a multigroup comparison (MANOVA) for the SS series, GN series, EF series, LF series, 3DP ground, and 3DP flight specimens was performed for each material property (ultimate tensile strength, modulus of elasticity, fracture elongation, compressive stress at 20% strain, compressive modulus, ultimate flexural stress, and flexural modulus). Data were restricted to results of room temperature mechanical tests. The summary of the comparative evaluation of the data from tensile testing, compression testing, and flexure testing for the classes of specimens identified in the preceding discussion appear in tables 28–30 in sections B.1–B.3. Scatterplots of tensile, compression, and flexure data for all six specimen sets are in figures 65–71 in sections B.1–B.3.

B.1 Comparison of Tensile Test Data

The comparison of tensile test data across the six specimen sets (SS, GN, EF, LF, 3DP ground, and 3DP flight) is summarized in table 28. The accompanying scatterplots for ultimate tensile strength, modulus, and fracture elongation appear in figures 65–67. In terms of ultimate tensile strength, the SS series exhibits lower than expected strength given that specimens were produced using a commercial off-the-shelf, industrial-grade printer. The important finding relative to 3DP is that the GN series, where specimens were inadvertently built with the extruder tip too close to the build tray as a consequence of the Lexan sheet necessitated by build tray damage, also exhibits greater ultimate tensile strength. An off-nominal tip-to-tray distance with the same bias was also present in the manufacture of the 3DP flight specimens. This observation lends supporting evidence to hypotheses that suggest greater densification in the flight specimens (and higher resulting mechanical properties) is a consequence of the closer tip-to-tray distances used during printer operations on orbit. Ground specimens for 3DP are in family with the LF series (built with a flight-like printer on the ground) in terms of ultimate tensile strength.

Table 28. Tensile data comparison for all specimen classes.

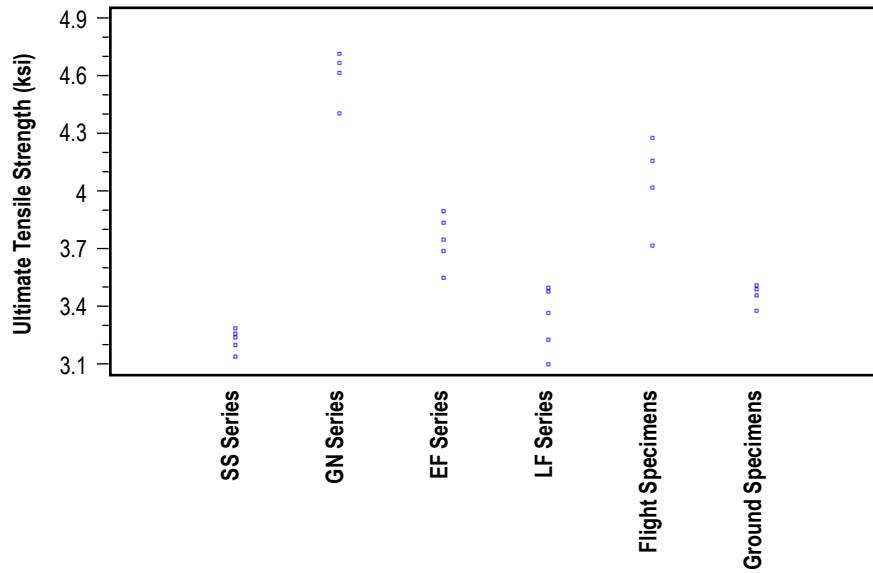| Group	Mean Ultimate Tensile Strength (ksi)	Coefficient of Variation (%)	Mean Modulus of Elasticity (msi)	Coefficient of Variation (%)	Mean Fracture Elongation (%)	Coefficient of Variation (%)
SS series	3.23	1.8	0.24	3.7	6.1	29.3
GN series	4.61	3.0	0.25	2.4	8.7	13.8
EF series	3.75	3.6	0.23	3.1	6.9	11.9
LF series	3.34	5.1	0.19	5.9	7.9	6.7
Ground specimens	3.46	1.7	0.22	2.7	7.5	9.9
Flight specimens	4.05	6.0	0.25	6.1	5.2	26.3

Figure 65. Scatterplot of ultimate tensile strength (measured from room temperature tensile tests) across six specimen sets.
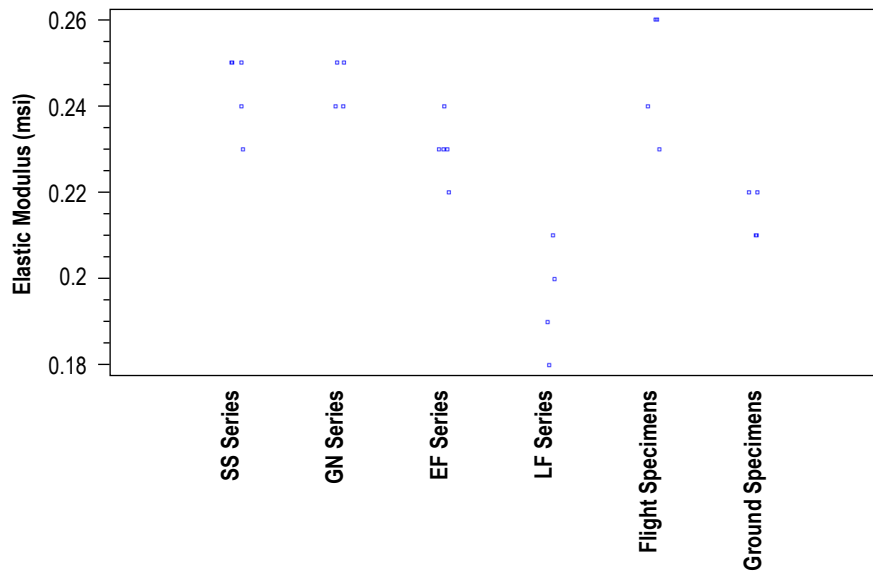

Figure 66. Scatterplot of elastic modulus (measured from room temperature tensile tests) across six specimen sets. Stratification of data (i.e., repeated values) is a consequence of rounding.
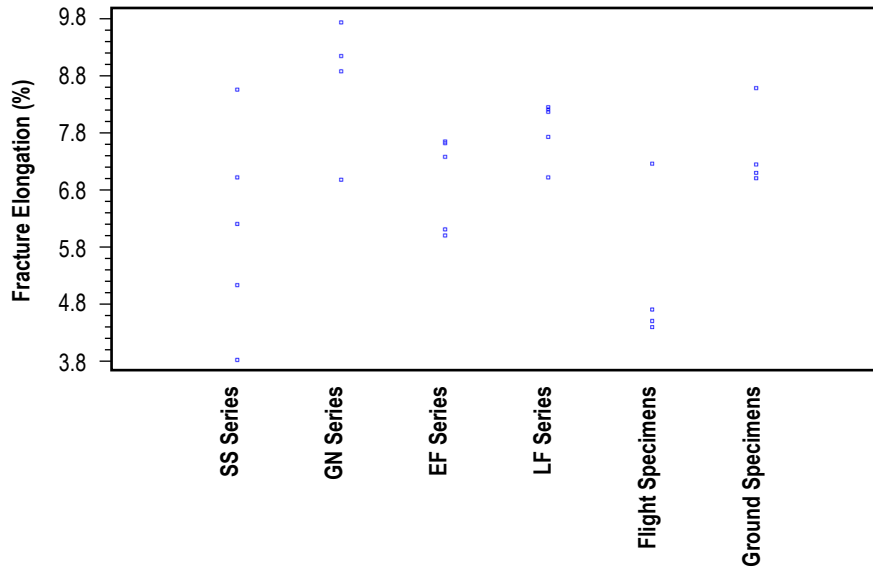
Figure 67. Scatterplot of fracture elongation (measured from room temperature
tensile tests) across six specimen sets.

The scatterplot of elastic modulus for all six datasets is shown in figure 66. The stratification of data (i.e., multiple specimens with the same modulus) is an artifact of rounding (modulus values are reported to two significant figures). Flight specimens from 3DP are statistically in family with the GN series (which also had a tip-to-tray distance commensurate with the extruder being too close to the build plate).

Fracture elongation data (fig. 67) are highly variable across all specimen classes. The most variability is observed in the SS series and the 3DP flight specimens (the coefficient of variation associated with these datasets is 29% and 26%, respectively). The large variability in the flight specimens is a product of F004 (tensile specimen 1), which, though not a true statistical outlier, has a fracture elongation that is ≈3% higher than the other flight tensile specimens. While GN specimens and 3DP flight specimens were both built with the extruder tip closer to the build tray than nominal, the specimen groups are not in family with one another in terms of fracture elongation. Reduced ductility may also be a consequence of the tensile specimen type (type IV from ASTM D638[5]), which has a larger stress concentration at the fillet than the type I specimen design (but fracture elongation of <5% is only observed in some datasets and thus does not show a clear linkage to coupon geometry).

B.2 Comparison of Compression Test Data

Material properties obtained from compression testing across the six datasets are summarized in table 29.

Table 29. Compression data comparison for all specimen classes.

Group	Mean Stress at 20% Strain (ksi)	Coefficient of Variation (%)	Mean Compressive Yield Strength (ksi)	Coefficient of Variation (%)	Mean Compressive Modulus (ksi)	Coefficient of Variation (%)
SS series	7.72	1.6	4.96	1.9	0.18	4.9
GN series	6.42	4.0	4.55	4.3	0.19	9.5
EF series	6.35	3.1	4.44	2.8	0.15	3.8
LF series	6.35	3.1	4.42	2.4	0.15	4.7
Ground specimens	7.45	5.0	5.42	7.9	0.24	4.2
Flight specimens	5.58	3.1	3.98	4.7	0.16	9.4

The compressive strengths (fig. 68) of the 3DP ground specimens are in family with the SS series and are also significantly higher than characteristic compressive strengths for specimens produced using other flight-like printers. The 3DP flight specimens exhibit the lowest compressive strengths of all data series.
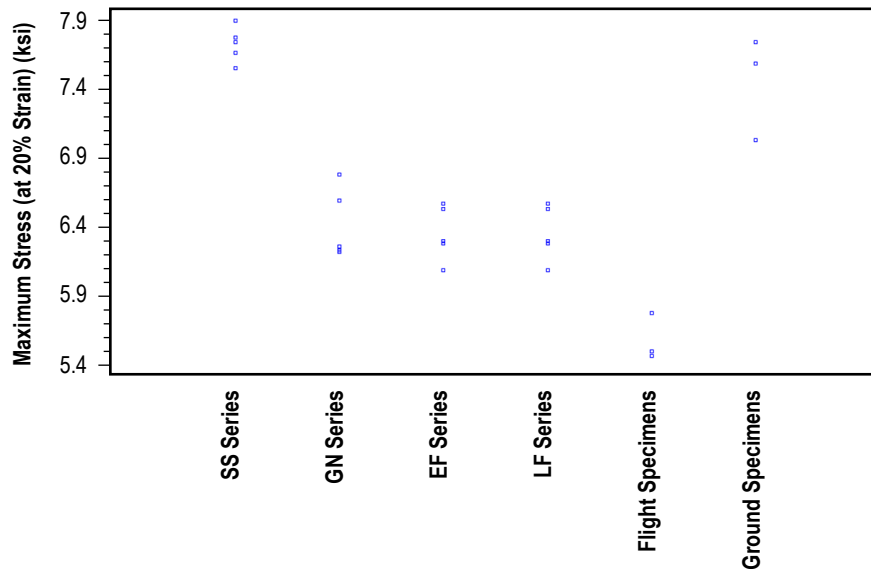

Figure 68. Scatterplot of compressive stress at 20% strain across six specimen sets.

As with elastic modulus, the stratification in the compressive modulus data (fig. 69) is attributable to rounding. For this metric, the 3DP ground specimens have the highest characteristic modulus and are distinct from all other datasets for this material property.
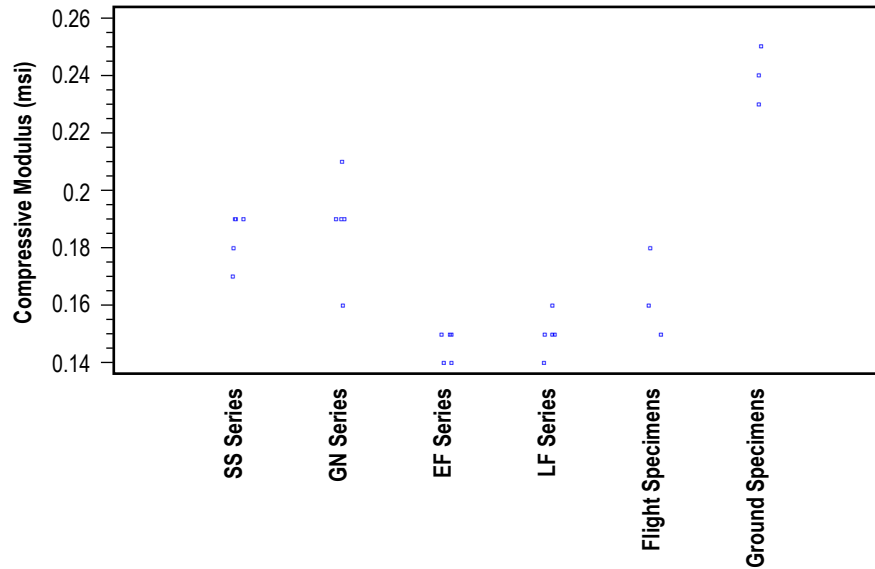

Figure 69. Scatterplot of compressive modulus across six specimen sets.
Stratification in data is due to rounding.

B.3 Comparison of Flexure Test Data

Material properties obtained from flexure testing at room temperature for all specimen sets are summarized in table 30.

Table 30. Flexural data comparison for all specimen classes.

Group	Ultimate Flexural Stress (ksi)	Coefficient of Variation (%)	Flexural Modulus (msi)	Coefficient of Variation (%)
SS series	5.687	9.5	0.22	1.3
GN series	6.951	5.8	0.22	4.3
EF series	6.560	6.8	0.24	7.0
LF series	5.329	14.6	0.17	1.7
Ground specimens	5.212	6.0	198.00	3.9
Flight specimens	6.544	9.3	241.00	9.6

Flexural strengths for the flight specimens (fig. 70) are in family with the EF and GN series. For flexural modulus (fig. 71), there is an overlap in the range of almost all the datasets.
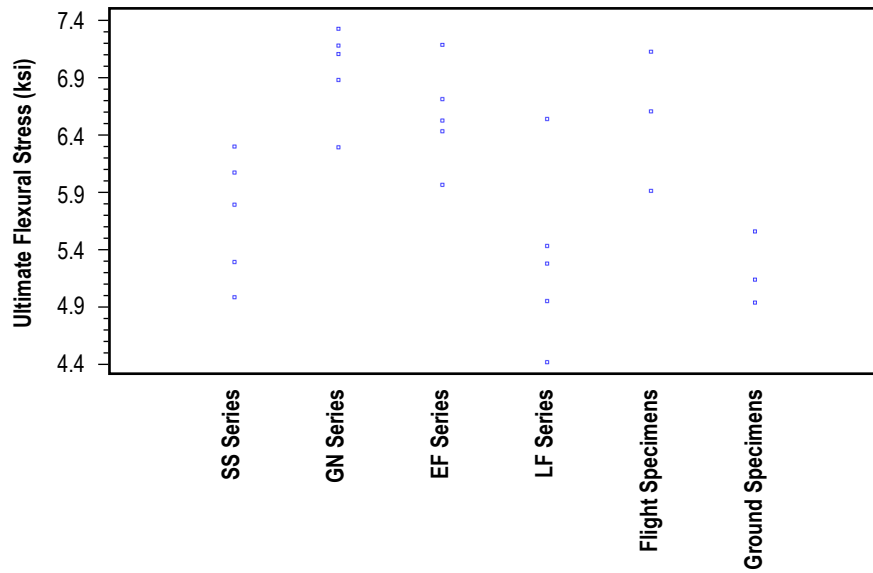

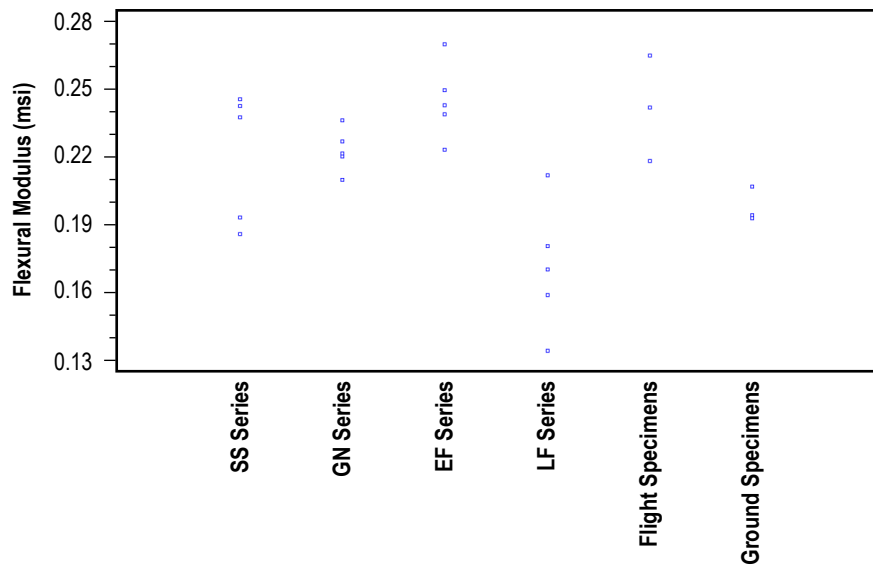Figure 70. Scatterplot of ultimate flexural stress across six specimen sets.

Figure 71. Scatterplot of flexural modulus across six specimen sets.

The SS, GN, EF, and LF series are not directly comparable with the 3DP data owing to differences in feedstock, manufacturing process controls, and printer hardware. However, much of the data from the 3DP flight specimens are in family with other ground-based datasets (SS, GN, EF, and LF series). The most puzzling dataset, when situated within the context of prior materials characterization work, is the compression properties for the 3DP specimens. The flight specimens have a characteristic value of compressive strength that is unique and lower than all other observed data. The ground specimens from 3DP have compressive moduli that are significantly greater than any other observations. Because of the multiple variables that are different between 3DP and other datasets, it is difficult to isolate and/or definitively identify the cause of this discrepancy. Further discussion of the compression specimens (and observed differences between ground and flight that may contribute to their unique behavior) appears in sections 6 and 7.

REFERENCES

1. Johnston, M.M.; Werkheiser, M.J.; Cooper, K.G.; et al.: "3D Printing in Zero-G ISS Technology Demonstration," in *Proc. AIAA SPACE 2014 Conference and Exposition*, August 5–7, 2014, AIAA, Reston, VA, 5 pp., doi:10.2514/6.2014-4470, 2014.

2. NASA TechPort, "Advanced Manufacturing Technologies (MAT): Additive Construction for Mobile Emplacement Project," <techport.nasa.gov/view/17558>, October 2014.

3. Mahoney, E.: "Future Engineers Finalists Get First Hand Look at Future of Space Exploration," <www.nasa.gov/feature/future-engineers-finalists-get-first-hand-look-at-future-of-space-exploration>, July 30, 2015.

4. Prater, T.J.; Bean, Q.A.; Werkheiser, M.J.; et al.: "Summary Report for the Technical Interchange Meeting on Development of Baseline Material Properties and Design Guidelines for In-Space Manufacturing Activities," NASA/TM—2016–218219, NASA Marshall Space Flight Center, 82 pp., March 2016.

5. ASTM D638, "Standard Test Method for Tensile Properties of Plastics," ASTM International, West Conshohocken, PA, 2014.

6. ASTM D790, "Standard Test Methods for Flexural Properties of Unreinforced and Reinforced Plastics and Electrical Insulating Materials," ASTM International, West Conshohocken, PA, 2015.

7. ASTM D695, "Standard Test Methods for Compressive Properties of Rigid Plastics," ASTM International, West Conshohocken, PA, 2015.

8. Forster, A.M.: "Materials Testing Standards for Additive Manufacturing of Polymer Materials: State of the Art and Standards Applicability," NISTIR 8059, National Institute of Standards and Technology, Gaithersburg, MD, 54 pp., May 2015.

9. National Institute of Standards and Technology, "Measurement Science Roadmap for Metal-Based Additive Manufacturing," <http://www.nist.gov/el/isd/upload/NISTAdd_Mfg_Report_FINAL-2.pdf>, May 2015.

10. DeGroh, K.K.; Banks, B.A.; McCarthy, C.E.; et al.: "MISSE 2 PEACE Polymers Atomic Oxygen Erosion Experiment on the International Space Station," *High Perform. Polym.*, Vol. 20, pp. 388–409, August 2008.

11. O'Donnell, J.H.: "Radiation Chemistry of Polymers," in *Effects of Radiation on High-Technology Polymers*, E. Reichmanis and J.H. O'Donnell (eds.), American Chemical Society, Washington, DC, pp. 1–13, 1989.

12. Snyder, M.P.; Dunn, J.J.; and Gonzalez, E.G.: "Effects of Microgravity on Extrusion based Additive Manufacturing," in *Proc. AIAA SPACE 2013 Conference and Exposition*, September 10–12, 2013, AIAA, Reston, VA, 6 pp., doi:10.2514/6.2013-5439, 2013.

13. Grugel, R.; Cotton, L.; Segre, P.; et al.: "The In-Space Soldering Investigation (ISSI): Melting and Solidification Experiments Aboard the International Space Station," in *Proc. 44th AIAA Aerospace Sciences Meeting and Exhibit*, January 9–12, 2006, AIAA, Reston, VA, doi:10.2514/6.2006-521, 2006.

14. Kulich, D.M.; Gaggar, S.K.; Lowry, V.; and Stepien, R.: "Acrylonitrile-Butadiene-Styrene (ABS) Polymers," in *Kirk-Othmer Encyclopedia of Chemical Technology*, John Wiley and Sons, Inc., 2001.

15. Rodriguez, J.F.; Thomas, J.P.; and Renaud, J.: "Characterization of the mesostructure of fused-deposition acrylonitrile-butadiene-styrene materials," *Rapid Prototyping J.*, Vol. 6, No. 3, pp. 175–186, doi:10.1108/13552540010337056, 2000.

16. ASTM D570, "Standard Test Method for Water Absorption of Plastics," ASTM International, West Conshohocken, PA, 2010.

17. Rodriguez, J.F.; Thomas, J.P.; and Renaud, J.: "Mechanical behavior of acrylonitrile-butadiene-styrene (ABS) fused deposition materials: experimental investigation," *Rapid Prototyping J.*, Vol. 7, pp. 148–158, 2001.

18. Kuhn, H.; and Medlin, D. (eds.): *ASM Handbook Volume 8*: *Mechanical Testing and Evaluation*, ASM International, Materials Park, OH, 998 pp., 2000.

19. Cole-Parmer: "Chemical Compatibility Database," <http://www.coleparmer.com/Chemical-Resistance>, 2016.

20. Agarwala, M.K.; Jamalabad, V.R.; Langrana, N.A.; et al.: "Structural quality of parts processed by fused deposition," *Rapid Prototyping J.*, Vol. 2, No. 4, pp. 4–19, doi:10.1108/13552549610732034, 1996.

21. Sun, Q.; Rizvi, G.M.; Bellehumeur, C.T.; and Gu, P.: "Effect of processing conditions on the bonding quality of FDM polymer filaments," *Rapid Prototyping J.*, Vol. 14, No. 2, pp. 72–80, doi:10.1108/13552540810862028, 1995.

REPORT DOCUMENTATION PAGE

1. REPORT DATE *(DD-MM-YYYY)* 01–07–2016	2. REPORT TYPE Technical Publication	3. DATES COVERED *(From - To)*

4. TITLE AND SUBTITLE

Summary Report on Phase I Results From the 3D Printing in Zero-G Technology Demonstration Mission, Volume I

5a. CONTRACT NUMBER

5b. GRANT NUMBER

5c. PROGRAM ELEMENT NUMBER

6. AUTHOR(S)

T.J. Prater, Q.A. Bean, R.D. Beshears, T.D. Rolin, N.J. Werkheiser, E.A. Ordonez, R.M. Ryan, and F.E. Ledbetter III

5d. PROJECT NUMBER

5e. TASK NUMBER

5f. WORK UNIT NUMBER

7. PERFORMING ORGANIZATION NAME(S) AND ADDRESS(ES)

George C. Marshall Space Flight Center
Huntsville, AL 35812

8. PERFORMING ORGANIZATION REPORT NUMBER

M–1415

9. SPONSORING/MONITORING AGENCY NAME(S) AND ADDRESS(ES)

National Aeronautics and Space Administration
Washington, DC 20546–0001

10. SPONSORING/MONITOR'S ACRONYM(S)

NASA

11. SPONSORING/MONITORING REPORT NUMBER

NASA/TP—2016–219101

12. DISTRIBUTION/AVAILABILITY STATEMENT

Unclassified-Unlimited
Subject Category 18
Availability: NASA STI Information Desk (757–864–9658)

13. SUPPLEMENTARY NOTES

Prepared by Materials and Processes Laboratory, Engineering Directorate

14. ABSTRACT

Human space exploration to date has been confined to low-Earth orbit and the Moon. The International Space Station (ISS) provides a unique opportunity for researchers to prove out the technologies that will enable humans to safely live and work in space for longer periods of time and venture beyond the Earth/Moon system. The ability to manufacture parts in-space rather than launch them from Earth represents a fundamental shift in the current risk and logistics paradigm for human spaceflight. In September 2014, NASA, in partnership with Made In Space, Inc., launched the 3D Printing in Zero-G technology demonstration mission to explore the potential of additive manufacturing for in-space applications and demonstrate the capability to manufacture parts and tools on orbit using fused deposition modeling. This Technical Publication summarizes the results of testing to date of the ground control and flight prints from the first phase of this ISS payload.

15. SUBJECT TERMS

in-space manufacturing, additive manufacturing, 3D printing, technology demonstration mission, material testing, ABS, ISS payload

16. SECURITY CLASSIFICATION OF:			17. LIMITATION OF ABSTRACT	18. NUMBER OF PAGES	19a. NAME OF RESPONSIBLE PERSON
a. REPORT	b. ABSTRACT	c. THIS PAGE			STI Help Desk at email: help@sti.nasa.gov
U	U	U	UU	156	19b. TELEPHONE NUMBER *(Include area code)* STI Help Desk at: 757–864–9658